ABSTRACT

SPATIO-TEMPORAL CORRELATION MODELS FOR INDOOR MIMO CHANNELS

by
Kaustubha Raghukumar

Accurate modeling of the spatio-temporal cross-correlation between the subchannels of a multiple-input multiple-output (MIMO) channel is an important prerequisite of multi-element antenna system design. In this thesis, a new model for indoor MIMO channels is proposed, and a closed form expression for the spatio-temporal cross-correlation function is derived. This new analytical correlation expression includes many physical parameters of interest such as the angle-of-arrivals at the base station and the user, the associated angle spreads, and other parameters, in a compact form. Comparison of this model with narrowband indoor MIMO data collected at Brigham Young University exhibits the utility of the model. Specifically, capacity calculations and the application of the model to maximum likelihood detection in correlated narrowband MIMO channels demonstrates close match to empirical data. As a different approach to indoor correlation modeling, the commonly used Kronecker product model is considered, which shows large deviation from the measured data in terms of correlation, capacity, and bit error rate.

SPATIO-TEMPORAL CORRELATION MODELS FOR INDOOR MIMO CHANNELS

by
Kaustubha Raghukumar

A Thesis
Submitted to the Faculty of
New Jersey Institute of Technology
in Partial Fulfillment of the Requirements for the Degree of
Master of Science in Telecommunications

Department of Computer Science
Department of Electrical and Computer Engineering

May 2003

APPROVAL PAGE

SPATIO-TEMPORAL CORRELATION MODELS FOR INDOOR MIMO CHANNELS

Kaustubha Raghukumar

Dr. Ali Abdi, Thesis Advisor — Date
New Jersey Center for Wireless Telecommunications
Center for Communications and Signal Processing Research
Assistant Professor of Electrical and Computer Engineering, NJIT

Dr. Yeheskel Bar-Ness, Committee Member — Date
Director, Center for Communications and Signal Processing Research
Distinguished Professor of Electrical and Computer Engineering, NJIT

Dr. Hongya Ge, Committee Member — Date
Center for Communications and Signal Processing Research
New Jersey Center for Wireless Telecommunications
Associate Professor of Electrical and Computer Engineering, NJIT

BIOGRAPHICAL SKETCH

Author: Kaustubha Raghukumar

Degree: Master of Science

Date: May 2003

Undergraduate and Graduate Education

- Master of Science in Telecommunications,
  New Jersey Institute of Technology, Newark, New Jersey, 2003
- Bachelor of Engineering in Electronics and Telecommunication,
  Goa College of Engineering, Goa, India, 1996

Major: Telecommunications

Presentations and Publications:

Kaustubha Raghukumar, Ali Abdi, Jon Wallace and Michael Jensen, "Spatial-Correlation in Indoor MIMO Channels: Analytic Model and Experimental Results", accepted for publication by *IEEE Vehicular Technology Conference*, Orlando, Florida, Oct. 2003.

To Popo

ACKNOWLEDGMENT

I would like to thank Dr. Ali Abdi for all the guidance, mentorship and support provided throughout my association with him. He has made me a better engineer. I also thank the New Jersey Center for Wireless Telecommunications (NJCWT) and Center for Communications and Signal Processing Research (CCSPR), for providing me with financial support and working space during the completion of this thesis. The efforts of Dr. Alexander Haimovich in providing financial support through NJCWT are greatly appreciated. I thank the members of the defense committee, Dr. Yeheskel Bar-Ness and Dr. Hongya Ge for sitting on the committee and taking time off to review this thesis. Dr. Jon Wallace and Dr. Michael Jensen of Brigham Young University deserve my gratitude for providing the measurement data used as part of this work, and for the many insightful comments over the past couple of months.

Finally, I thank all my friends and colleagues at CCSPR for the long lunches and longer coffee breaks that have made things so interesting around here.

TABLE OF CONTENTS

TABLE OF CONTENTS
(Continued)

Chapter **Page**

LIST OF TABLES

Table **Page**

LIST OF FIGURES

Figure **Page**

LIST OF FIGURES
(Continued)

Figure **Page**

CHAPTER 1
INTRODUCTION

A foreseeable increase in demand for higher data rates and reliability in wireless communications has led to the proposal of several attractive schemes to achieve these goals. One of these was to use antenna arrays at the base station (transmit diversity) which results in increased reliability but no gain in the channel capacity. This lead to an investigation by [1][2] to study the use of multiple antennas at both the receiver and transmitter from an information theoretic point of view. Their findings reported increases in capacity as the number of sub-channels between the transmitter and receive arrays increased. There now exist several coding schemes [3] and experimental setups [4] that have exploited the availability of additional antenna elements to achieve significant increases in both capacity and diversity. Multi-element antenna systems have been shown to be capable of delivering tremendous increases in channel capacities by exploiting a sufficiently rich multipath scattering environment. It has been shown that the channel capacity of such systems can increase linearly with the number of spatial sub-channels between the transmitter and receiver. This capacity, however, may not be as high as envisioned when the sub-channels between the different antenna elements are correlated. The correlation can depend on a number of factors, such as geometry of the layout, absence of a line-of-sight component, and the presence of scatterers local to the transmitter and receiver.

This report consists of various findings where we use a series of measurements taken by Dr. Jon Wallace and Prof. Michael Jensen of Brigham Young University, in order to compare the measured correlations and channel capacities with those obtained by several analytical correlation models, including one proposed in this thesis. The models that have been used for performance comparison with the measured correlation are the widely used Kronecker product model proposed in [5], the one-ring model proposed in [6], and the two-ring model developed in this body

of work. The Kronecker product model assumes independence between the transmit and receive correlations, an assumption that may not always be valid, although it greatly simplifies the computation of the correlation. The one-ring model is not analytically sound for an indoor MIMO channel, where there are scattering objects around both the transmitter and receiver. The two-ring model takes care of this deficit in the one-ring model, while at the same time showing a good fit to measured data.

1.1 Multiple Antenna System Model

A typical setup involving a MIMO system is shown in Fig.1.1, taken from [7]. The number of transmit antennas may or may not be equal to the number of receive antennas, but a common requirement is that the number of transmit antennas be less than the number of receive antennas. The capacity has been shown to increase linearly with $min(n_T, n_R)$ where n_T and n_R are the number of transmit and receive antenna elements respectively, until a limit is reached, after which no further increases in capacity are possible. Various transmission schemes exist that try and exploit the availability of additional antennas at on either side of the communication link, and significant effort has been put in by the wireless research community to achieve increased data rates. As shown in Fig.1.1, the bit stream at the transmitter needs to pass through a serial-to-parallel converter before it can be modulated and transmitted from one of the n_T transmit antennas. We now introduce the system model that we use as the basis for further investigations.

Let us consider the down-link with no transmit beamforming. Let $s_p(t)$ represent the complex envelope of the signal transmitted from the pth BS array element and $r_l(t)$ the complex envelope of the signal received by the $l$the user's array element. For the frequency non-selective communication link between the element BS_p and the element U_l, the complex low-pass equivalent channel response

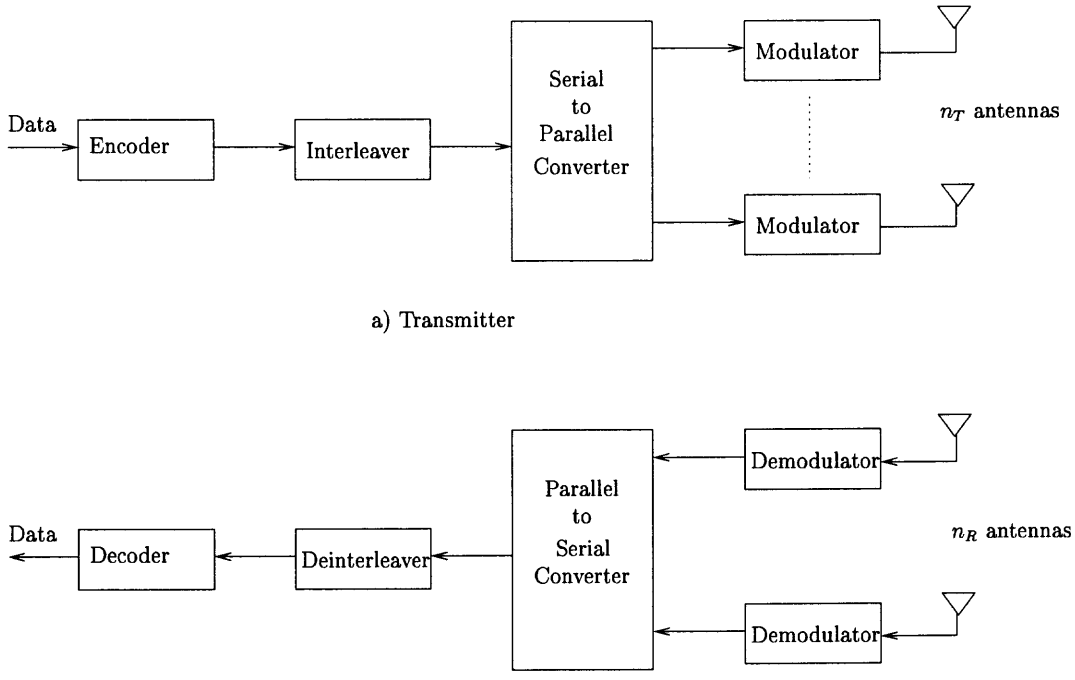

Figure 1.1: A MIMO system.

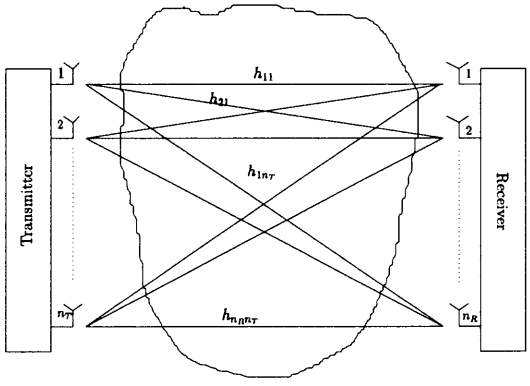

Figure 1.2: The MIMO channel.

$h_{lp}(t)$ appears as a multiplicative factor. Note that such a link comprises of many *paths* that can be drawn from BS_p to U_l through the local and remote scatterers enclosing the user, as well as a possible line-of-sight path. Based on vector notation, $\mathbf{s}(t) = [s_1(t) \dots s_{n_{BS}}(t)]'$ and $\mathbf{r}(t) = [r_1(t) \dots r_{n_U}(t)]'$, with $'$ as the transpose operator, the input-output equation for the frequency non-selective MIMO fading channel can be written as,

$$\mathbf{r}(t) = \mathbf{H}(t)\mathbf{s}(t) + \mathbf{n}(t) \tag{1.1}$$

where $\mathbf{H}(t)$ is the $n_U \times n_{BS}$ channel matrix complex envelope such that $[\mathbf{H}(t)]_{lp} = h_{lp}(t)$, and $\mathbf{n}(t)$ stands for the complex envelope of the additive white Gaussian noise(AWGN) with zero mean vector and the diagonal covariance matrix, i.e., $E[\mathbf{n}(t)\mathbf{n}^H(t)] = P_{noise}\mathbf{I}_{n_U}$, where $\mathbf{I}$ is the $n_U \times n_U$ real identity matrix, and ^{H} stands for the Hermitian operator. The dependence of $\mathbf{H}(t)$ on time is a result of user mobility (Doppler effect). This implies that we need to take into account the effect of channel time selectivity. However, as we will see in a later section, the data available to us represents a fixed wireless scenario (no relative movement between the transmitter and receiver), as a result of which, at this stage, the accounting of the time selectivity in this thesis is merely for the sake of completeness. The channel matrix $\mathbf{H}(t)$ is assumed to be a multivariate Gaussian process, which, for most practical purposes, is correlated,

with non-zero mean and non-unit variance. However, in most literature , $\mathbf{H}(t)$ is assumed to be IID complex Gaussian, i.e Rayleigh distributed. In this thesis, an attempt is made to demonstrate the effect of correlation between the elements of the channel matrix on important wireless system performance criteria such as channel capacity and bit error rate.

1.2 Correlation Modeling of MIMO Systems

In order to understand the need for correlation modeling of MIMO systems, it is helpful to first look at correlation modeling of wireless systems from a historical perspective. The origins of correlation modeling may be traced to Clark's correlation model [8], where the temporal correlation in the received signal envelope is developed. This correlation model, developed in the early days of cellular radio, still remains a fundamental model, and most modern correlation models for a variety of wireless applications, can be shown to reduce to this fundamental model, under simplifying conditions. With the advent of antenna arrays for use at the base station, the need arose for a correlation model that could take care of the spatial characteristics of the received signal envelope, such as angle of arrival, time delay spread and the antenna array geometries [9]. These spatial models too, under some conditions can be found to reduce to the classical Clark's correlation, with the temporal variable replaced by a spatial variable. Typical approaches to correlation usually involve starting with field measurements, and then using various statistical properties of the communication system and environment to construct the correlation model. This model is then validated against the field measurements. The model developed needs to be able to capture the essential physical properties of the environment, and should be able to predict, with reasonable accuracy, the behavior of the wireless communication channel. With the advent of multielement antenna systems, employing multiple antennas at both transmitter and receiver, the need arose to develop models that

capture the multidimensionality of the resulting radio channel. The effect of fading correlation is first treated in [10], where the authors have built upon a one-ring correlation model, first proposed by [11]. Using the classification scheme used in [12] for a variety of correlation models, the one-ring model used in [10] may be classified as a physical scatterer model, where a particular geometry of scatterers around either the base station or the user is used to obtain various physical characteristics of the channel being studied. Models are often defined by the geometry of the scatterers which may be a ring [10][11], an ellipse [13] or a virtual array between the transmitter and receiver [14]. Further, the statistical distribution of the scatterers is also an important consideration when it comes to correlation modeling.

1.3 Drawbacks of Existing Models and the Need for New Models

A popular approach to correlation modeling in MIMO systems is the Kronecker product model which assumes separability between the signals at the transmitter and receiver, and models the correlation as the product between the transmit and receive covariance matrices. This assumption of separability, though extremely attractive for analytical purposes, has been shown in [6] and in this contribution, to give erroneous results in terms of correlation and capacity. In fact, the error as far as correlation alone is concerned can be quite high (upto 70%). An improvement to the model in [10] was proposed in [6] which made use of the von Misses distribution to model the scatterer distribution at the user. Further, this model proposed a easily implementable closed-form expression for the spatio-temporal correlation between any two pairs of antenna elements at the transmitter and receiver, without making the assumption of separability between the transmitter and receiver. In fact, this model treats the whole propagation phenomenon between the transmitter and receiver as one irreducible system. It must, however, be pointed out that the model developed in [6], while useful for the outdoor MIMO case, is not entirely accurate for the indoor

MIMO scenario. This is because the model assumes that the base station is at an elevation, and hence has no scatterers local to it. In the indoor case, both the transmitter (base station) and the receiver (user) are at the same level, and in fact, may often be in the same room. Thus, it is important to account for scatterers local to the base station in indoor MIMO correlation models.If one were to start with the one-ring model, and were to try and enhance it to take care of the indoor scenario as well, it is logical to include the scatterers local to the base station as an additional ring surrounding the base station. This two-ring model, so to speak, has been proposed in literature, but the authors have usually run into analytical difficulties [15]. Other examples of two-ring models may be found in [12], [16]-[21].

1.4 New Contributions

The contributions of this thesis are the proposal of a new spatio-temporal correlation model which maybe classified as a two-ring model, which takes into account several physical parameters of interest, such as angle of arrival, angle of departure, scatterer geometries and distributions, and other relevant parameters. Further, some capacity calculations have been made that demonstrate the large errors that can occur with the use of the separable model, while at the same time, showing the utility of the new two-ring model when it comes to capacity calculations. Finally, some calculations of the bit error rate that is predicted by the use of various correlation models have been made, which again shows the close fit of the predictions made by the new model with measurement results. It is believed that such calculations on the effect of correlation on bit error rate have not been previously made.

1.5 Outline

The organization of this thesis is as follows: In Chapter 2 we talk about the measurement data available from Brigham Young University and the various

parameters that need to be taken into consideration when working with this data. Chapter 3 delves into the one-ring and two-ring spatio-temporal correlation models and the need for such models in indoor wireless systems. Chapter 4 discusses the utility of the new two-ring model in MIMO capacity calculations while Chapter 5 utilizes the same two-ring correlation model to study the bit error rate of a MIMO maximum likelihood detector. Chapter 6 concludes this thesis while the appendices include the room layouts, all the correlation, capacity CDF and bit error rate plots generated

CHAPTER 2

THE MEASUREMENT SYSTEM

A series of detailed MIMO measurements were carried out by Dr. Jon Wallace at Brigham Young University in the year 2000. The measurements were taken on the fourth floor of the engineering building using custom built hardware. This data , graciously made available to the public, was used for this study. Fig.2, taken

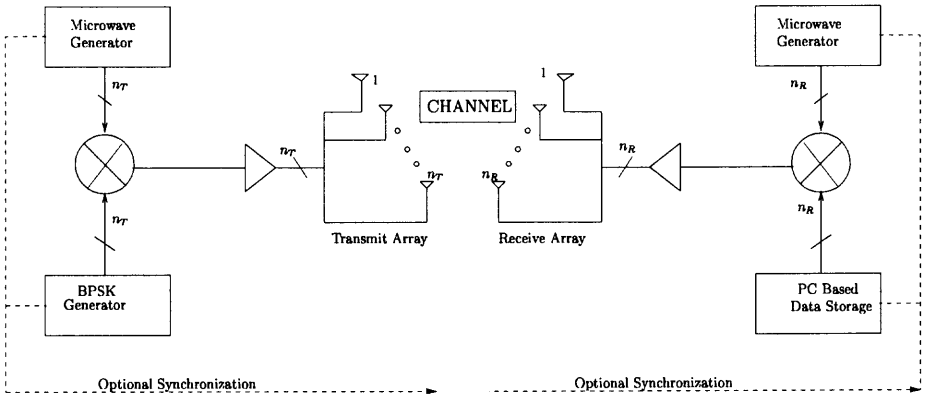

Figure 2.1: The measurement system.

from [22], illustrates the high level measurement system that was used to make the measurements. Two different antenna arrays were used during the measurements. The first design consisted of four-element dual-polarization patch antennas with half-wavelength spacing on either end of the MIMO link. The second design was a two-dimensional grid of holes spaced at a quarter wavelength. In this study, the data belonging to the latter design had 10 element monopole antennas on either end of the MIMO link.

2.1 The Measured Channel Matrix

The data was collected at a center frequency of 2.45 GHz using a 1000-bit binary(+1,-1) codes at a chip rate of 12.5 kbps. This chip rate results in channel matrix estimate every 80 ms. Although line-of-sight data was available for a particular setting, it was

found to be statistically insufficient to conduct detailed study. Also, no relative motion between the transmitter and receiver was present, and hence, there is no Doppler spread, which in turn results in a correlation result that is independent of time. The data is organized into data files with each data set containing 124 channel matrices. It should be emphasized that the 124 sample snapshot in any data set is *not* the channel impulse response. A data set containing these 124 channel matrices

$$\mathbf{h} = \overbrace{\begin{Bmatrix} h_{11} & h_{12} & h_{13} & h_{14} \\ h_{21} & h_{22} & h_{23} & h_{24} \\ h_{31} & h_{32} & h_{33} & h_{34} \\ h_{41} & h_{42} & h_{43} & h_{44} \end{Bmatrix}}^{1} \quad \cdots \quad \overbrace{\begin{Bmatrix} h_{11} & h_{12} & h_{13} & h_{14} \\ h_{21} & h_{22} & h_{23} & h_{24} \\ h_{31} & h_{32} & h_{33} & h_{34} \\ h_{41} & h_{42} & h_{43} & h_{44} \end{Bmatrix}}^{124}$$

is illustrated above for a 4×4 setup. Several such sets are collected and stored as part of the data pertinent to a particular *location*. Different locations may have data collected at physically different spots but the data in each location is always collected at the exact same spot under the exact same conditions. This approach results in data which is sizable in volume, hence providing statistically sufficient samples. In addition to being collected at the same physical locations, the data across locations may also have differences in transmit- receive antenna orientations, and discrete motion of the receiver/transmitter from one location to another. It is thus seen that when dealing with the data, one has to be extremely cautious in using the correct data sets and locations when performing any kind of averaging process. Table 2.1 summarizes the information pertinent to the various data sets used. For the sake of uniformity, only those data sets that have the transmitter in room 484 and receiver in room 400 have been used for correlation fitting and capacity calculations. Also shown is a room layout for a 4x4 setup (Fig. 2.1), which shows the transmit and receive rooms, antenna orientations and arrangement of locations. The remainder of the room layouts, i.e. for the 10x10 data sets may be found in the Appendix A. Although

Table 2.1: Important Features of the Data Sets

Antennas	Antenna Sep.	Date	Carrier Frequency	Locations	Sets
4×4 patch	$\lambda/2$	08/22/00	2.45 GHz	8	5
10×10 monopole	$\lambda/4$	11/07/00	2.42 GHz	24	20
		11/08/00		4	20
		12/21/00		8	21

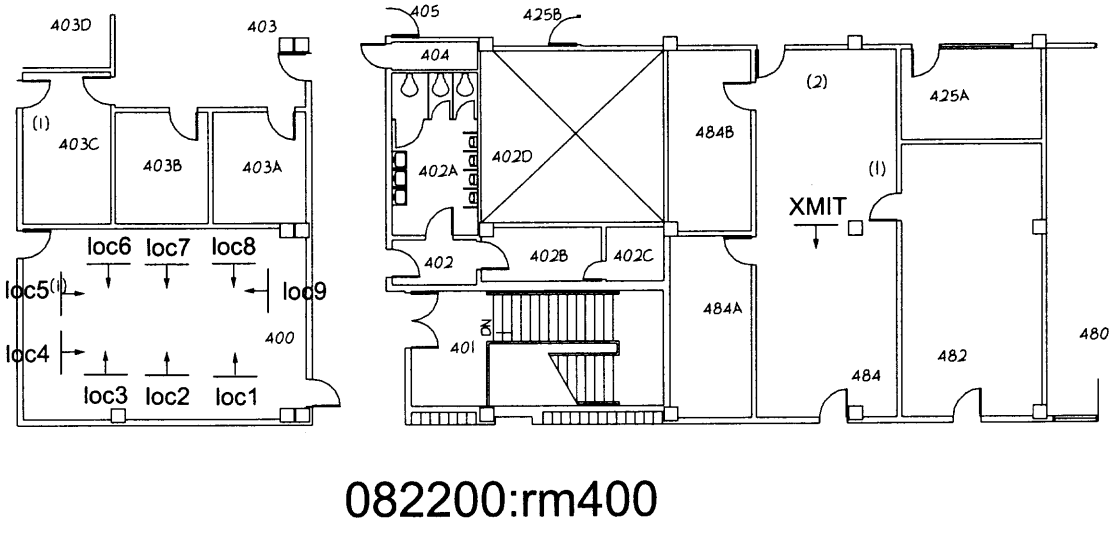

Figure 2.2: Location of 4x4 measurement.

channel data was available for different antenna polarizations, it was found to be in different transmit and receive locations, as a result of which, statistical consistency may be lost while examining the effect of polarization on various parameters of interest.

2.2 Normalization of the Channel Matrix

The variety of scenarios in which the data were collected causes the received power in each of the locations to vary considerably. In order to make a fair comparison of the channel matrix properties across data sets and locations, one needs to perform some kind of normalization on the channel data. There is also the effect of path loss, which could lead to a distortion of effects such as spatial correlation of transmit and receive signals. The effect of path loss may be removed through appropriate channel normalization.

In this thesis, channel matrix normalization is performed to force a unit single-input-single-output (SISO) gain. If this normalization is performed across all the **H** matrices in a set, then the effect of path loss is removed. If the normalization is performed on each **H** matrix separately, the effect of path loss is not removed. This kind of normalization (each **H** matrix separately), though useful for some purposes, is not required to study correlated fading, which is primarily a product of small-scale fading. Thus, the normalization is performed such that,

$$\frac{1}{N}\sum_{i=1}^{N}\|\mathbf{H}_i\|_F^2 = n_T n_R, \tag{2.1}$$

where $\|\cdot\|$ denotes the Frobenius norm, defined as,

$$\|\mathbf{H}\|_F = \sqrt{\sum_{i=1}^{n_T}\sum_{k=1}^{n_R}|h_{ik}|^2} \tag{2.2}$$

and N is the sum total of the number of **H** matrices available. For example, for the 10×10 data collected on 11/07/00, 11/08/00 and 12/21/00 N is equal to 7184,

11532, 14756 respectively. For the 4×4 data collected on 08/22/00, N is equal to 4588 for Room 400, which has a layout consistent with the 10×10 measurements. This normalization is carried out prior to any kind of analysis and simulations conducted using the available measured data.

CHAPTER 3

CORRELATION MODELS

Having dispensed with the preliminaries, it is now appropriate to begin an investigation into the correlation properties of MIMO channels, and to attempt capturing the essential features through an analytical model. The measurement data available serves as a benchmark against which the model can be tested. This chapter is organized as follows: Section 3.1 first details the methods followed to estimate the measured covariance matrix and the covariance estimated using the Kronecker product model. This is then followed by a comparison of the model errors between the covariance matrices in section 3.2. Section 3.3 defines the various types of correlation that are used in the comparison of the two-ring correlation model with the measured correlations, also obtained using these definitions. Section 3.4 develops the analytic two-ring model in detail, and in Section 3.5, a comparison between the correlations returned by the measurements and those returned by the new model is made. In Section 3.6, an attempt is made to interpret the parameters returned by the two-ring model in terms of the room layouts. By the end of this chapter, it is thus possible to observe the utility of the new two-ring model in correlation measurements.

3.1 Calculation of Measured Correlation

We define $vec\{\mathbf{H}(t)\}$ as an $n_U n_{BS} \times 1$ vector, constructed by stacking the columns of $\mathbf{H}(t)$, the $n_U \times n_{BS}$ channel matrix. If $\mathbf{H}(t) = [\mathbf{h}_1(t) \;\; \mathbf{h}_2(t) \ldots \mathbf{h}_{n_{BS}}(t)]$, where $\mathbf{h}_s(t)$ is an $n_U \times 1$ vector,corresponding to the sth BS antenna element. Then, $vec\{\mathbf{H}(t)\} = [\mathbf{h}_1'(t) \;\; \mathbf{h}_2'(t) \ldots \mathbf{h}_{n_{BS}}'(t)]'$. Based on these definitions, we may write the measured (empirical) correlation matrix as,

$$\mathbf{R}_H = E[vec\{\mathbf{H}(t)\}vec\{\mathbf{H}(t)\}^H], \tag{3.1}$$

where $E[\cdot]$ denotes the expected value. $\mathbf{R}_H$ is the $n_U n_{BS} \times n_U n_{BS}$ channel covariance matrix obtained from the normalized channel data. It should be kept in mind that in all simulations involving the channel covariance matrix or when covariance matrices need to be generated according to an analytic model, one must work with $vec\{\mathbf{H}(t)\}$ and not $\mathbf{H}(t)$ in order to maintain consistency of matrix dimensions. It should also be noticed that the empirical covariance matrix in Eq. (3.1) is *not* a function of time. This is because, as mentioned earlier, the data does not incorporate relative motion between transmitter and receiver, as a result of which there is no Doppler spread.

3.2 The Kronecker Product Model

This widely used model makes use of the assumption that the spatial correlation at the transmitter and receiver are independent and the correlation between a pair of sub-channels between the transmitter and receiver can be expressed as the product of transmit and receive correlations. In [5], the authors have found a good match between the empirical covariance matrix and the covariance matrix obtained through the use of the Kronecker product. It must, however, be pointed out that in [5] the authors have not developed a model based on the Kronecker product, and have merely obtained the transmit and receive covariance matrices from the empirical data themselves. Although they have reported a good match between the two, the measurement procedure involved averaging across several frequency bands in a wideband (120 MHz bandwidth) measurement, without taking into account possible correlation between the frequency bands themselves.[6] reports large errors and concludes that system modeling based on the Kronecker product model may result in a too optimistic characterization of a multi-element antenna system.

In the light of the above, the Kronecker product model is investigated in the context of the data available.

The BS and user covariance matrices are defined as,

$$\mathbf{R}_{\mathbf{H}}^{BS} = E[(\mathbf{h}_i(t)^H \mathbf{h}_i(t))^T], \qquad i = 1, \cdots, n_U \tag{3.2}$$

$$\mathbf{R}_{\mathbf{H}}^{U} = E[\mathbf{h}^k(t)(\mathbf{h}^k(t))^H], \qquad k = 1, \cdots, n_{BS} \tag{3.3}$$

where $(\cdot)^T$ is the matrix transpose. $\mathbf{h}_i(t)$ is the ith row of $\mathbf{H}(t)$, and $\mathbf{h}^k(t)$ is the kth column of $\mathbf{H}(t)$. The Kronecker product model suggests the following representation for $\mathbf{R_H}$

$$\mathbf{R_H} = \mathbf{R}_{\mathbf{H}}^{BS} \otimes \mathbf{R}_{\mathbf{H}}^{U} \tag{3.4}$$

where $\otimes$ denotes the Kronecker product, defined for two arbitrary matrices $\mathbf{A}$ and $\mathbf{B}$ as,

$$\mathbf{A} \otimes \mathbf{B} \triangleq \begin{pmatrix} \{\mathbf{A}\}_{11}\mathbf{B} & \{\mathbf{A}\}_{12}\mathbf{B} & \cdots \\ \{\mathbf{A}\}_{21}\mathbf{B} & \{\mathbf{A}\}_{22}\mathbf{B} & \cdots \\ \vdots & \vdots & \ddots \end{pmatrix} \tag{3.5}$$

This definition of the covariance matrix, adopted in [10] provides us with mathematical convenience and compact notation, but may not always return reliable results in practical cases. In the following pages, we provide the model error when applied to the data available.

The model error between the empirical and Kronecker covariance matrices is defined as [5],

$$\psi = \frac{\|\hat{\mathbf{R}}_{\mathbf{H}} - (\hat{\mathbf{R}}_{\mathbf{H}}^{BS} \otimes \hat{\mathbf{R}}_{\mathbf{H}}^{U})\|_F}{\|\hat{\mathbf{R}}_{\mathbf{H}}\|_F} \tag{3.6}$$

The tables on the following pages for the 10×10 and 4×4 data sets show the large model errors that are accrued through the use of the Kronecker product model, even when measurement data are being used. It is argued that when one averages over a large number of locations, then the Kronecker model has been known to perform better. However, the process of averaging across many locations causes a loss of information about the physical characteristics of the channel. Thus, although the *model* may perform well after such averaging, it is of no utility if it contains no information about the physical characteristics of the channel.

Table 3.1: Kronecker Product Model Errors for 11/07/00 10×10 Data

Location	Model Error(%)
1_1, 1_6, 2_1, 2_6	77.49
1_2, 2_5, 2_2, 2_5	85.00
1_3, 1_4, 2_3, 2_4	76.97
3_1, 3_6, 4_1, 4_6	80.88
3_2, 3_5, 4_2, 4_5	82.19
3_3, 3_4, 4_3, 4_4	73.80
OverallAverage	59.96

Table 3.2: Kronecker Product Model Errors for 11/08/00 10×10 Data

Location	Model Error(%)
OverallAverage	44.58

Note that averaging across all locations is not possible in Tables 3.3, 3.4, due to different transmit of receive antenna orientations for the different locations (See room layouts Fig. A.2 and Fig. 2.1)

As seen in Tables 3.1 - 3.4, the Kronecker product model produces extremely high model errors. This is perhaps explained by the fact that the calculation of the covariance itself involves one multiplication, while the calculation of the covariance matrix via the Kronecker product method (Eq.3.4) involves a multiplication for each of the transmit and receive covariance matrices, followed by an additional multiplication between the two. This obviously results in a correlation estimate that can often be a lot lower than the actual correlation, as calculated by Eq. 3.1. This motivates the need to develop a correlation model that is not separable but, in fact, takes into account parameters relevant to both the transmitter and receiver sides.

Table 3.3: Kronecker Product Model Errors for 12/21/00 10×10 Data

Location	Model Error(%)
1, 2	57.76
3, 4	57.12
5, 6	55.46
7, 8	58.27

Table 3.4: Kronecker Product Model Errors for 08/22/00 4×4 Data

Location	Model Error(%)
2, 3	79.07
4, 5	74.01
6, 7, 8	60.55

3.3 The Two-Ring Model

The channel model developed around the two-ring model is shown in Fig. 3.1. As can be seen, the channel model in the figure is for a 2×2 setup, but can be expanded to any antenna configuration without loss of generality. Scatterers are present local to the BS and user, and either ring can be enlarged arbitrarily to include the effect of additional scatterers. The rings of scatterers are assumed to be fixed at any point of time, and only the receiver is assumed to exhibit motion at a speed ν, in the direction γ. These assumptions are necessary to obtain a stationary spatio-temporal cross-correlation function. The user receives a non-line-of-sight signal from scatterer S_k around the BS and scatterer S_i around the user. Thus, the overall signal received by at the user array will be the sum of two single-bounce signals. This is different from the two-ring model proposed in [24], where only one signal is received at the user after a bounce in each ring. It is felt that this sort of propagation (double bounce) mechanism will result in very weak signals at the receiver, and may not be more significant than signals received after just one bounce in either ring. Further,

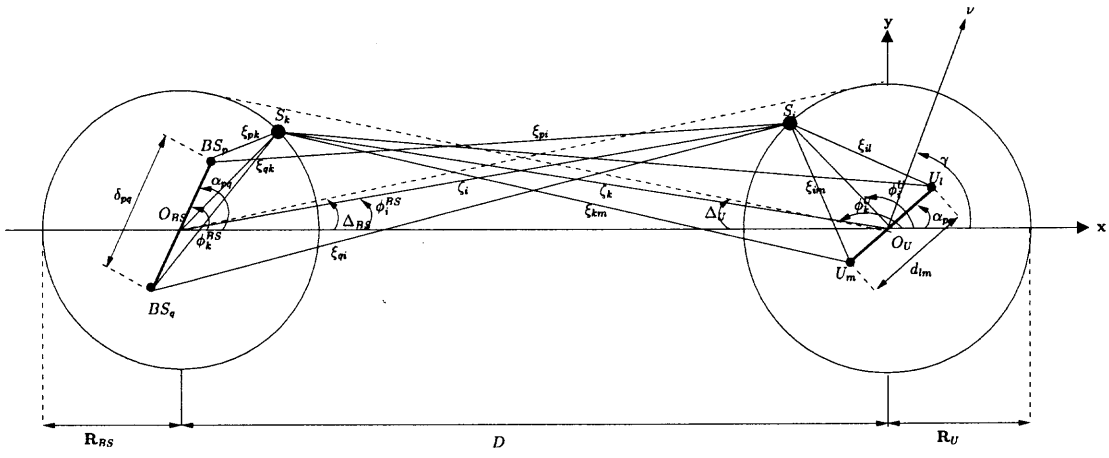

Figure 3.1: The two-ring model.

the modeling of the propagation phenomenon as a sum of two independent bounces yields advantages such as computational simplicity as compared to a product model.

The BS receives the signal through the narrow beamwidth Δ_{BS} while the user receives signals through a narrow beamwidth Δ_U. It is assumed that the waves are planar. D is the distance between the BS and user, R_U and R_{BS} are the radii of the rings of scatterers around the user and BS respectively. For the case of indoor MIMO, where the transmitter and receiver are in different rooms, it is reasonable to assume that no line-of-sight component exists. Thus the signal will suffer Rayleigh and not Ricean fading.

For the frequency non-selective communication link between the BS_p and the element U_l, let h_{lp} denote the complex low-pass equivalent time-invariant channel gain. For a unit transmit power, suppose the power transferred thorough the $BS_p - U_l$ link is Ω_{lp}, i.e., $\Omega_{lp} = E[|h_{lp}(t)|^2] \leq 1$. The plane waves emitted from the array element BS_p travel over paths with different lengths and after being scattered by scatterers local to the BS or the mobile user, impinge the array element U_l from different directions. Mathematical representation of this propagation mechanism

results in the following expressions for the diffuse components, h_{lp} and h_{mq}.

$$h_{lp}(t) = \sqrt{\Omega_{lp}} \lim_{N\to\infty} \frac{1}{\sqrt{N}} \sum_{k=1}^{N} g_k^{BS} exp\{j\psi_k^{BS} - \frac{j2\pi}{\lambda}[\xi_{pk}(\phi_k^{BS}) + \xi_{kl}(\phi_k^{BS})] + j2\pi f_D \cos(\phi_k^U - \gamma)t\} + \sqrt{\Omega_{lp}} \lim_{M\to\infty} \frac{1}{\sqrt{M}} \sum_{i=1}^{M} g_i^U exp\{j\psi_i^U - \frac{j2\pi}{\lambda}[\xi_{pi}(\phi_i^U) + \xi_{il}(\phi_i^U)] + j2\pi f_D \cos(\phi_i^U - \gamma)t\}$$

$$h_{mq}(t) = \sqrt{\Omega_{mq}} \lim_{N\to\infty} \frac{1}{\sqrt{M}} \sum_{k=1}^{N} g_k^{BS} exp\{j\psi_k^{BS} - \frac{j2\pi}{\lambda}[\xi_{qk}(\phi_k^{BS}) + \xi_{km}(\phi_k^{BS})] + j2\pi f_D \cos(\phi_k^U - \gamma)t\} + \sqrt{\Omega_{lp}} \lim_{M\to\infty} \frac{1}{\sqrt{M}} \sum_{i=1}^{M} g_i^U exp\{j\psi_i^U - \frac{j2\pi}{\lambda}[\xi_{qi}(\phi_i^U) + \xi_{im}(\phi_i^U)] + j2\pi f_D \cos(\phi_i^U - \gamma)t\} \quad (3.7)$$

N is the number of independent scatterers S_k around the the BS, g_k^{BS} represents the amplitude of the wave scattered by the kth scatterer toward the user such that $N^{-1}\sum_{k=1}^{N} E[g_k^{BS^2}] = 0.5$ as $N \to \infty$. ψ_k^{BS} denotes the phase shift introduced by the kth scatterer, ξ_{pk} and ξ_{kl} as the distances shown in Fig. 3.3, which are functions of ϕ_k^{BS}, the AOA of the wave traveling from the kth scatterer toward the user, λ is the wavelength, $j^2 = -1$, $f_D = \nu/\lambda$ is the maximum Doppler shift. The set $\{g_k^{BS}\}_{k=1}^{\infty}$ consists of independent positive random variables with finite variances, independent of $\{\psi_k^{BS}\}_{k=1}^{\infty}$. It is reasonable to assume that $\{\psi_k^{BS}\}_{k=1}^{\infty}$ are independent and identically distributed (iid) random variables with uniform distributions over $[0, 2\pi)$. This representation of h_{lp}, together with the assumption of $N^{-1}\sum_{k=1}^{\infty} E[g_k^{BS^2}] + M^{-1}\sum_{i=1}^{\infty} E[g_i^{U^2}] \to 1$ as $N, M \to \infty$, guarantees that $E[|h_{lp}(t)|)^2] = \Omega_{lp}$.

According to the statistical properties of the channel described above, the central limit theorem implies that $h_{lp}(t)$ is a low-pass non-zero mean complex

Gaussian process. Hence, the envelope $|h_{lp}|$ is a Rayleigh process. In other words, the model described represents a MIMO frequency non-selective Rayleigh fading channel.

Let us define the spatio-temporal cross-correlation between the gains of two arbitrary communication links $h_{lp}(t)$ and $h_{mq}(t)$ as,

$$\rho_{lp,mq}(\tau,t) = \frac{E[h_{lp}(t)h^*_{mq}(t+\tau)]}{\sqrt{\Omega_{lp}\Omega_{mq}}}, \tag{3.8}$$

where * is the complex conjugate. Based on the statistical properties of $\{g_k\}_{k=1}^{\infty}$, the spatio-temporal correlation between $h_{lp}(t)$ and $h_{mq}(t)$, according to Eq. (3.7), can be written as,

$$\begin{aligned}
&\rho_{lp,mq}(\tau,t) = \rho_{lp,mq}(\tau) \\
&= \lim_{N\to\infty}\frac{1}{N}\sum_{k=1}^{N} E[g_k^{BS^2}]exp\Big\{-j\frac{2\pi}{\lambda}[\xi_{pk}(\phi_k^{BS}) - \xi_{qk}(\phi_k^{BS}) + \xi_{kl}(\phi_k^{BS}) - \xi_{km}(\phi_k^{BS})] \\
&\qquad\qquad - j2\pi f_D\cos(\phi_k^U - \gamma)\tau\Big\} \\
&\quad + \lim_{M\to\infty}\frac{1}{M}\sum_{i=1}^{M} E[g_i^{U^2}]exp\Big\{-j\frac{2\pi}{\lambda}[\xi_{pi}(\phi_i^U) - \xi_{qi}(\phi_i^U) + \xi_{il}(\phi_i^U) - \xi_{im}(\phi_i^U)] \\
&\qquad\qquad - j2\pi f_D\cos(\phi_i^U - \gamma)\tau\Big\}
\end{aligned} \tag{3.9}$$

Notice that the cross-terms go to zero due to the assumed statistics of ψ_k^{BS} and ψ_i^U. For a large N and M,the small contribution of the kth and ith scatterers, out of the total Ω_{lp}, is proportional to $E[g_k^{BS^2}]/N$ and $E[g_i^{U^2}]/M$ respectively. This is equal to the infinitesimal power coming from the differential angle $d\phi^{BS}$ and $d\phi^U$ with probability $f(\phi_k^{BS})$ and $f(\phi_i^U)$, i.e $E[g_k^{BS^2}]/N = f(\phi^{BS})d\phi^{BS}$ and $E[g_i^{U^2}]/M = f(\phi^U)d\phi^U$, where $f(\phi^{BS})$ is the continuous pdf of the AOD ϕ_k^{BS} seen by the BS while $f(\phi^U)$ is the continuous pdf of the AOA ϕ_i^U seen by the user. Therefore, Eq. 3.9 can

be written in the following integral form,

$$\rho_{lp,mq}(\tau) = \int_{-\pi}^{\pi} exp\Big\{ -\frac{j2\pi}{\lambda}[\xi_{px}(x) - \xi_{qx}(x) + \xi_{xl}(x) - \xi_{mk}(x)] - j2\pi f_D \cos(v-\gamma)\tau \Big\} f(x)dx + \int_{-\pi}^{\pi} exp\Big\{ \frac{j2\pi}{\lambda}[\xi_{py}(y) - \xi_{qy}(y) + \xi_{yl}(y) - \xi_{ym}(y)] - j2\pi f_D \cos(y-\gamma)\tau \Big\} f(y)dy \quad (3.10)$$

x, y, v, w denote a functional dependence on $\phi_k^{BS}, \phi_i^U, \phi_k^U, \phi_i^{BS}$. ξ_{px} denotes the path length between the antenna element and the point on the ring of scatterers determined by ϕ_k^{BS}, and so forth.

For any given $f_U(\cdot)$ and $f_{BS}(\cdot)$, Eq. (3.10) can be calculated numerically, according to the following relations, derived based on the application of the law of cosines in appropriate triangles.

$$\begin{aligned}
\xi_{px}^2(x) &= (\delta_{pq}^2/4) + R_{BS}^2 - \delta_{pq} R_{BS} \cos(\alpha_{pq} - x) \\
\xi_{qx}^2(x) &= (\delta_{pq}^2/4) + R_{BS}^2 + \delta_{pq} R_{BS} \cos(\alpha_{pq} - x) \\
\xi_{xl}^2(x) &= (d_{lm}^2/4) + \zeta_x^2 - \zeta_x d_{lm} \cos(v - \beta_{lm}) \\
\xi_{mx}^2(x) &= (d_{lm}^2/4) + \zeta_x^2 + \zeta_x d_{lm} \cos(v - \beta_{lm}) \\
\xi_{py}^2(y) &= (\delta_{pq}^2/4) + \zeta_y^2 - \zeta_y \delta_{pq} \cos(\alpha_{pq} - w) \\
\xi_{qy}^2(y) &= (\delta_{pq}^2/4) + \zeta_y^2 + \zeta_y \delta_{pq} \cos(\alpha_{pq} - w) \\
\xi_{yl}^2(y) &= (d_{lm}^2/4) + R_U^2 - d_{lm} R_U \cos(y - \beta_{lm}) \\
\xi_{ym}^2(y) &= (d_{lm}^2/4) + R_U^2 + d_{lm} R_U \cos(y - \beta_{lm})
\end{aligned} \quad (3.11)$$

ζ_x and ζ_y are continuous versions of ζ_k and ζ_i respectively (Fig. 3.1). For any given x, v can be determined by the application of the law of sines to the triangle $O_{BS}S_kO_U$,

$$\frac{D}{\sin(v-x)} = \frac{R_{BS}}{\sin(v)} = \frac{\zeta_x}{\sin(x)} \quad (3.12)$$

Similarly, for any given y, w and ζ_y can be determined by the application of the law of sines in the triangle $O_{BS}S_iO_U$,

$$\frac{D}{\sin(y-w)} = \frac{R_U}{\sin(w)} = \frac{\zeta_y}{\sin(y)} \tag{3.13}$$

Using Eqns. (3.11), (3.12), and (3.13) in Eq. (3.10), we can compute the exact spatial correlation for any AOA and AOD distributions. A positive feature in the above methodology of expressing the correlation is that it can be written as the sum of two integrals, which can be calculated numerically. An approximation is derived in later pages, which vastly reduce the computational time by presenting a closed-form function for the correlation. Therefore, the exact correlation function can be expressed as,

$$\begin{aligned}\rho_{lp,mq}(\tau) = \int_{-\pi}^{\pi} exp\Big\{\frac{j4\pi}{\lambda}[R_{BS}\delta_{pq}\cos(\alpha_{pq}-x) + \zeta_x d_{lm}\cos(v-\beta_{lm})] \\ - j2\pi f_D\cos(v-\gamma)\tau\Big\} f(x)dx \\ + \int_{-\pi}^{\pi} exp\Big\{\frac{j4\pi}{\lambda}[\zeta_y\delta_{pq}\cos(\alpha_{pq}-v) + d_{lm}R_U\cos(y-\beta_{lm})] \\ - j2\pi f_D\cos(y-\gamma)\tau\Big\} f(y)dy\end{aligned} \tag{3.14}$$

The above expression can be evaluated numerically to give the exact correlation. Values for v, w, ζ_x and ζ_y in Eq. 3.14 may either be found by solving Eqns. 3.12, 3.13, or derived using trigonometry to give,

$$v = \pi - \tan^{-1}\left(\frac{\tan(\Delta_U\sin(x))}{1-\tan(\Delta_U\cos(x)}\right) \tag{3.15}$$

$$w = \tan^{-1}\left(\frac{\tan(\Delta_{BS}\sin(y))}{1-\tan(\Delta_B S\cos(y)}\right) \tag{3.16}$$

$$\zeta_x^2 = D^2\Big(1+\tan^2(\Delta_U)\sin^2(x) + (1-\tan(\Delta_U)\cos(x))^2\Big) \tag{3.17}$$

$$\zeta_y^2 = D^2\Big(1+\tan^2(\Delta_{BS})\sin^2(y) + (1-\tan(\Delta_{BS})\cos(y))^2\Big) \tag{3.18}$$

However, the assumption of of $D \gg (R_U, R_{BS} \gg max(\delta_{pq}, d_{lm}))$ is valid for many practical cases of interest, which also implies that Δ_U, Δ_{BS} are small, simplifies

equations drastically. Using the relations $\sqrt{1+\chi} \approx 1 + \chi/2$, $\sin(\chi) \approx \chi$,and $\cos(\chi) \approx 1$, when χ is small. To begin with, the first equation in Eq. (3.12), (3.13) yields $v = -\Delta_{BS}\sin(x)$ and $w = \Delta_U \sin(y)$. Further, Eq.(3.11) can be approximated by,

$$\begin{aligned}
\xi_{px}(x) &\approx R_{BS} - (\delta_{pq}/2)cos(\alpha_{pq} - x) \\
\xi_{qx}(x) &\approx R_{BS} + (\delta_{pq}/2)cos(\alpha_{pq} - x) \\
\xi_{xl}(x) &\approx \zeta_x - (d_{lm}/2)[cos(\beta_{lm}) - \Delta_U \sin(\beta_{lm})\sin(x)] \\
\xi_{xm}(x) &\approx \zeta_x + (d_{lm}/2)[cos(\beta_{lm}) - \Delta_U \sin(\beta_{lm})\sin(x)] \\
\xi_{py}(y) &\approx \zeta_y - (\delta_{pq}/2)[cos(\alpha_{pq} + \Delta_{BS}\sin(\alpha_{pq})\sin(y)] \\
\xi_{qy}(y) &\approx \zeta_y + (\delta_{pq}/2)[cos(\alpha_{pq} + \Delta_{BS}\sin(\alpha_{pq})\sin(y)] \\
\xi_{yl}(y) &\approx R_U - (d_{lm}/2)cos(y - \beta_l m) \\
\xi_{mx}(y) &\approx R_U + (d_{lm}/2)cos(y - \beta_l m)
\end{aligned} \tag{3.19}$$

Substitution of Eq. (3.19) into Eq. (3.14) yields,

$$\begin{aligned}
\rho_{lp,mq}(\tau) \approx \int_{-\pi}^{\pi} exp\Big\{ \frac{j2\pi}{\lambda}\big(\delta_{pq}\cos(\alpha_{pq} - x) + d_{lm}[\cos(\beta_{lm}) - \Delta_U \sin(\beta_{lm})\sin(x)]\big) \\
- j2\pi f_D \cos(v - \gamma)\tau \Big\} f(x)dx \\
+ \int_{-\pi}^{\pi} exp\Big\{ \frac{j2\pi}{\lambda}\big(d_{lm}\cos(y - \beta_{lm}) + \delta_{pq}[\cos(\alpha_{pq}) + \Delta_{BS}\sin(\alpha_{pq})\sin(y)]\big) \\
- j2\pi f_D \cos(y - \gamma)\tau \Big\} f(y)dy
\end{aligned} \tag{3.20}$$

The approximate cross-correlation defined in Eq. (3.20) holds for any AOA and AOD PDF's $f(y)$ and $f(x)$. Here the von Misses PDF is used, which is defined by,

$$f(y) = \frac{exp[\kappa_U \cos(y - \mu_U)]}{2\pi I_0(\kappa_U)}, \qquad y \in [-\pi, \pi] \tag{3.21}$$

where $I_0(\cdot)$ is the zeroth-order modified Bessel function, $\mu_U \in [-\pi, \pi)$ accounts for the mean direction of AOA seen by the user, and $\kappa_U \geq 0$ controls the width of

AOA. $\kappa_U = 0$ results in isotropic scattering, while for $\kappa_U = \infty$, the von Misses PDF becomes a Dirac delta function, concentrated at $y = \mu_U$.

To simplify the notation, we define $a = 2\pi f_D \tau$, $b_{lm} = 2\pi d_{lm}/\lambda$, and $c_{pq} = 2\pi\delta_{pq}/\lambda$. By inserting Eq. (3.21) into Eq. (3.20), and calculating the integral exactly, according to [25],eq.3.338-4, p.357,

$$\int_{-\pi}^{\pi} exp(x\sin z + y\cos z)dz = 2\pi I_0(\sqrt{x^2+y^2}) \tag{3.22}$$

we get the final approximate correlation expression,

$$\begin{aligned}
\rho_{lp,mq}(\tau) \approx{}& \frac{exp\{j[b_{lm}\cos(\beta_{lm}) - a\ cos(\gamma)]\}}{2I_0(\kappa_{BS})} \times \\
& I_0\Big(\{\kappa_{BS}^2 - a^2\Delta_U^2\sin^2\gamma - b_{lm}^2\Delta_U^2\sin^2(\beta_{lm}) - c_{pq}^2 + 2b_{lm}c_{pq}\Delta_U\sin(\alpha_{pq})\sin(\beta_{lm}) \\
& \quad + 2a\Delta_U\sin(\gamma)[c_{pq}\sin(\alpha_{pq}) - b_{lm}\Delta_U\sin\beta_{lm}] \\
& \quad - j2\kappa_{BS}[a\Delta_U\sin\mu_{BS}\sin(\gamma) + b_{lm}\Delta_U\sin(\beta_{lm})\sin(\mu_{BS}) \\
& \quad - c_{pq}\cos(\alpha_{pq} - \mu_{BS})]\}^{1/2}\Big) + \\
& \frac{exp\{j[c_{pq}\cos(\alpha_{pq})]\}}{2I_0(\kappa_U)} \times I_0\Big(\{\kappa_U^2 - a^2 - b_{lm}^2 - c_{pq}^2\Delta_{BS}^2\sin^2(\alpha_{pq}) + 2c_{pq}\Delta_{BS}\sin(\alpha_{pq}) \\
& \quad [a\sin(\gamma) - b_{lm}\sin(\beta_{lm})] + 2ab_{lm}\cos(\beta_{lm} - \gamma) \\
& \quad - j2\kappa_U[a\cos(\mu_U - \gamma) - b_{lm}\cos(\beta_{lm} - \mu_U) + \\
& \quad c_{pq}\Delta_{BS}\sin(\alpha_{pq})\sin(\mu_U)]\}^{1/2}\Big)
\end{aligned} \tag{3.23}$$

The proposed spatio-temporal correlation function, although initially derived using the assumption of small Δ's has been shown to be valid for Δ's up-to 50°. Further, this model, which includes all parameters relevant to a MIMO frequency non-selective channel, is in a compact form, suitable for both mathematical calculations and simulations. In fact, in later sections, this model is extensively used in variety of scenarios to test the properties of the derived correlation and its impact on various parameters of interest such as channel capacity and bit error rate. The authors in [6] compare a simpler form of this model with various classical correlation models

and show this model's conformity with those classical models under simplifying conditions. In the following sections, various forms of correlation are defined together with their expression obtained using Eq. (3.23), and these correlations, as obtained from the measurements, are compared with the same correlations derived using the proposed two-ring model.

3.4 Correlation Definitions

Given transmit antenna elements, p *and* q, and receive antenna elements l *and* m, the following types of correlations are defined along with an explanatory figure below:

1. Parallel Sub-Channel Correlation

$$\rho_{parallel} \triangleq E[h_{lp}h^*_{(l+n)(p+n)}] = \rho_{(l+n)(p+n)}(\tau) \qquad n = 1, 2 \ldots \min(n_T, n_R)$$

$$\begin{aligned}
\rho_{(l+n)(p+n)}(\tau) \approx{}& \frac{exp\{j[b_{l(l+n)}\cos(\beta_{l(l+n)}) - a\ cos(\gamma)]\}}{2I_0(\kappa_{BS})} \times \\
& I_0\Big(\{\kappa^2_{BS} - a^2\Delta^2_U \sin^2(\gamma) - b^2_{l(l+n)}\Delta^2_U \sin^2(\beta_{l(l+n)}) - c^2_{p(p+n)} + \\
& 2b_{l(l+n)}c_{p(p+n)}\Delta_U \sin(\alpha_{p(p+n)})\sin(\beta_{l(l+n)}) \\
& + 2a\Delta_U \sin(\gamma)[c_{p(p+n)}\sin(\alpha_{p(p+n)}) - b_{l(l+n)}\Delta_U \sin(\beta_{l(l+n)})] \\
& - j2\kappa_{BS}[a\Delta_U \sin(\mu_{BS})\sin(\gamma) + b_{l(l+n)}\Delta_U \sin(\beta_{l(l+n)})\sin(\mu_{BS}) \\
& - c_{p(p+n)}\cos(\alpha_{p(p+n)} - \mu_{BS})]\}^{1/2}\Big) + \\
& \frac{exp\{j[c_{p(p+n)}\cos(\alpha_{p(p+n)})]\}}{2I_0(\kappa_U)} \times I_0\Big(\{\kappa^2_U - a^2 - b^2_{l(l+n)} - c^2_{p(p+n)}\Delta^2_{BS}\sin^2(\alpha_{p(p+n)}) \\
& + 2c_{p(p+n)}\Delta_{BS}\sin(\alpha_{p(p+n)})[a\sin(\gamma) - b_{l(l+n)}\sin(\beta_{l(l+n)})] \\
& + 2ab_{l(l+n)}\cos(\beta_{l(l+n)} - \gamma) - j2\kappa_U[a\cos(\mu_U - \gamma) - b_{l(l+n)}\cos(\beta_{l(l+n)} - \mu_U) + \\
& c_{p(p+n)}\Delta_{BS}\sin(\alpha_{p(p+n)})\sin(\mu_U)]\}^{1/2}\Big) \qquad (3.24)
\end{aligned}$$

2. Crossing Sub-Channel Correlation

$$\rho_{crossing} \triangleq E[h_{lp}h^*_{pl}] = \rho_{lp,pl}(\tau)$$

$$\rho_{lp,pl}(\tau) \approx \frac{exp\{j[b_{lp}\cos(\beta_{lp}) - a\ cos(\gamma)]\}}{2I_0(\kappa_{BS})} \times$$
$$I_0\Big(\{\kappa_{BS}^2 - a^2\Delta_U^2\sin^2(\gamma) - b_{lp}^2\Delta_U^2\sin^2(\beta_{lp}) - c_{pl}^2 + 2b_{lp}c_{pl}\Delta_U\sin(\alpha_{pl})\sin(\beta_{lp})$$
$$+ 2a\Delta_U\sin(\gamma)[c_{pl}\sin(\alpha_{pl}) - b_{lp}\Delta_U\sin(\beta_{lp})]$$
$$- j2\kappa_{BS}[a\Delta_U\sin(\mu_{BS})\sin(\gamma) + b_{lp}\Delta_U\sin(\beta_{lp})\sin(\mu_{BS})$$
$$- c_{pl}\cos(\alpha_{pl} - \mu_{BS})]\}^{1/2}\Big) +$$
$$\frac{exp\{j[c_{pl}\cos(\alpha_{pl})]\}}{2I_0(\kappa_U)} \times I_0\Big(\{\kappa_U^2 - a^2 - b_{lp}^2 - c_{pl}^2\Delta_{BS}^2\sin^2(\alpha_{pl}) + 2c_{pl}\Delta_{BS}\sin(\alpha_{pl})$$
$$[a\sin(\gamma) - b_{lp}\sin(\beta_{lp})] + 2ab_{lp}\cos(\beta_{lp} - \gamma)$$
$$- j2\kappa_U[a\cos(\mu_U - \gamma) - b_{lp}\cos(\beta_{lp} - \mu_U) +$$
$$c_{pl}\Delta_{BS}\sin(\alpha_{pl})\sin(\mu_U)]\}^{1/2}\Big) \quad (3.25)$$

Note that $c_{pl} = -c_{lp}$

3. Common Transmit Sub-Channel Correlation

$$\rho_{common\ tx.} \triangleq E[h_{lp}h_{mp}^*] = \rho_{lp,mp}(\tau)$$

$$\rho_{lp,mp}(\tau) \approx \frac{exp\{j[b_{lp}\cos(\beta_{lp}) - a\ cos(\gamma)]\}}{2I_0(\kappa_{BS})} \times$$
$$I_0\Big(\{\kappa_{BS}^2 - a^2\Delta_U^2\sin^2(\gamma) - b_{lp}^2\Delta_U^2\sin^2(\beta_{lp})$$
$$- 2a\Delta_U\sin(\gamma)b_{lm}\Delta_U\sin(\beta_{lm})$$
$$- j2\kappa_{BS}[a\Delta_U\sin(\mu_{BS})\sin(\gamma) + b_{lm}\Delta_U\sin(\beta_{lm})\sin(\mu_{BS})]\}^{1/2}\Big) +$$
$$\frac{1}{2I_0(\kappa_U)} \times I_0\Big(\{\kappa_U^2 - a^2 - b_{lm}^2 + 2ab_{lm}\cos(\beta_{lm} - \gamma)$$
$$- j2\kappa_U[a\cos(\mu_U - \gamma) - b_{lm}\cos(\beta_{lm} - \mu_U)]\}^{1/2}\Big) \quad (3.26)$$

4. Common Receive Sub-Channel Correlation

$$\rho_{common\ rx.} \triangleq E[h_{lp}h_{lq}^*] = \rho_{lp,lq}(\tau)$$

$$\rho_{lp,lq}(\tau) \approx \frac{exp\{-ja\ cos(\gamma)]\}}{2I_0(\kappa_{BS})} \times$$
$$I_0\Big(\{\kappa_{BS}^2 - a^2\Delta_U^2 \sin^2(\gamma) - c_{pq}^2 + 2a\Delta_U \sin(\gamma)[c_{pq}\sin(\alpha_{pq})]$$
$$- j2\kappa_{BS}[a\Delta_U \sin(\mu_{BS})\sin(\gamma) - c_{pq}\cos(\alpha_{pq} - \mu_{BS})]\}^{1/2}\Big) +$$
$$\frac{exp\{j[c_{pq}\cos(\alpha_{pq})]\}}{2I_0(\kappa_U)} \times I_0\Big(\{\kappa_U^2 - a^2 - c_{pq}^2\Delta_{BS}^2 \sin^2(\alpha_{pq}) + 2c_{pq}\Delta_{BS}\sin(\alpha_{pq})[a\sin(\gamma)]$$
$$- j2\kappa_U[a\cos(\mu_U - \gamma) + c_{pq}\Delta_{BS}\sin(\alpha_{pq})\sin(\mu_U)]\}^{1/2}\Big) \quad (3.27)$$

Note that $|\rho_{parallel}|$, $|\rho_{crossing}|$, $|\rho_{common\ tx}|$ and $|\rho_{common\ rx}|$ as obtained by Equations 3.24, 3.25, 3.26 and 3.27 are fit to the empirical parallel, common transmit or common receive correlations. The empirical correlations are estimated in MATLAB as shown below.

```
c1=(xcov(tx11,tx22,0,'biased')/sqrt(xcov(tx11,tx11,0,'biased')
                                    *xcov(tx22,tx22,0,'biased')));
```

where tx11 and tx22 are 1×124 vectors of a channel coefficient. Note that following this method of empirical correlation estimation guarantees that the correlations are obtained from zero-mean unit-variance channel coefficents.

3.5 Results

In order to compare the correlation obtained using the two-ring model with the measurement data, the optimum values for κ_U, κ_{BS}, Δ_U, Δ_{BS}, μ_U, and μ_{BS} need to be determined. This has been done by conducting a parameter estimation using a simple numerical search that minimizes the error over a large set of possible values. For each possible set of parameter values, correlations are calculated for various antenna spacings, and matched using the least squares error criterion to the each one of the measured parallel, common-transmit and common-receive sub-channel correlations separately. The three sets of optimum parameters are then averaged

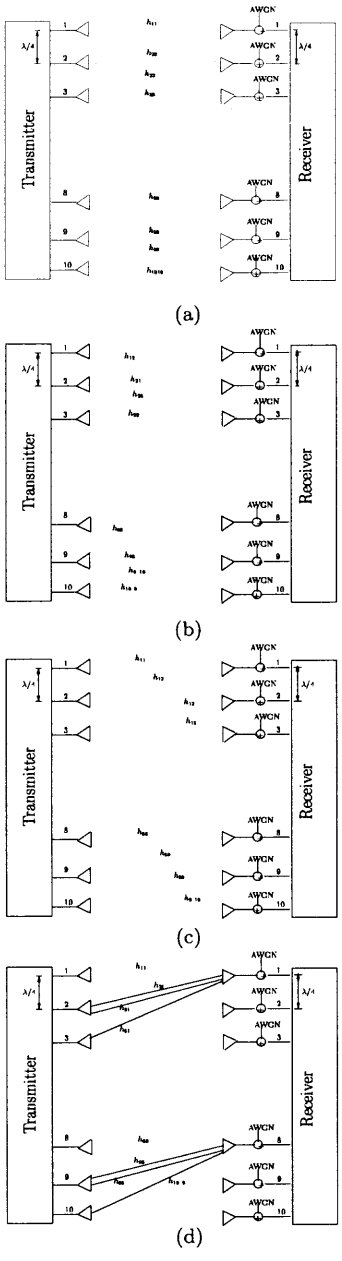

Figure 3.2: Various types of correlation in a MIMO Channel: a) parallel, b) crossing, c) common-transmit, d) common-receive correlations.

to give the final parameter set for that particular measurement setting. It should be noted that while averaging in order to obtain the Δ's, one only need average two parameters, since for the common-transmit and common-receive correlations, either one of the two Δ's does not appear in the approximate correlation expression Eq. (3.23).

When performing correlation calculations for the 4×4 data, it is assumed that $\kappa_{BS} = 1$ and $\mu_{BS} = 87°$. This is a reasonable assumption because patch antennas were used during the 4×4 measurements, whose antenna pattern closely matches the von Misses distribution with $\kappa_{BS} = 1$. Therefore, no matter what the actual distribution of the scatterers around the BS is, only the scatterers that are within the antenna pattern of the BS are illuminated. The fixed value for μ_{BS} was inferred from the room layouts. Thus, instead of estimating six parameters, only four parameters need estimation.

When performing correlation calculations for the 10×10 data, it is assumed that $\kappa_{BS} = 0$ and $\mu_{BS} = 0°$. This conforms to a uniform scatterer distribution around the BS, which is a reasonable assumption in the light of the fact that monopole antennas were used during the 10×10 measurements. Again, only four parameters need estimation, as opposed to six as given by Eq. (3.23).

The optimum parameters obtained for the 10×10 and 4×4 data are now presented in Tables 3.5- 3.19. Note that the parameters in Table 3.11 are not the average of the entries of Tables 3.5-3.10, but have been estimated using data collected over all locations, on 11/07/00.

Table 3.5: Optimum Parameters for 10×10 Data Collected on 11/07/00, Locations 1-1,1-6,2-1,2-6, $\alpha = 172°$, $\beta = 80°$

Parameter	Parallel	Common Transmit	Common Receive	Average
Δ_U	51.6o	57.3°	–	54.4°
Δ_{BS}	57.3°	–	57.3°	57.3°
κ_U	1.8	2.4	0.4	1.53
κ_{BS}	0	0	0	0
μ_U	343.8°	343.8°	286.5°	324.7°
μ_{BS}	0°	0°	0°	0°

Table 3.6: Optimum Parameters for 10×10 Data Collected on 11/07/00, Locations 1-2,1-5,2-1,2-5, $\alpha = 173°$, $\beta = 79°$

Parameter	Parallel	Common Transmit	Common Receive	Average
Δ_U	57.3°	57.3°	–	57.3°
Δ_{BS}	57.3°	–	57.3°	57.3°
κ_U	1.8	0.6	0.2	0.86
κ_{BS}	0	0	0	0
μ_U	343.8°	229.2°	286.5°	286.5°
μ_{BS}	0°	0°	0°	0°

Table 3.7: Optimum Parameters for 10×10 Data Collected on 11/07/00, Locations 1-3,1-4,2-3,2-4, $\alpha = 174°$, $\beta = 83°$

Parameter	Parallel	Common Transmit	Common Receive	Average
Δ_U	34.4°	57.3°	–	45.85°
Δ_{BS}	57.3°	–	57.3°	57.3°
κ_U	2.2	2.6	0.2	1.67
κ_{BS}	0	0	0	0
μ_U	343.8°	343.8°	286.5°	324.7°
μ_{BS}	0°	0°	0°	0°

Table 3.8: Optimum Parameters for 10×10 Data Collected on 11/07/00, Locations 3-1,3-6,4-1,4-6, $\alpha = 164°$, $\beta = 70°$

Parameter	Parallel	Common Transmit	Common Receive	Average
Δ_U	17.18°	57.3°	–	37.24°
Δ_{BS}	57.3°	–	57.3°	57.3°
κ_U	2.2	1.8	0.2	1.4
κ_{BS}	0	0	0	0
μ_U	171.9°	171.9°	286.5°	210.1°
μ_{BS}	0°	0°	0°	0°

Table 3.9: Optimum Parameters for 10×10 Data Collected on 11/07/00, Locations 3-2,3-5,4-2,4-5, $\alpha = 169°$, $\beta = 75°$

Parameter	Parallel	Common Transmit	Common Receive	Average
Δ_U	57.3°	51.6°	–	54.45°
Δ_{BS}	57.3°	–	57.3°	57.3°
κ_U	1.4	2.4	0.2	1.33
κ_{BS}	0	0	0	0
μ_U	343.8°	171.9°	286.5°	267.4°
μ_{BS}	0°	0°	0°	0°

Table 3.10: Optimum Parameters for 10×10 Data Collected on 11/07/00, Locations 3-3,3-4,4-3,4-4, $\alpha = 168°$, $\beta = 75°$

Parameter	Parallel	Common Transmit	Common Receive	Average
Δ_U	57.3°	51.6°	–	54.45°
Δ_{BS}	57.3°	–	57.3°	57.3°
κ_U	1.6	2.4	0.2	1.4
κ_{BS}	0	0	0	0
μ_U	171.9°	171.9°	286.5°	210.1°
μ_{BS}	0°	0°	0°	0°

Table 3.11: Optimum Parameters for 10×10 Data Collected on 11/07/00, Average Over All locations, $\alpha = 171°$, $\beta = 78°$

Parameter	Parallel	Common Transmit	Common Receive	Average
Δ_U	51.6°	57.3°	–	54.45°
Δ_{BS}	57.3°	–	57.3°	57.3°
κ_U	1.8	2.2	0.2	1.4
κ_{BS}	0	0	0	0
μ_U	343.8°	343.8°	286.5°	324.7°
μ_{BS}	0°	0°	0°	0°

Table 3.12: Optimum Parameters for 10 × 10 Data Collected on 11/08/00, α = 170°, β = 78°

Parameter	Parallel	Common Transmit	Common Receive	Average
Δ_U	40.1°	57.3°	–	48.7°
Δ_{BS}	57.3°	–	57.3°	57.3°
κ_U	2	1.6	0.4	1.33
κ_{BS}	0	0	0	0
μ_U	171.9°	343.8°	286.5°	267.4°
μ_{BS}	0°	0°	0°	0°

Table 3.13: Optimum Parameters for 10×10 Data Collected on 12/21/00, Locations 1,2, α = 173°, β = 83°

Parameter	Parallel	Common Transmit	Common Receive	Average
Δ_U	45.83°	40.1°	–	43°
Δ_{BS}	57.3°	–	57.3°	57.3°
κ_U	1.8	2.2	0.4	1.5
κ_{BS}	0	0	0	0
μ_U	0°	230°	286.5°	172°
μ_{BS}	0°	0°	0°	0°

Table 3.14: Optimum Parameters for 10×10 Data Collected on 12/21/00, Locations 3,4, α = 175°, β = 87°

Parameter	Parallel	Common Transmit	Common Receive	Average
Δ_U	45.83°	40.1°	–	43°
Δ_{BS}	57.3°	–	57.3°	57.3°
κ_U	1.2	1.6	0.6	1.6
κ_{BS}	0	0	0	0
μ_U	343.8°	286.5°	286.5°	305.6°
μ_{BS}	0°	0°	0°	0°

Table 3.15: Optimum Parameters for 10×10 Data Collected on 12/21/00, Locations 5,6, α = 81°, β = 83°

Parameter	Parallel	Common Transmit	Common Receive	Average
Δ_U	0°	23°	–	11.5°
Δ_{BS}	51.3°	–	40.1°	37.24°
κ_U	2	1.4	2.8	1.13
κ_{BS}	0	0	0	0
μ_U	171.9°	57.3°	0°	76.3°
μ_{BS}	0°	0°	0°	0°

Table 3.16: Optimum Parameters for 10×10 Data Collected on 12/21/00, Locations 7,8, $\alpha = 79°$, $\beta = 87°$

Parameter	Parallel	Common Transmit	Common Receive	Average
Δ_U	0°	57.3°	–	28.65°
Δ_{BS}	51.6°	–	45.84°	32.5°
κ_U	0.4	1	2	1.6
κ_{BS}	0	0	0	0
μ_U	114.6°	57.3°	343.8°	171.9°
μ_{BS}	0°	0°	0°	0°

Table 3.17: Optimum Parameters for 4 × 4 Data Collected on 08/22/00, Locations 2,3, $\alpha = 167°$, $\beta = 168°$

Parameter	Parallel	Common Transmit	Common Receive	Average
Δ_U	57.3°	57.3°	–	57.3°
Δ_{BS}	51.6°	–	57.3°	54.45°
κ_U	4.2	5	0.2	3.1
κ_{BS}	1	1	1	1
μ_U	57.3°	57.3°	286.5o	133.7°
μ_{BS}	87°	87°	87°	87°

Table 3.18: Optimum Parameters for 4 × 4 Data Collected on 08/22/00, Locations 4,5, $\alpha = 173°$, $\beta = 83°$

Parameter	Parallel	Common Transmit	Common Receive	Average
Δ_U	0°	45.84°	–	22.92°
Δ_{BS}	0°	–	57.3°	28.65°
κ_U	5	5	1	3.66
κ_{BS}	1	1	1	1
μ_U	114.5°	343.8°	286.5o	248.3°
μ_{BS}	87°	87°	87°	87°

Table 3.19: Optimum Parameters for 4 × 4 Data Collected on 08/22/00, Locations 6,7,8, $\alpha = 177°$, $\beta 177°$

Parameter	Parallel	Common Transmit	Common Receive	Average
Δ_U	0°	0°	–	0°
Δ_{BS}	57.3°	–	57.3°	57.3°
κ_U	5	5	5	5
κ_{BS}	1	1	1	1
μ_U	57.3°	286.5°	286.5o	210.1°
μ_{BS}	87°	87°	87°	87°

On the following pages, one plot each from various 10×10 locations are presented in Figs. 3.3- 3.5, followed by one 4×4 correlation plot in Fig. 3.6.

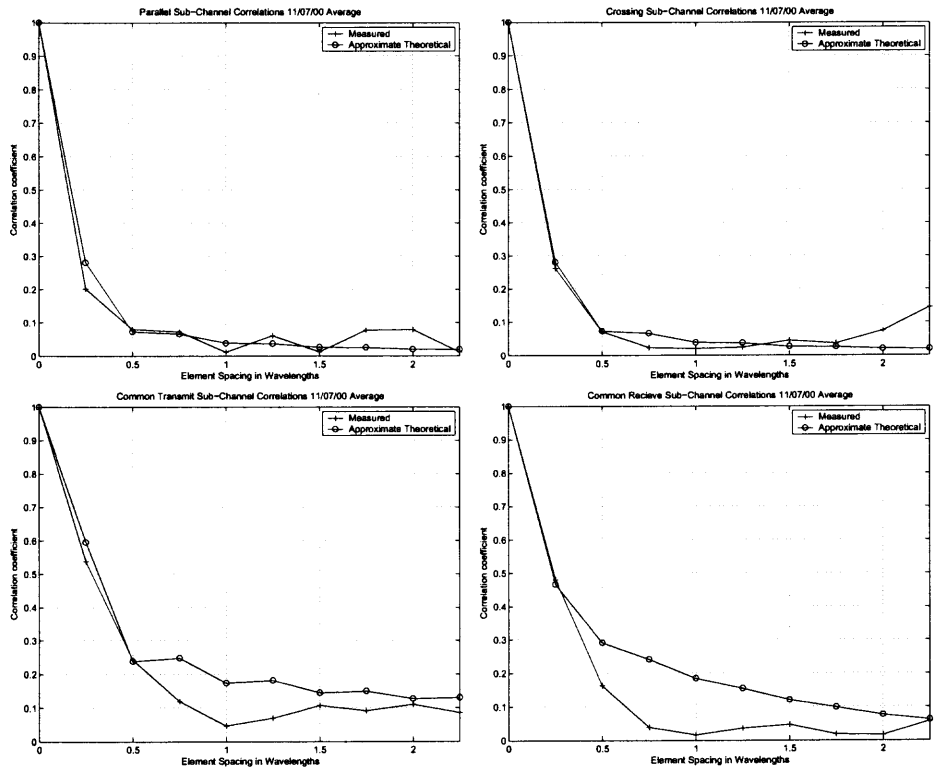

Figure 3.3: Correlation plots for 10×10 data collected on 11/07/00, average over all locations.

Table 3.20: Parameters Taken from the Last Column of Table 3.11

Δ_U	Δ_{BS}	κ_U	κ_{BS}	μ_U	μ_{BS}
54.45°	57.3°	1.4	0	324.7°	0°

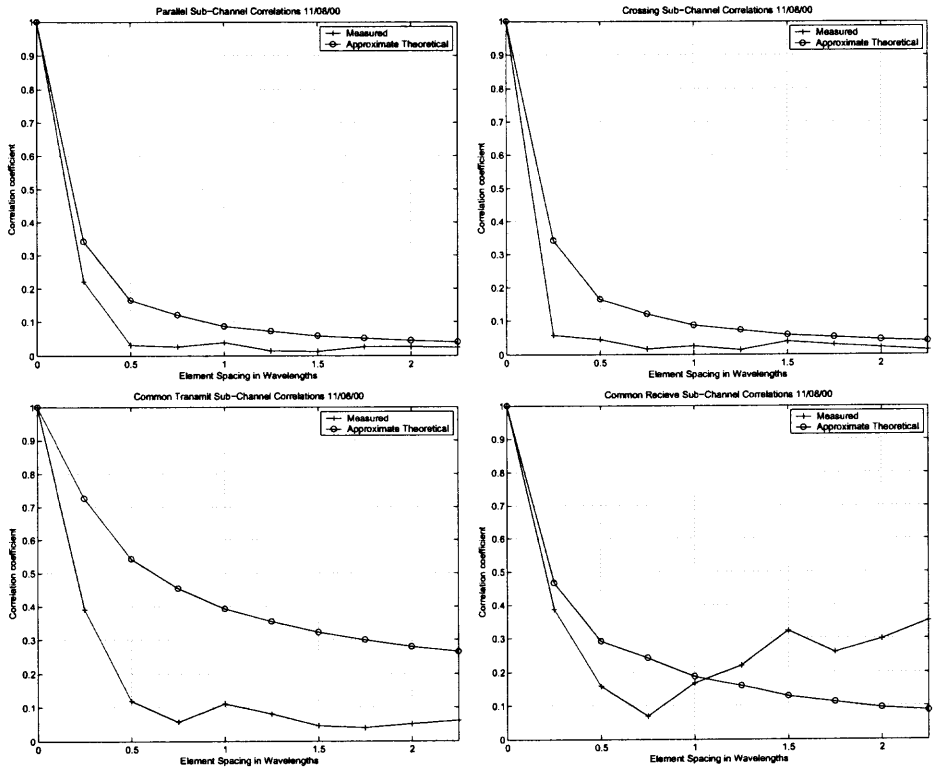

Figure 3.4: Correlation plots for 10×10 data collected on 11/08/00.

Table 3.21: Parameters Taken from the Last Column of Table 3.12

Δ_U	Δ_{BS}	κ_U	κ_{BS}	μ_U	μ_{BS}
48.7°	57.3°	1.33	0	267.4°	0°

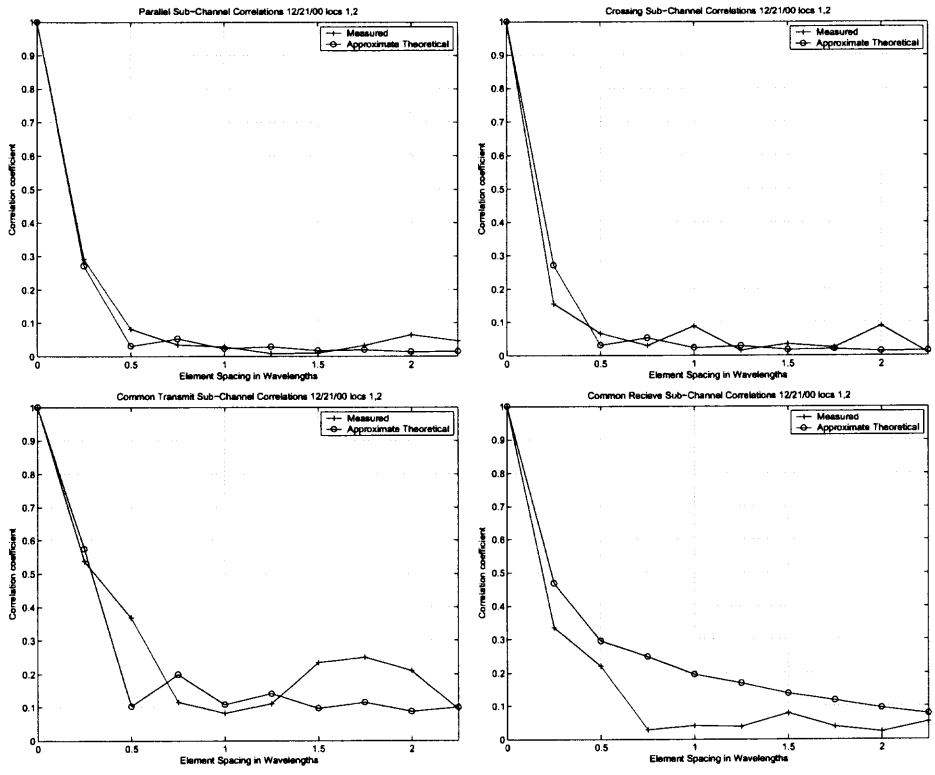

Figure 3.5: Correlation plots for 10×10 data collected on 12/21/00, locations 1,2.

Table 3.22: Parameters Taken from the Last Column of Table 3.13

Δ_U	Δ_{BS}	κ_U	κ_{BS}	μ_U	μ_{BS}
43°	57.3°	1.5	0	172°	0°

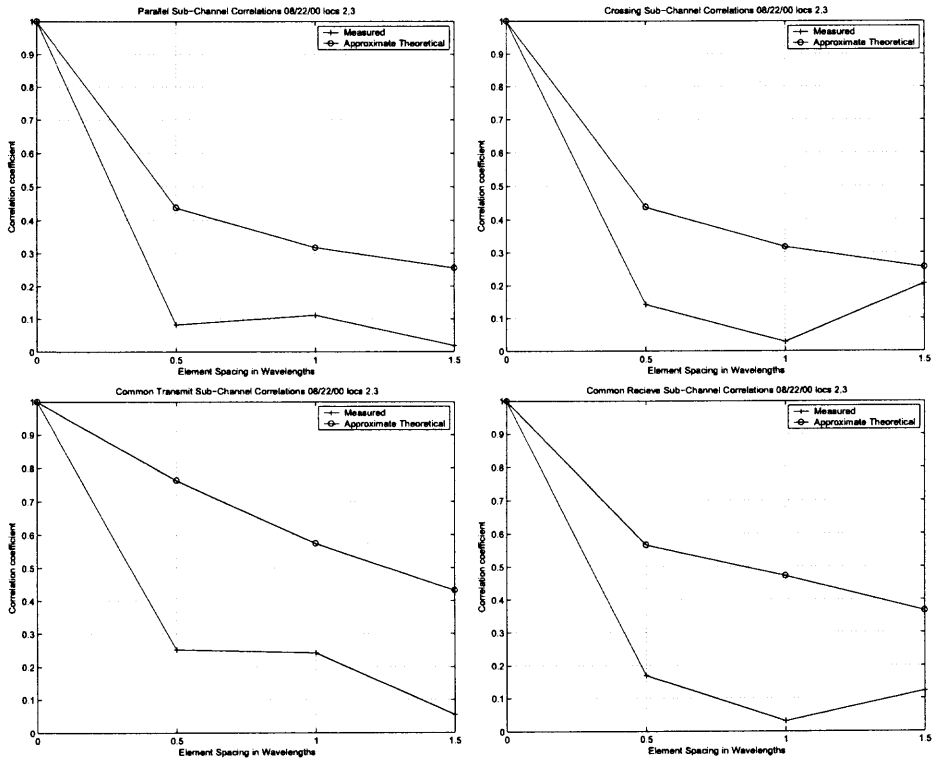

Figure 3.6: Correlation plots for 4×4 data collected on 08/22/00, locations 2,3.

Table 3.23: Parameters Taken from the Last Column of Table 3.14

Δ_U	Δ_{BS}	κ_U	κ_{BS}	μ_U	μ_{BS}
57.3°	54.45°	3.1	1	133.7°	87°

3.6 Interpretation of Parameters in Terms of Room Layout

Owing to the nature of measurement campaigns and the results obtained therein, it must be admitted that making conclusive judgements based on the results of modeling is not an easy task. Any judgements made from comparison of the parameters returned by the numerical searches with the room layouts can be a rule-of-thumb at best. Yet, it is interesting to note several regularities in this approach. Upon comparison of the values of the Δ's (Table. 3.17) with the room layout for the 4×4 data (Fig. 2.1), one sees that as the location of the receiver moves from $1, 2$ to $4, 5$, the values for the Δ's roughly halve. This could be explained by the fact that when the receiver is close to the lower wall, as in locations $1, 2$, the upper walls, which could possibly determine Δ is approximately twice as far away as it is when the receiver is moved to locations $4, 5$. Further, when the receiver is moved close to the upper wall, as in locations $6, 7, 8$, the values of Δ again drop to approximately half that in locations $4, 5$. As for the κ's, the relatively high values seem to reflect the use of directional patch antennas. Also, for the locations $4, 5, 6, 7, 8$, the value of μ_U seems to roughly point in the direction of the transmitter.

A similar pattern in the Δ's can be found for the 10×10 data collected in the same rooms as the 4×4 data. The values for the Δ's (Tables 3.18,3.19,3.5) for locations $\{1\text{–}1, 1\text{–}6, 2\text{–}1, 2\text{–}6\}$, $\{1\text{–}2, 1\text{–}5, 2\text{–}1, 2\text{–}5\}$, $\{1\text{–}3, 1\text{–}4, 2\text{–}4, 2\text{–}4\}$ remain fairly steady. However, for locations $\{3\text{–}1, 3\text{–}6, 4\text{–}1, 4\text{–}6\}$, $\{3\text{–}2, 3\text{–}5, 4\text{–}2, 4\text{–}5\}$, $\{3\text{–}3, 3\text{–}4, 4\text{–}3, 4\text{–}4\}$, where the transmitter moves up a little, the value for Δ_U drops by about $20°$. The small values for κ's seem to reflect the use of isotropic monopole antennas. Also, for the last set of locations, the value of μ_U roughly points in the direction of the transmitter.

CHAPTER 4

EFFECT OF CORRELATION ON CHANNEL CAPACITY

The main motivation behind the development of MIMO systems was the need for higher capacities and increased reliability in communications. The capacity increases reported in [1] were for uncorrelated (iid) channels and the effect of correlation on MIMO channel capacity was first studied in [10]. The authors in [10] first develop a model for the fading correlation (the correlation between the sub-channels of a MIMO channel matrix), and then study the effect of this fading correlation on channel capacity. They then proceeded to study the effect of angle spreads on capacity, and report that fading correlation does indeed reduce attainable capacity. Their work was further extended by [6], where the effect of non-isotropic scattering on channel capacity was studied using a newly developed correlation model. [23] compared the effectiveness of various correlation models in capturing the reduction of capacity and has compared these models with measurements. It must be pointed out that the capacity calculations made in [23] made use of the water-filling principle which assumes that the transmitter as well as the receiver has perfect knowledge of the channel and can allocate power to various antennas based on this *a priori* knowledge.

This part of the thesis follows a path similar to the one taken by [23], but assumes that the transmitter does not have any channel knowledge, and hence, cannot implement any power allocation scheme. Further, a comparison is made between the capacity curves predicted by the two-ring model developed in this thesis with another two-ring model [24], which makes use of the Kronecker product model. It is shown that the Kronecker product model exhibits a performance inferior to the model developed in this thesis, a result that once again throws doubt on the validity of the separability argument widely found in literature.

4.1 MIMO Channel Capacity

Suppose the underlying frequency non-selective fading channel is such that the symbol duration is much smaller than the channel coherence time, $1/f_D$. Hence, the channel matrix $\mathbf{H}(t)$ can be regarded as a random constant matrix over a long data block. It is also assumed that $\mathbf{H}(t)$ is known at the user but not the BS. If the total finite transmitted BS power, $P_{BS_{total}}$, is allocated uniformly to all the n_{BS} antennas of the BS array , then the capacity of the MIMO channel, in bits/s/Hz, is given by [1][2],

$$C/W = \log_2 \left(det \left(\mathbf{I}_{n_U} + \frac{P_{BS_{total}}}{n_{BS} P_{noise}} \mathbf{H}\mathbf{H}^H \right) \right) \tag{4.1}$$

where $det(\cdot)$ is the determinant. Note that the capacity in Eq. (4.1) is a random variable whose distribution depends on the distribution of the random complex matrix $\mathbf{H}\mathbf{H}^H$. If ρ is used to denote the SNR $P_{BS_{total}}/P_{noise}$, then Eq. (4.1) can be expressed as,

$$C/W = \log_2 \left(det \left(\mathbf{I}_{n_U} + \frac{\rho}{n_{BS}} \mathbf{H}\mathbf{H}^H \right) \right) \tag{4.2}$$

In literature, the value of ρ is usually assumed to take any value between 10 dB and 20 dB and is kept constant for all capacity calculations. This way, the effect of ρ only appears as a scaling factor for all curves. Obviously, higher values for ρ mean higher capacities. For the measurement data available, ρ was found to be close to 30 dB. For consistency with other capacity curves widely found in literature, we chose $\rho = 20\ dB$

While studying the effect of correlation on capacity, it is important to be able to find an expression for the channel capacity , which directly reflects the covariance matrix $\mathbf{R_H}$. This can be accomplished by finding the Cholesky factor of the channel covariance matrix $\mathbf{R_H}$, such that,

$$\mathbf{R_H} = \mathbf{R_H^{1/2}} (\mathbf{R_H^{1/2}})^H \tag{4.3}$$

A colored channel matrix $\mathbf{H}$ can then be obtained from an iid channel matrix $\mathbf{H}_{iid}$ as,

$$vec(\mathbf{H}) = \mathbf{R}_{\mathbf{H}}^{1/2} vec(\mathbf{H}_{iid}) \tag{4.4}$$

Eq. (4.4) when used in Eq. (4.2) allows the study of the effect of correlation on channel capacity. In this study, the correlation matrix used for coloring is either estimated directly from measured $\mathbf{H}$ matrices, according to Eq. (3.1), or is the Kronecker product of estimated transmit and receive correlation matrices, following Eq. (3.4), or is constructed based on Eq. (3.23), the new two-ring model, or based on the one-ring Kronecker model of [24]. In Figs. 4.2 - 4.5, the associated capacity curves are labelled as 'Empirical correlation matrix', 'Empirical Kronecker correlation matrix', 'Two-ring model', and 'One-ring Kronecker model' respectively. The correlation expression proposed in [24] is reproduced below for completeness sake using the notation of this thesis,

$$\rho_{mp,nq}(\tau) = \rho_{pq}^{BS} \cdot \rho_{mn}^{U}(\tau) \tag{4.5}$$

where,

$$\rho_{pq}^{BS} \approx \frac{1}{I_0(\kappa_{BS})} \times I_0\Big\{[\kappa_{BS}^2 - c_{pq}^2 + 2j\kappa_{BS}c_{pq}\cos(\alpha_{pq} - \mu_{BS})]^{1/2}\Big\} \tag{4.6}$$

and,

$$\rho_{mn}^{U}(\tau) \approx \frac{1}{I_0(\kappa_U)} \times I_0\Big\{[\kappa_U^2 - a^2 - b_{lm}^2 + 2ab_{lm}\cos(\beta_{lm} - \gamma) + 2j\kappa_U b_{lm}\cos(\beta_{lm} - \mu_U) - 2ja\kappa_U\cos(\gamma - \mu_U)]^{1/2}\Big\} \tag{4.7}$$

The notations for the BS and user antenna elements are somewhat different from that proposed in this thesis and the reader is referred to [24] for further details.

Fig.4.1 shows the methodology followed in order to study the effect of correlation on channel capacity

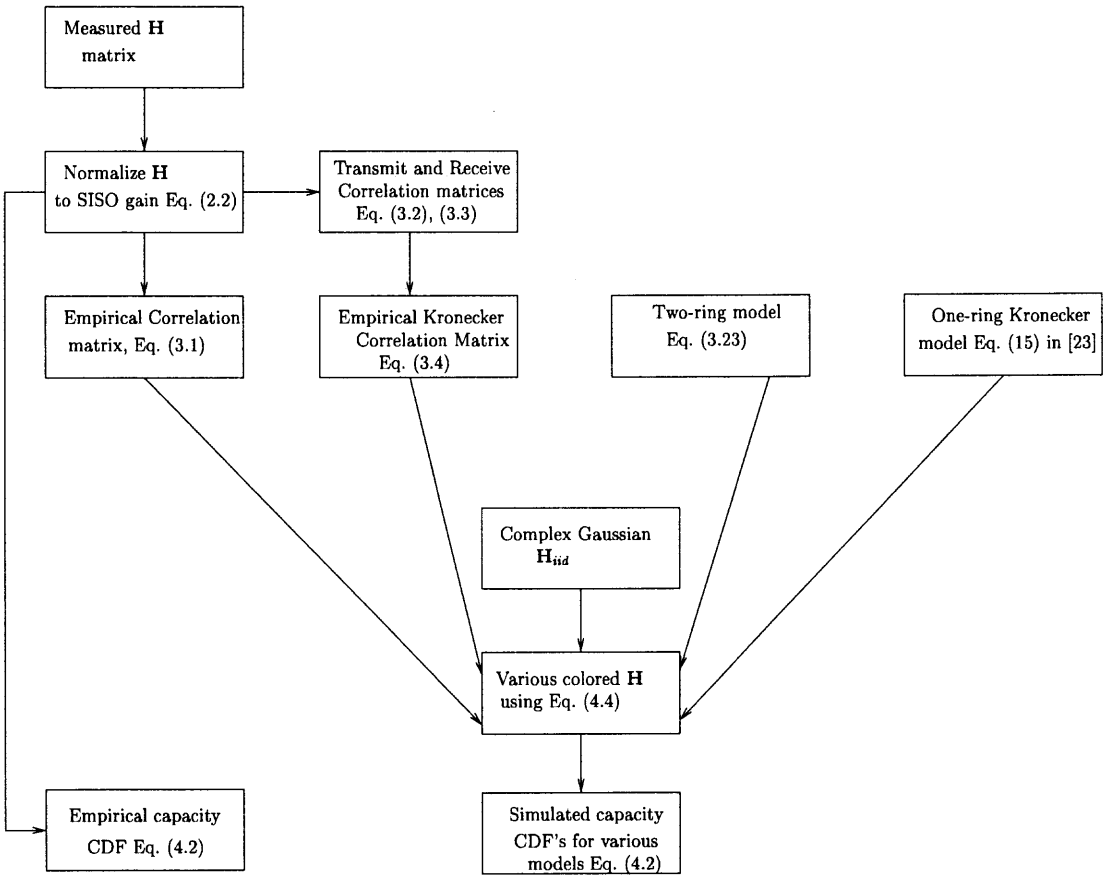

Figure 4.1: Methodology followed in capacity calculations

4.2 Results

Using the methods outlined in the Fig. 4.1, capacity plots are calculated for the various 10×10 and 4×4 correlations. The number of Monte Carlo simulations concucted in order to obtain the capacity CDF curve is equal to the total number of emprical $\mathbf{H}$ available, given on p. 13. For example, the 10×10 data collected on 11/07/00 had 7184 $\mathbf{H}$ matrices.

The remaining plots may be found in Appendix C. The transmit and receive correlation matrices for the one-ring Kronecker model may be found in Appendix E.

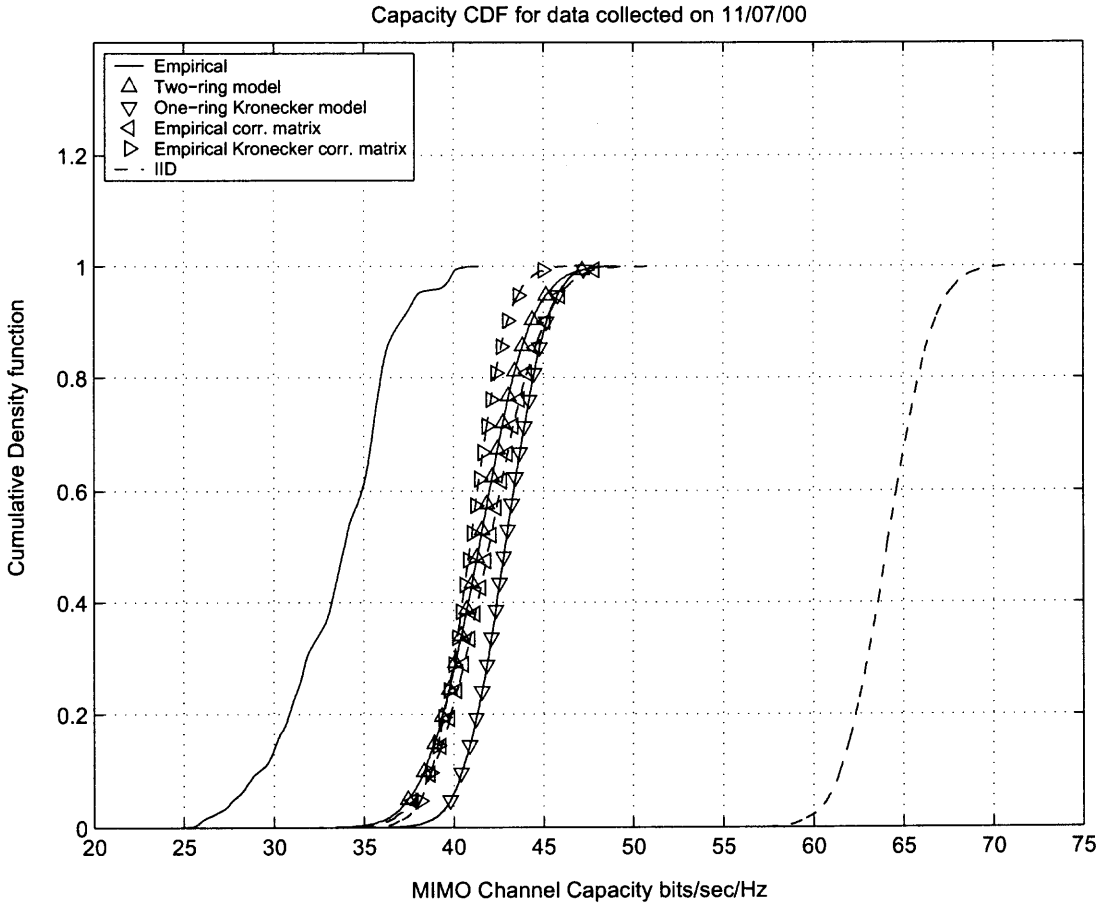

Figure 4.2: Capacity CDF for 10×10 data collected on 11/07/00, average over all locations.

Model	Δ_U	Δ_{BS}	κ_U	κ_{BS}	μ_U	μ_{BS}
Two-ring (Table 3.11)	54.45°	57.3°	1.4	0	324.7°	0°
One-ring Kronecker	–	–	1.67	0	222.5°	0°

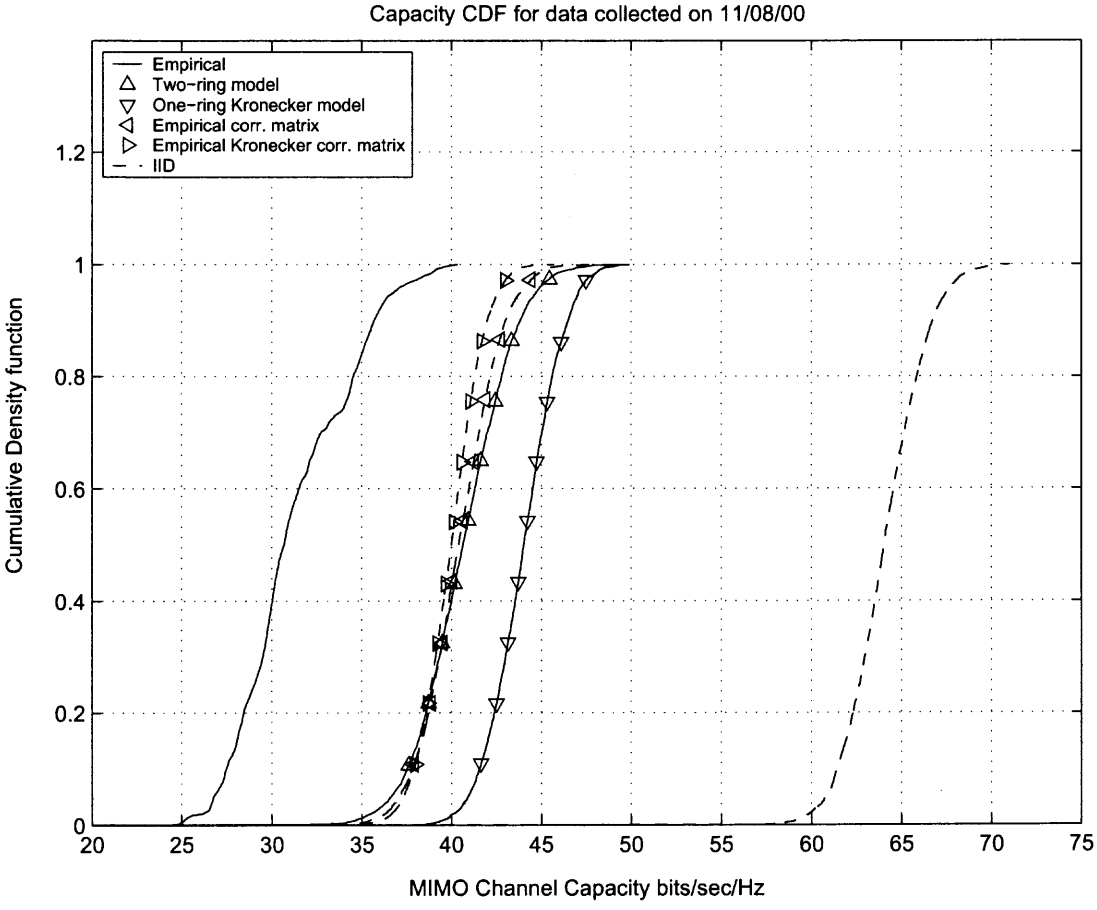

Figure 4.3: Capacity CDF for 10×10 data collected on 11/08/00.

Model	Δ_U	Δ_{BS}	κ_U	κ_{BS}	μ_U	μ_{BS}
Two-ring (Table 3.12)	48.7°	57.3°	1.33	0	267.4°	0°
One-ring Kronecker	–	–	0	0	226.3°	0°

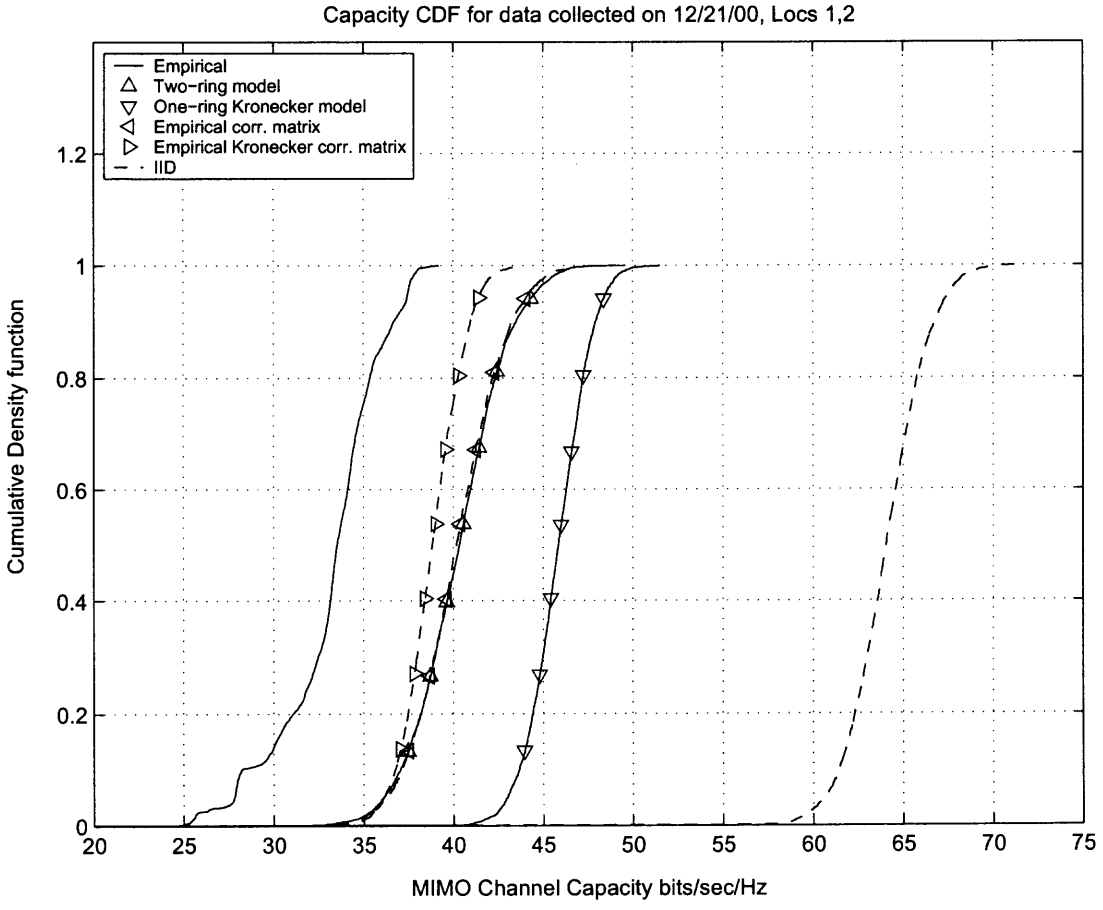

Figure 4.4: Capacity CDF for 10×10 data collected on 12/21/00, locations 1,2.

Model	Δ_U	Δ_{BS}	κ_U	κ_{BS}	μ_U	μ_{BS}
Two-ring (Table 3.13)	43°	57.3°	1.5	0	172°	0°
One-ring Kronecker	–	–	1.33	0	177.6°	0°

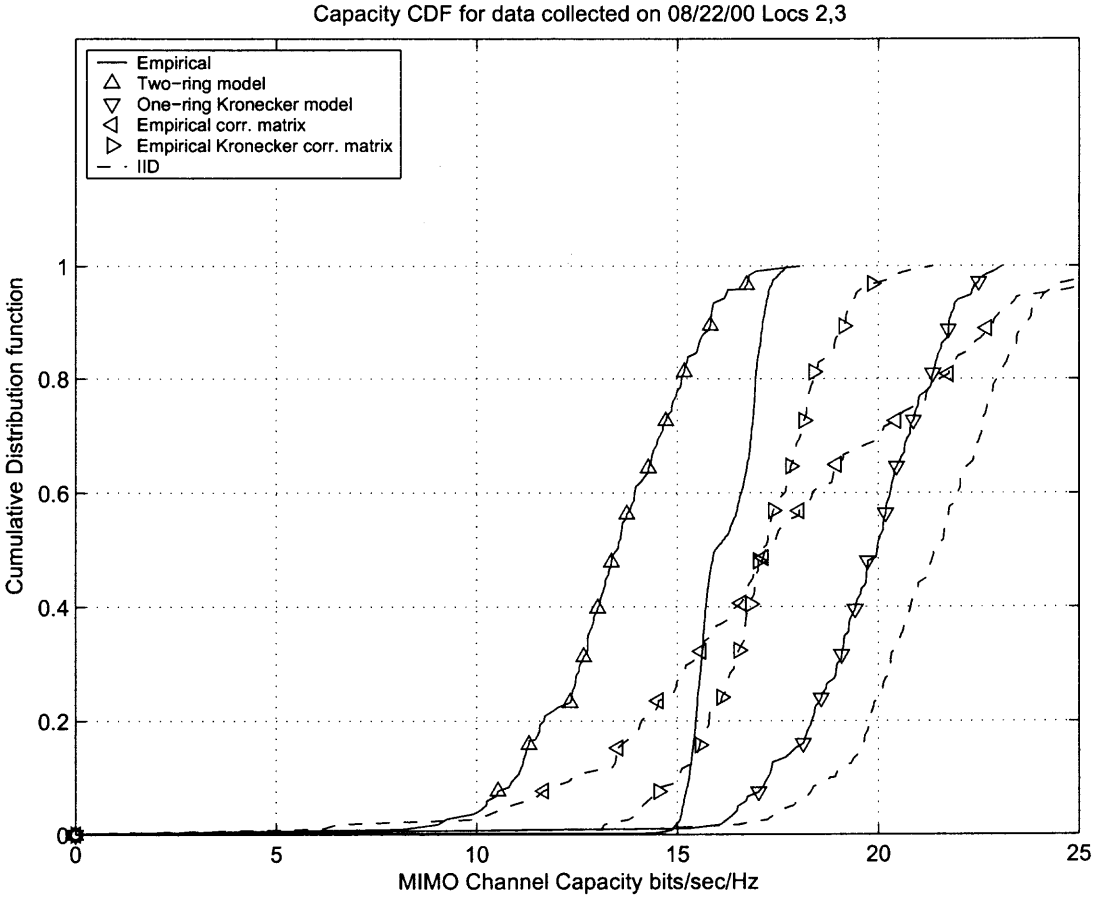

Figure 4.5: Capacity CDF for 4×4 data collected on 08/22/00, locations 2,3.

Model	Δ_U	Δ_{BS}	κ_U	κ_{BS}	μ_U	μ_{BS}
Two-ring (Table 3.17)	57.3°	54.45°	3.1	1	133.7°	87°
One-ring Kronecker	–	–	2.1	1	39.2°	87°

The parameters of the one-ring Kronecker model are estimated in exactly the same way as was done for the two-ring model, i.e least-squares fitting of $|\rho_{parallel}|$, $|\rho_{common\ tx}|$ and $|\rho_{common\ rx}|$ to the empirical correlation and then averaging over three sets of parameters.

As can seen be seen Figs. 4.2, 4.3 and 4.4, the two-ring model proposed in this thesis always performs better than the one-ring Kronecker product model in terms of the proximity to the capacity curve obtained from the empirical correlation matrix. It should also be noted that the capacity CDF obtained from the empirical Kronecker correlation matrix is very close to that obtained from the empirical correlation matrix. This, however, is to be expected, since both correlation matrices are obtained directly from the measurements. Note also that all curves are quite distant from the measured capacity CDF curve. However, the curves obtained from the measurements may not always available prior to system design, and those obtained through modeling are the best that can be obtained. In other words, the capacity CDF predicted by the empirical correlation matrix is the best that can be obtained. Hence, in this respect, the capacity CDF curve predicted by the two-ring model performs the best. One explanation for the large deviation of all the simulated curves from the measured curve could be that the simulated curves were generated using the assumption that the distribution of the channel coefficients is complex Gaussian. The reality, however, may be different, where the actual distribution of the channel coefficients may not be complex Gaussian but something else. This, however, is very likey in indoor radio channels [26]. This investigation is beyond the scope of this thesis and is an active research topic.

As regards the 4×4 curves (Fig. 4.5), there are no conclusive results, which is explained by the fact that there is insufficient data available which results in statistical inconsistency. Hence, making any judgment based on Fig. 4.5 would be incorrect.

CHAPTER 5

EFFECT OF CORRELATION ON BIT ERROR RATE

Having seen the favorable performance of the two-ring correlation model and the empirical Kronecker correlation matrix in capacity calculations, one question still lingers: in what aspect of system design do the large model errors reported in Tables. 3.2, 3.3, 3.4, 3.1 for the empirical Kronecker correlation matrix manifest themselves? The capacity plots did not reflect the large model errors between the empirical correlation matrix and the empirical Kronecker correlation matrix. In order to answer this question, another system performance criterion, the bit error rate of a MIMO system using maximum likelihood detection (MIMO-ML) is studied in the hope that this form of performance analysis will throw some light on the large model errors observed for the empirical Kronecker correlation matrix. Further, this performance criterion will show the usefulness of the new model developed in one more aspect of MIMO system design.

5.1 MIMO Maximum Likelihood Detection

For the sake of readability, the system model proposed in Eq. (1.1) is reproduced below,

$$\mathbf{r}(t) = \mathbf{H}(t)\mathbf{s}(t) + \mathbf{n}(t) \tag{5.1}$$

where $\mathbf{H}(t)$ is the $n_U \times n_{BS}$ channel matrix complex envelope such that $[\mathbf{H}(t)]_{lp} = h_{lp}(t)$, and $\mathbf{n}(t)$ stands for the complex envelope of the additive white Gaussian noise(AWGN) with zero mean vector and the diagonal covariance matrix, i.e., $E[\mathbf{n}(t)\mathbf{n}^H(t)] = P_{noise}\mathbf{I}_{n_U}$, where $\mathbf{I}$ is the $n_U \times n_U$ real identity matrix, and ^{H} stands for the Hermitian operator. $\mathbf{r}(t)$ is the $n_{BS} \times 1$ received vector, while $\mathbf{s}(t)$ is the $n_U \times 1$ transmitted vector. All values are complex baseband values of the real system.

Assuming an iid data stream, the maximum likelihood detector for the the MIMO system is tasked with finding [27],

$$\mathbf{s}_{ML} = arg \min_{\mathbf{s} \in Q} ||\mathbf{y} - \mathbf{Hs}||^2 \tag{5.2}$$

$$= arg \min_{\mathbf{s} \in Q} (\mathbf{y} - \mathbf{Hs})^H (\mathbf{y} - \mathbf{Hs}) \tag{5.3}$$

where Q denotes the constellation set. Hence, as can be seen, the maximum likelihood solution involves an exhaustive search. The algorithm followed for the MIMO ML simulations is shown in Fig. 5.1.

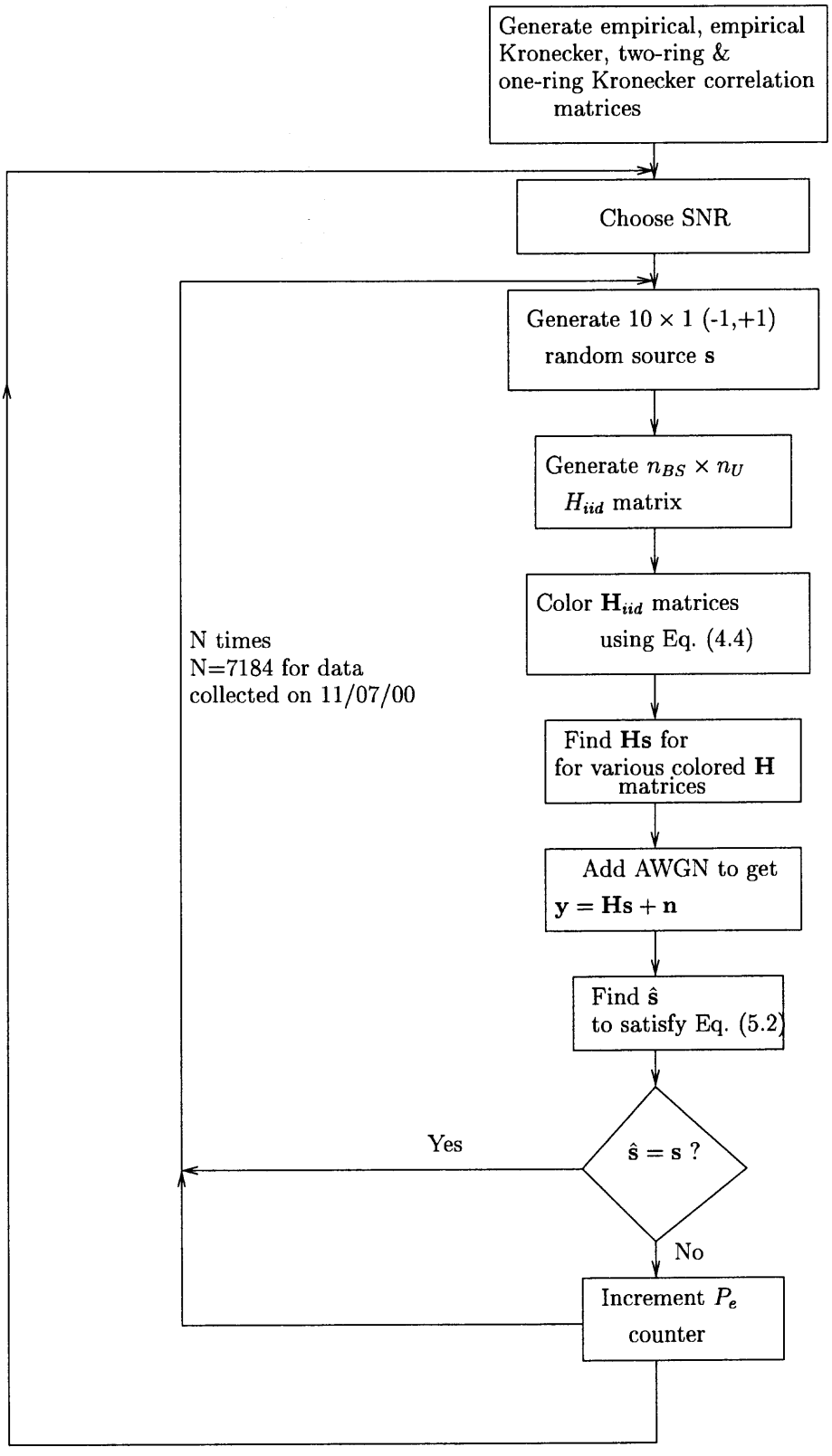

Figure 5.1: Methodology followed in MIMO ML simulations.

5.2 Results

Using the method outlined in Fig. 5.1, the bit error rate curves for various rooms and antenna configurations were generated. Two such plots are shown on the following pages.The remaining BER plots may be found in Appendix D. The transmit and receive correlation matrices for the one-ring Kronecker model may be found in Appendix E.

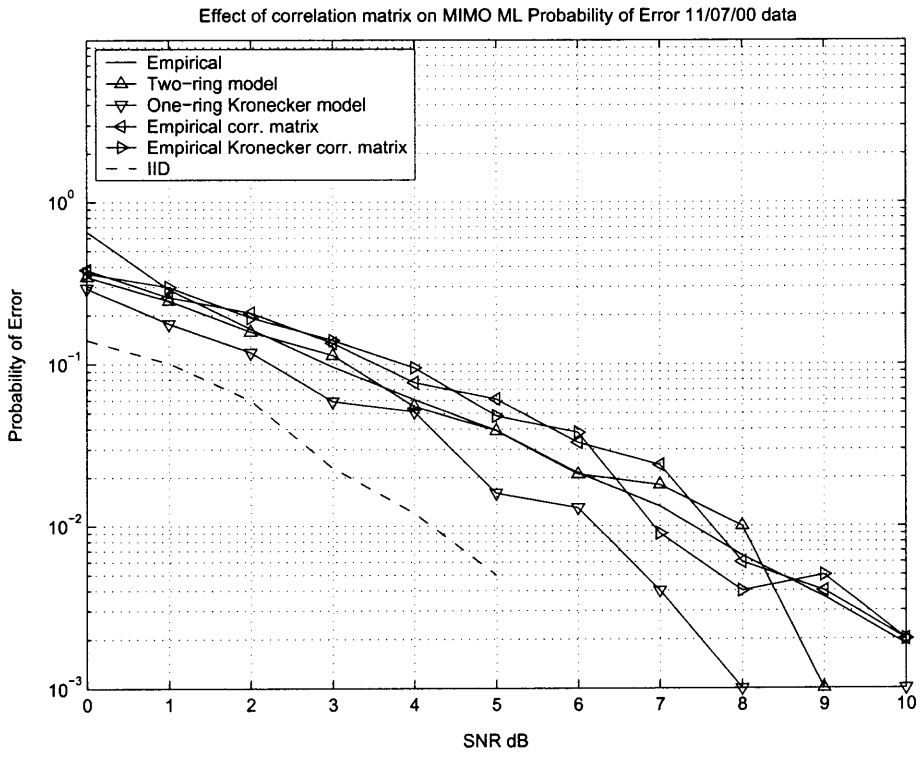

Figure 5.2: MIMO ML bit error rate curve for data collected on 11/07/00.

Model	Δ_U	Δ_{BS}	κ_U	κ_{BS}	μ_U	μ_{BS}
Two-ring	54.45°	57.3°	1.4	0	324.7°	0°
One-ring Kronecker	0°	0°	1.67	0	222.5°	0°

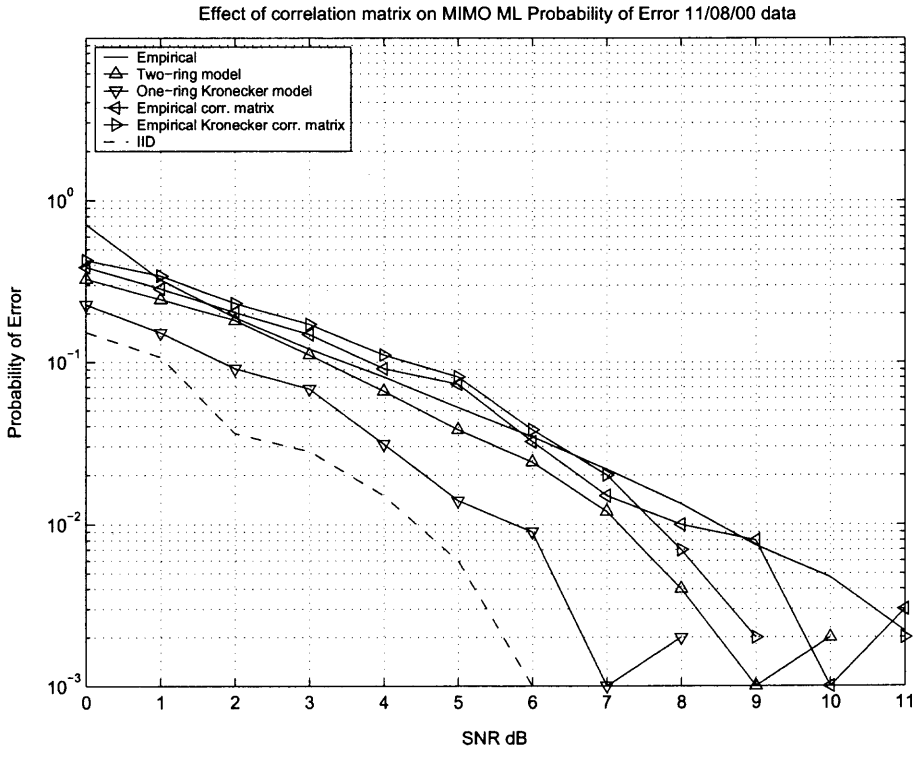

Figure 5.3: MIMO ML bit error rate curve for data collected on 11/08/00.

Model	Δ_U	Δ_{BS}	κ_U	κ_{BS}	μ_U	μ_{BS}
Two-ring	48.7°	57.3°	1.33	0	267.4°	0°
One-ring Kronecker	0°	0°	0	0	226.3°	0°

Figs. 5.2 and 5.3 show the utility of the model when it comes to bit error rate predictions . In both plots, the bit error rate curve predicted by the two-ring model closely follows that obtained from the measurements and that simulated using the empirical correlation matrix. The one-ring Kronecker model consistently underestimates the bit error rate and is closest to the iid curve. Also note that the curves are only plotted for an SNR up-to 11 dB. This is because of the limited numerical precision available with the number of Monte Carlo simulations, which had to be constrained in order to have consistency with the amount of measurement data available.

However, as can be seen, the large model error between the empirical and empirical Kronecker correlation matrices reported in Tables 3.1 - 3.4 does not manifest itself in any of the concerned curves. However modeling based on the assumption of separability does not quite return reliable results, as judged by the large difference between the two-ring and one-ring Kronecker model curves.

CHAPTER 6

CONCLUSIONS

This work has developed a new two-ring cross-correlation model and demonstrated the utility of the model when applied to a variety of MIMO performance analysis criteria. Chapter 1 presents a brief overview of MIMO systems and the need for accurate models that capture the various physical parameters involved. It also pointed out the drawbacks of currently used correlation models and paved the way for the development of a new parametric model. Chapter 2 addresses the measurement system used and attempts to explain the various complexities involved in dealing with measured data. The normalization process for the data is explained together with the need for such normalization. Important features of the data are presented that need consideration when used to fit models.

Chapter 3 marks the beginning of the contributions of this thesis, and starts with pointing out the deficiencies of the assumption of separability in correlation modeling. This deficiency is quantized in terms of the model error where the correlation matrices obtained directly from the measurements are compared with those obtained using the separability argument. Large errors are shown to occur, which point to the invalidity of the assumption of separability. Chapter 3 then goes on to develop a new parametric two-ring model, which is based on the contributions of [6]. Some handy correlation definitions are presented and the model developed is compared with measurements, based on these correlation definitions. Optimum parameters for the two-ring model are found using a least squares approach. Finally, an attempt is made to interpret these parameters in terms of the actual room layouts.

Chapter 4 utilizes the two-ring correlation model and attempts to compare the capacity curves obtained with that obtained from other models. The superiority of the two-ring model in this regard is demonstrated over the one-ring Kronecker model.

Chapter 5 attempts to find a performance criterion in which the large model error between the empirical correlation matrix and empirical Kronecker correlation matrix manifests itself. While showing that the two-ring model again performs better than the one-ring Kronecker model, the large model error does not seem to manifest itself in the the bit error rate curves obtained.

APPENDIX A

ROOM LAYOUTS

The room layout for the 4×4 setting was given in Fig. 2.1. The other room layouts are given in this chapter.

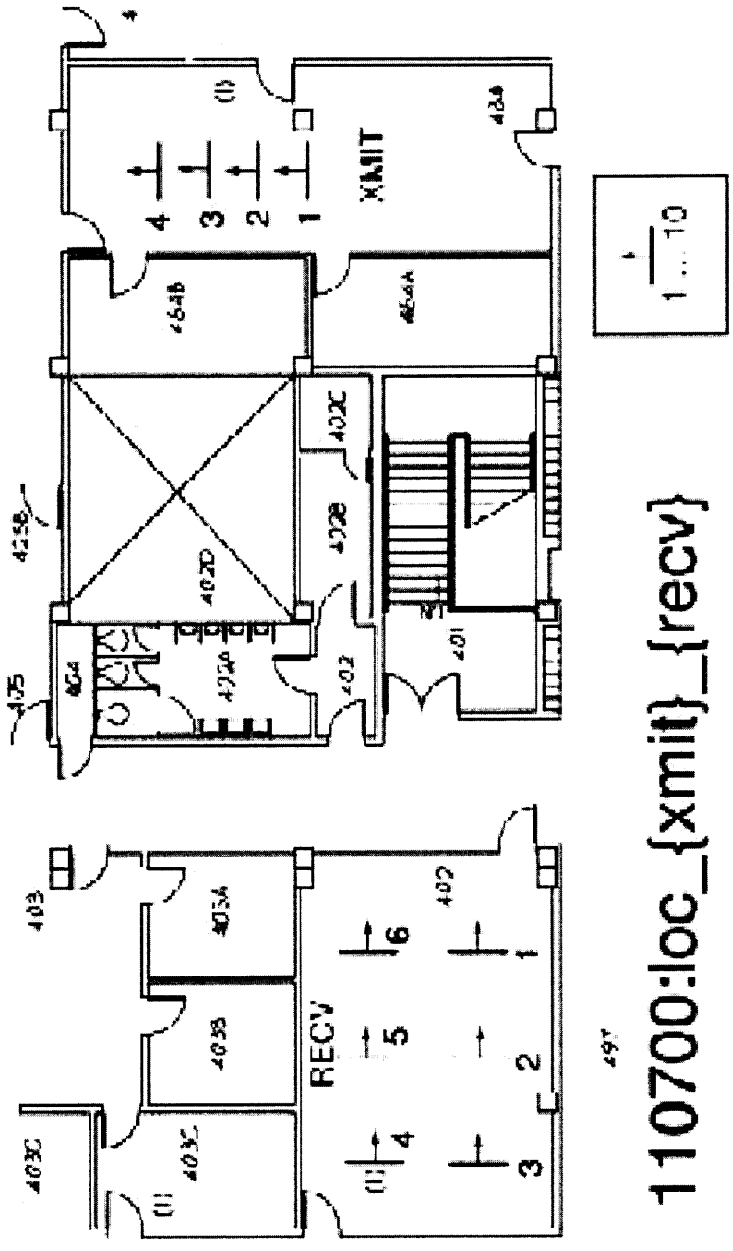

Figure A.1: Room layout for data collected on 11/07/00.

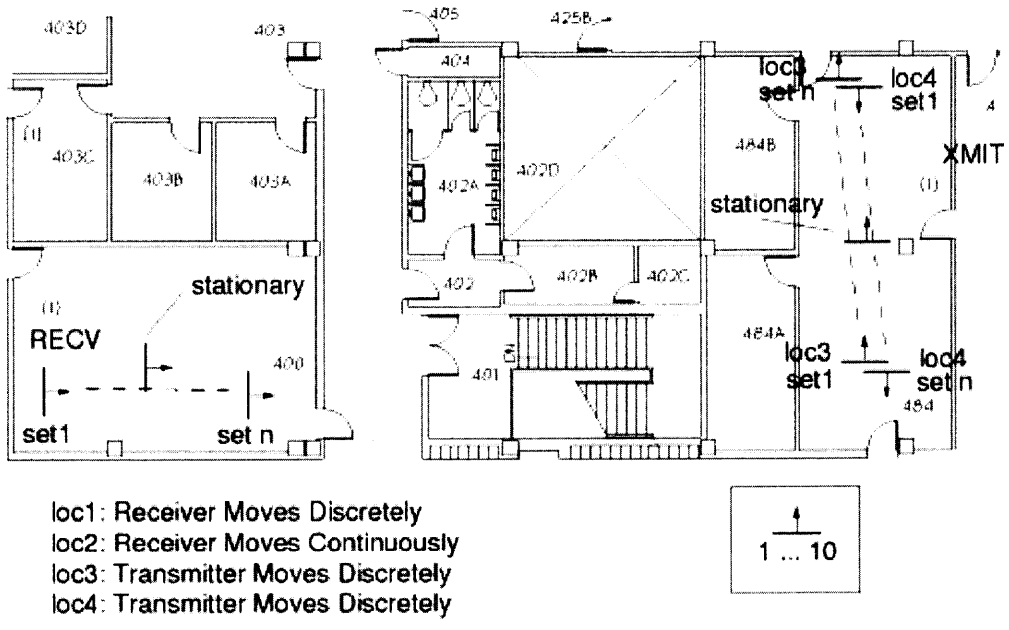

Figure A.2: Room layout for data collected on 11/08/00.

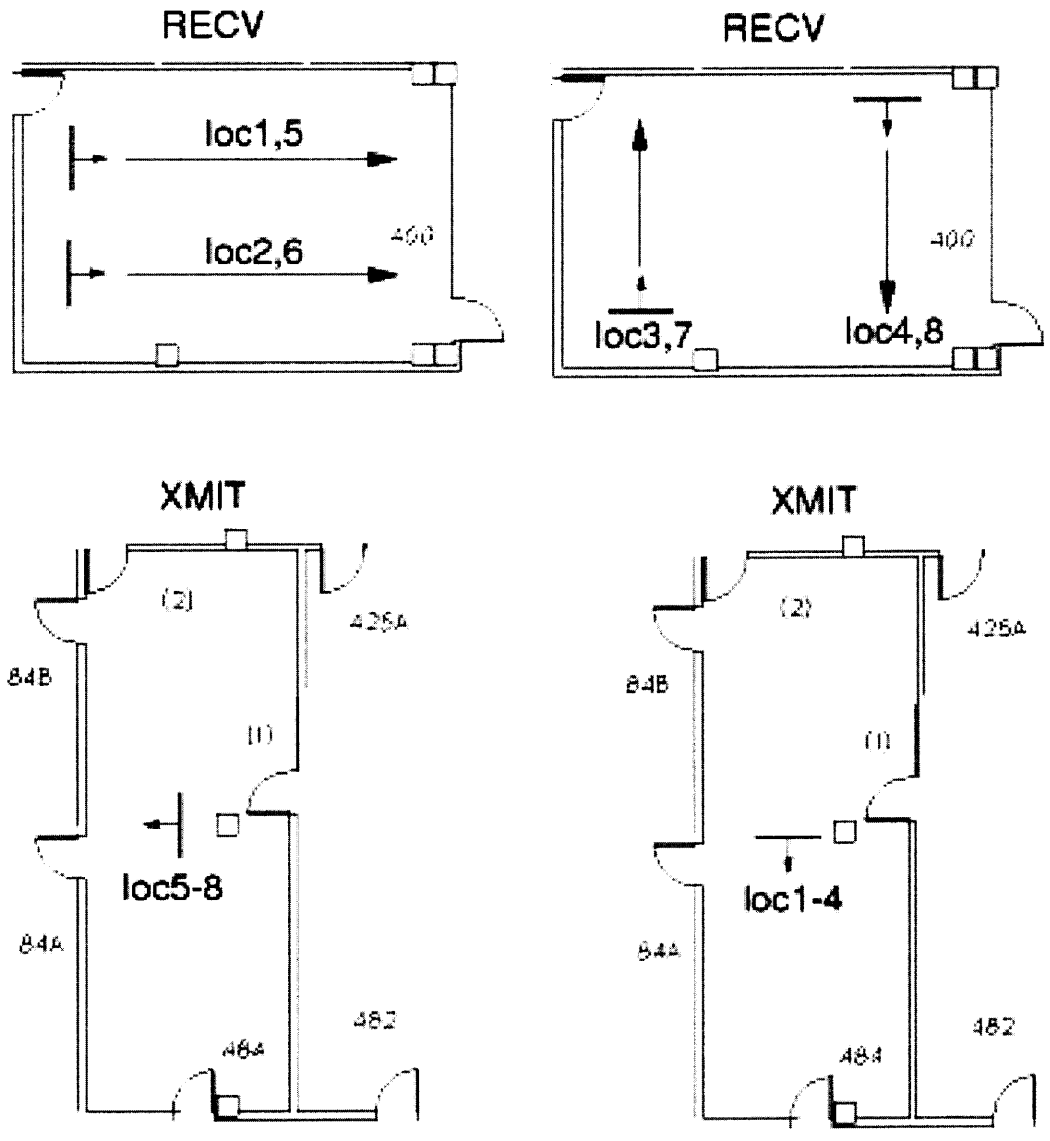

Figure A.3: Room layout for data collected on 12/21/00.

APPENDIX B

CORRELATION PLOTS

The remainder of the correlation plots are presented here.

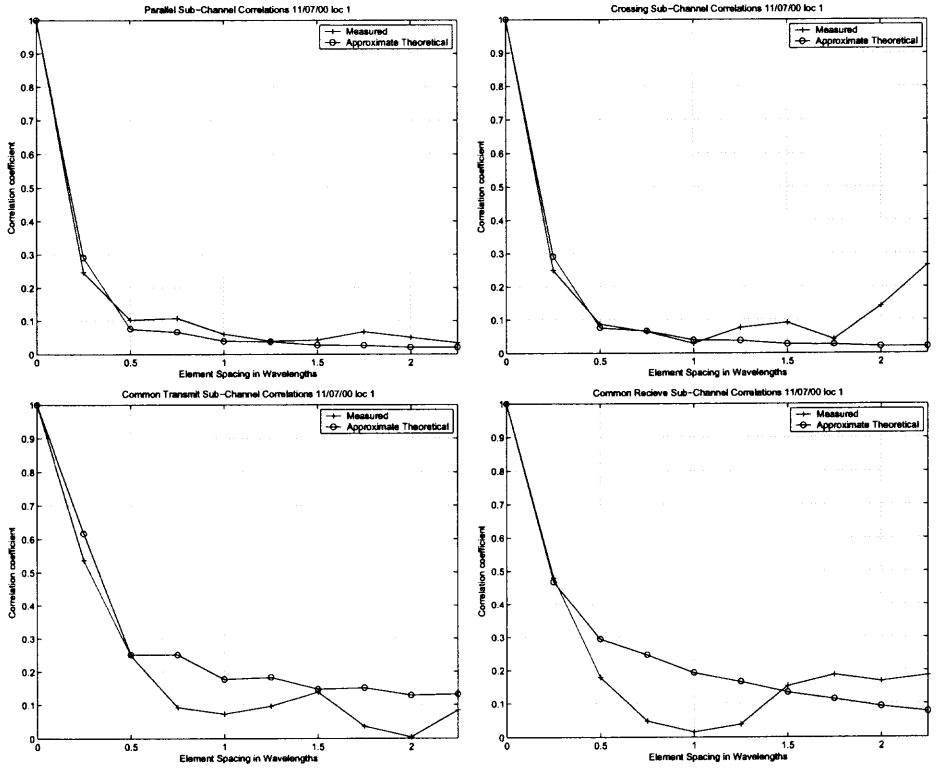

Figure B.1: Correlation Plots for 10×10 data collected on 11/07/00, locations 1-1,1-6,2-1,2-6.

Table B.1: Parameters Taken from the Last Column of Table 3.5

Δ_U	Δ_{BS}	κ_U	κ_{BS}	μ_U	μ_{BS}
54.45°	57.3°	1.53	0	324.7°	0°

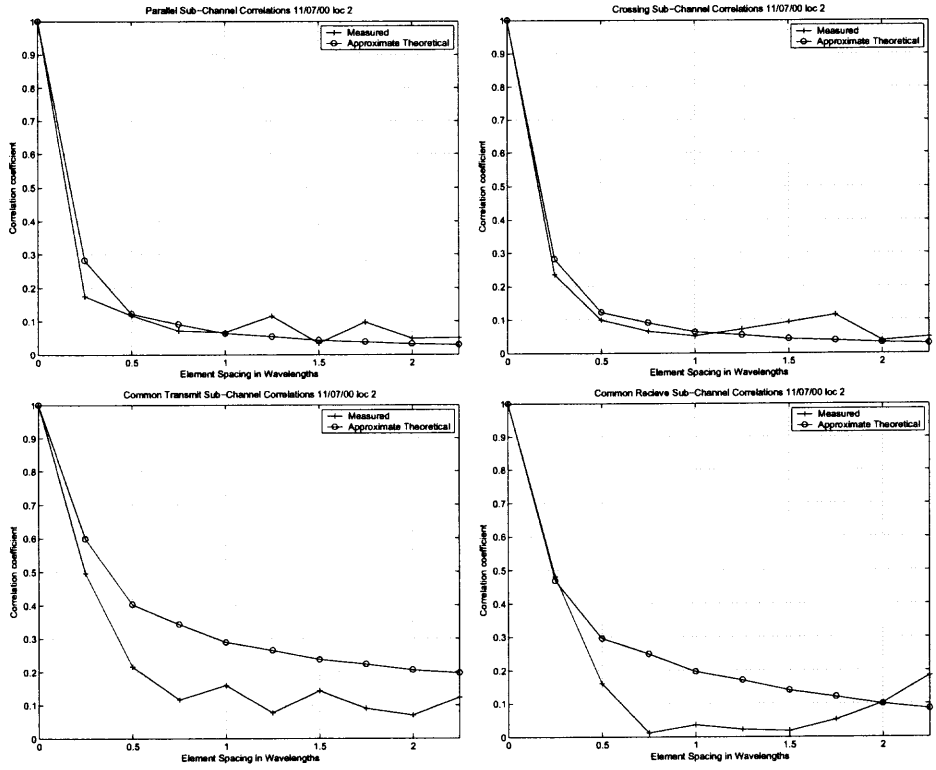

Figure B.2: Correlation Plots for 10×10 data collected on 11/07/00, location 1-2,1-5,2-2,2-5.

Table B.2: Parameters Taken from the Last Column of Table 3.6

Δ_U	Δ_{BS}	κ_U	κ_{BS}	μ_U	μ_{BS}
57.3°	57.3°	0.86	0	286.5°	0°

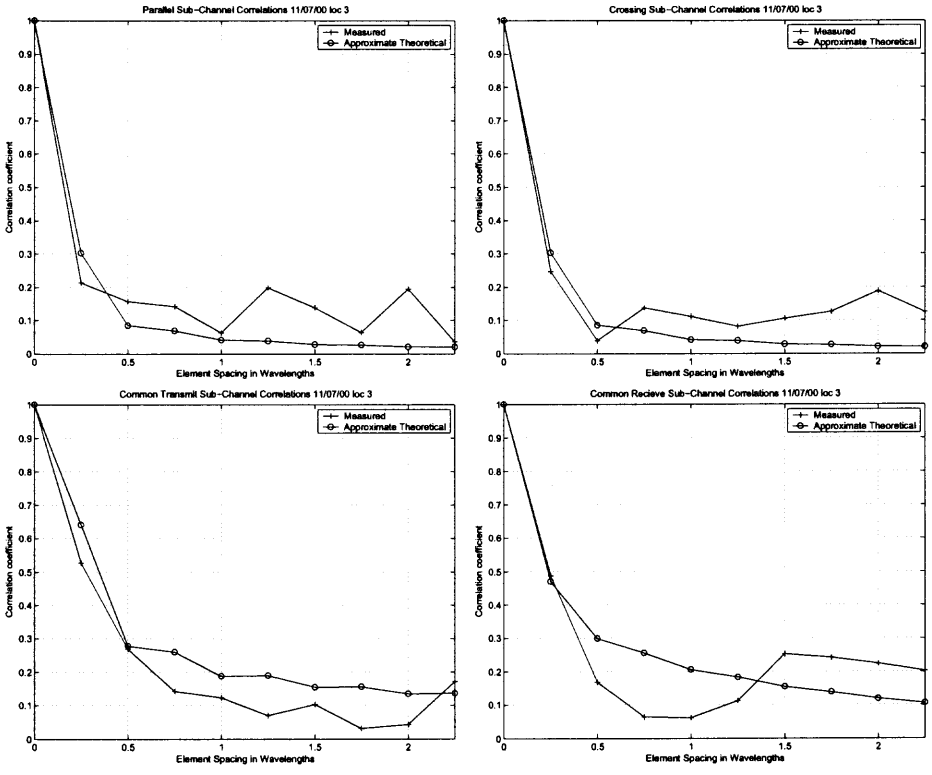

Figure B.3: Correlation Plots for 10×10 data collected on 11/07/00, location 1-3,1-4,2-3,2-4.

Table B.3: Parameters Taken from the Last Column of Table 3.7

Δ_U	Δ_{BS}	κ_U	κ_{BS}	μ_U	μ_{BS}
45.85°	57.3°	1.67	0	324.7°	0°

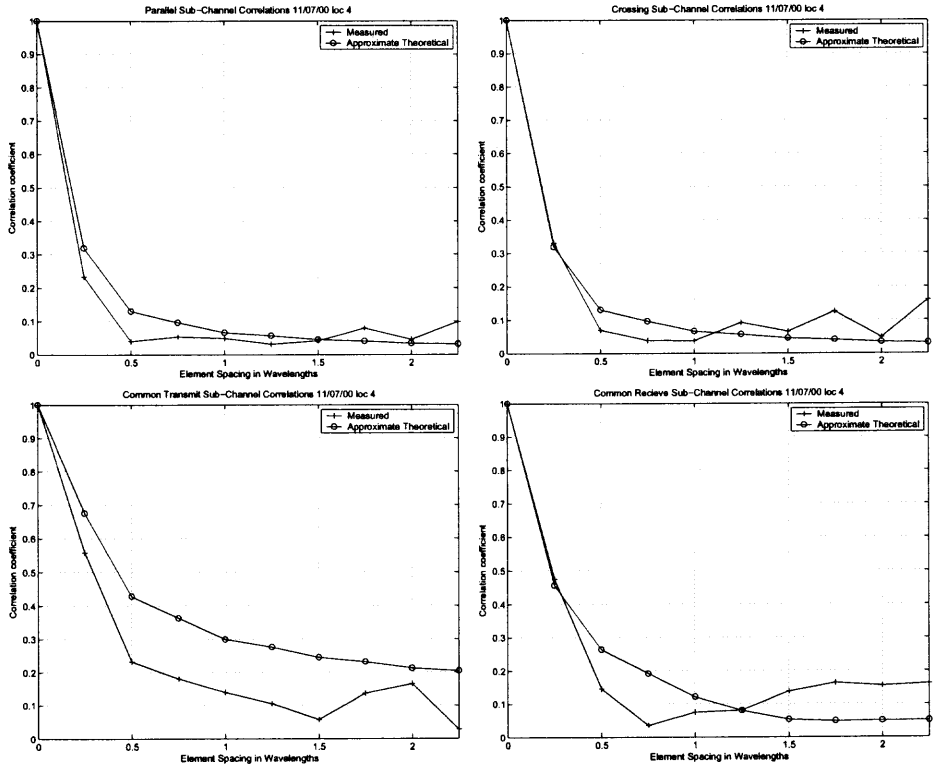

Figure B.4: Correlation Plots for 10×10 data collected on 11/07/00, location 3-1,3-6,4-1,4-6.

Table B.4: Parameters Taken from the Last Column of Table 3.8

Δ_U	Δ_{BS}	κ_U	κ_{BS}	μ_U	μ_{BS}
37.24°	57.3°	1.4	0	210.1°	0°

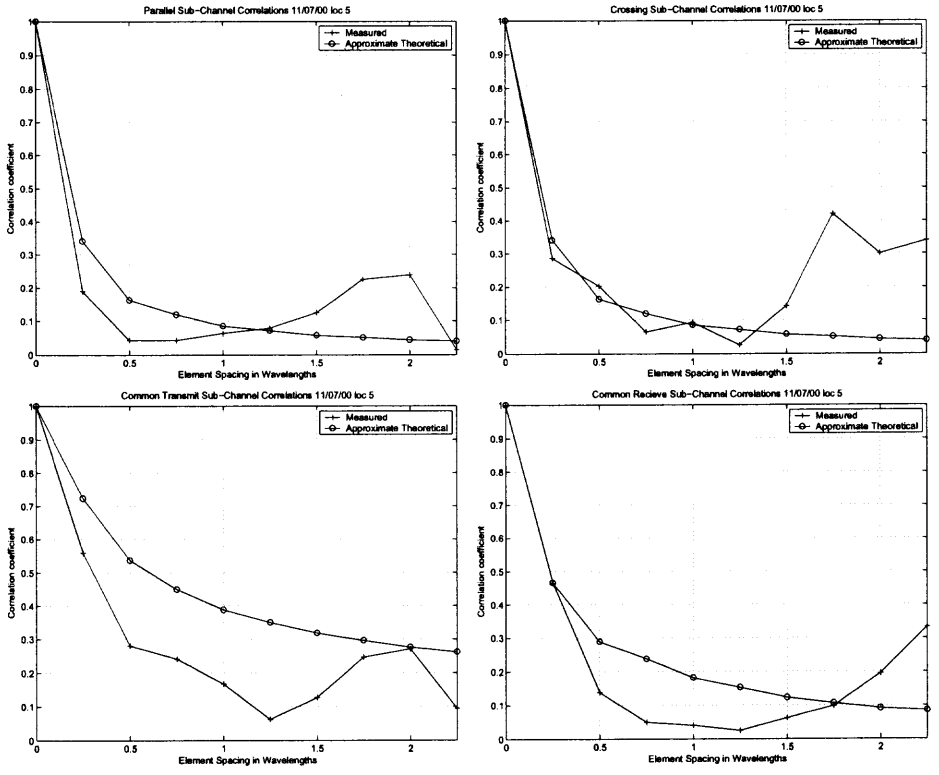

Figure B.5: Correlation Plots for 10×10 data collected on 11/07/00, location 3-2,3-5,4-2,4-5.

Table B.5: Parameters Taken from the Last Column of Table 3.9

Δ_U	Δ_{BS}	κ_U	κ_{BS}	μ_U	μ_{BS}
54.45°	57.3°	1.33	0	267.4°	0°

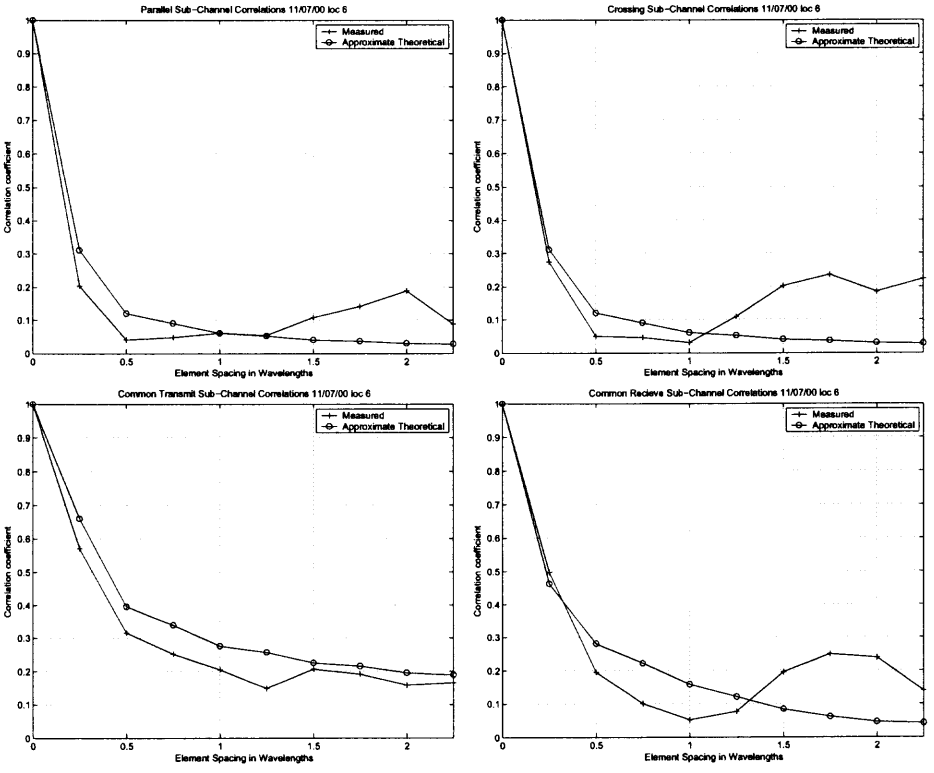

Figure B.6: Correlation Plots for 10×10 data collected on 11/07/00, location 3-3,3-4,4-3,4-4.

Table B.6: Parameters Taken from the Last Column of Table 3.10

Δ_U	Δ_{BS}	κ_U	κ_{BS}	μ_U	μ_{BS}
54.45°	57.3°	1.4	0	210.1°	0°

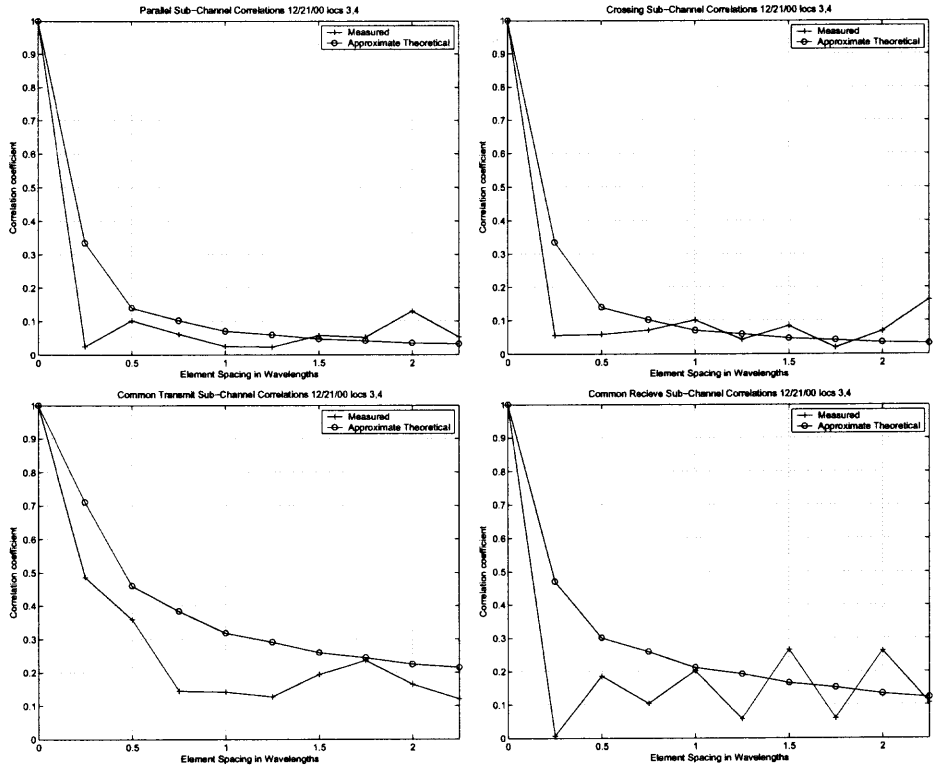

Figure B.7: Correlation Plots for 10×10 data collected on 12/21/00, location 3,4.

Table B.7: Parameters Taken from the Last Column of Table 3.14

Δ_U	Δ_{BS}	κ_U	κ_{BS}	μ_U	μ_{BS}
43°	57.3°	1.6	0	305.6°	0°

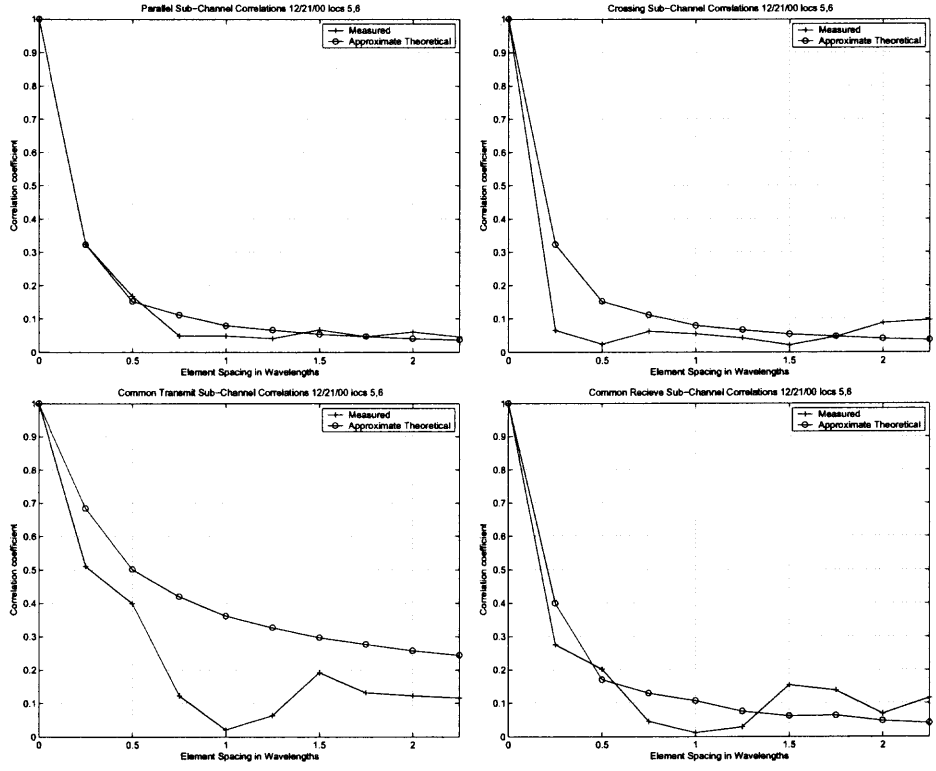

Figure B.8: Correlation Plots for 10×10 data collected on 12/21/00, location 5,6.

Table B.8: Parameters Taken from the Last Column of Table 3.15

Δ_U	Δ_{BS}	κ_U	κ_{BS}	μ_U	μ_{BS}
11.5°	37.24°	1.13	0	76.3°	0°

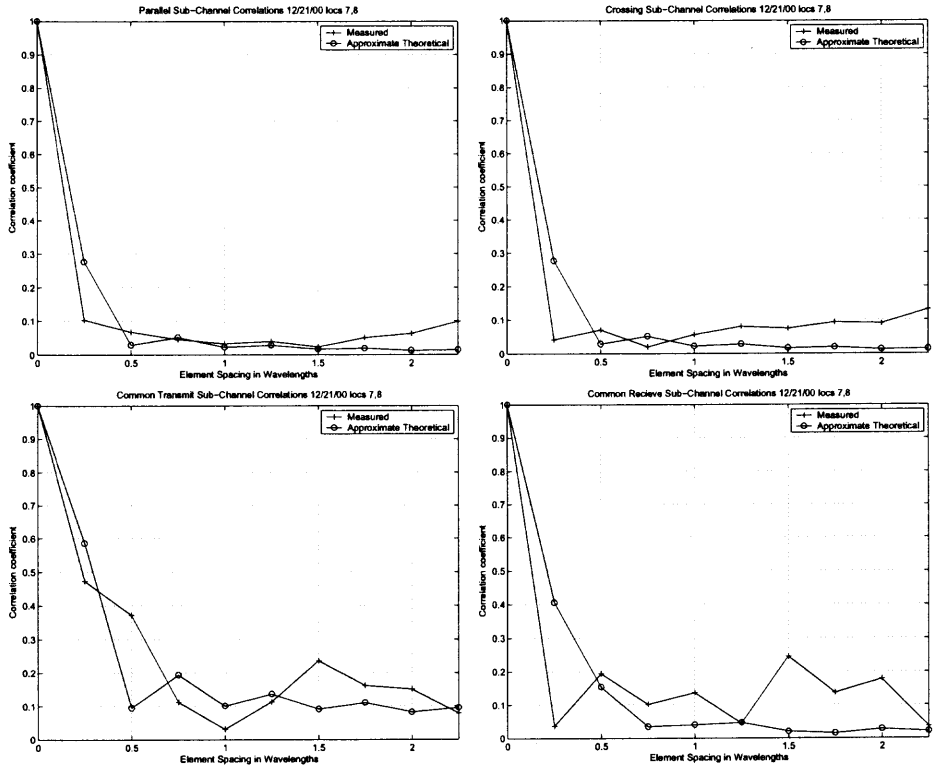

Figure B.9: Correlation Plots for 10×10 data collected on 12/21/00, location 7,8.

Table B.9: Parameters Taken from the Last Column of Table 3.16

Δ_U	Δ_{BS}	κ_U	κ_{BS}	μ_U	μ_{BS}
28.65°	32.5°	1.6	0	171.9°	0°

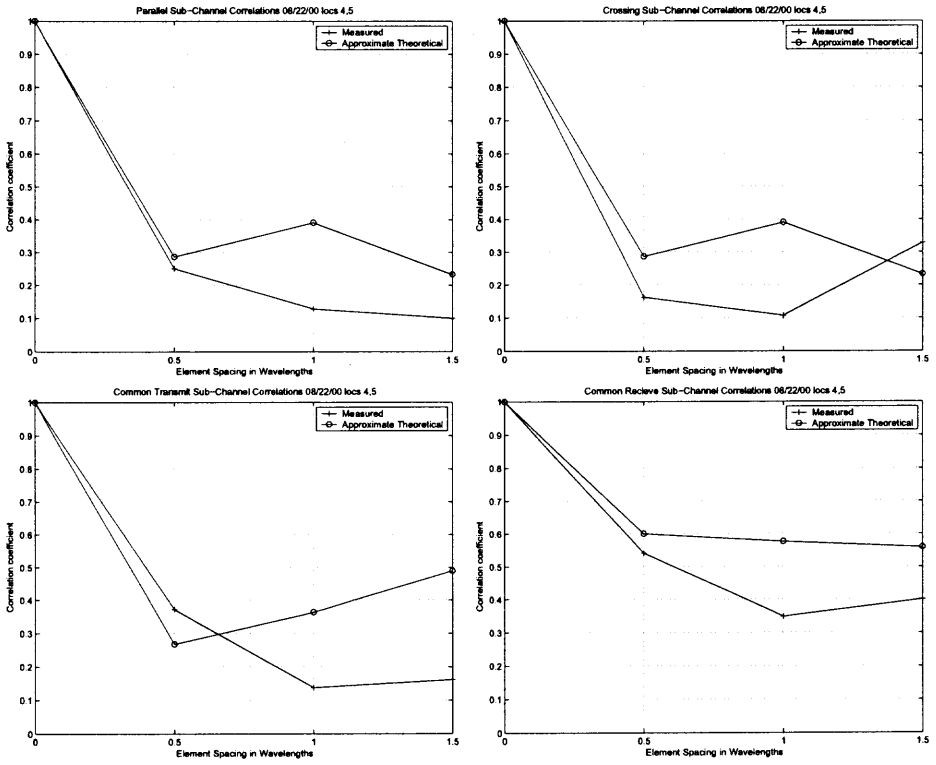

Figure B.10: Correlation Plots for 4×4 data collected on 08/22/00, location 4,5.

Table B.10: Parameters Taken from the Last Column of Table 3.18

Δ_U	Δ_{BS}	κ_U	κ_{BS}	μ_U	μ_{BS}
22.92°	28.65°	3.66	1	248.3°	87°

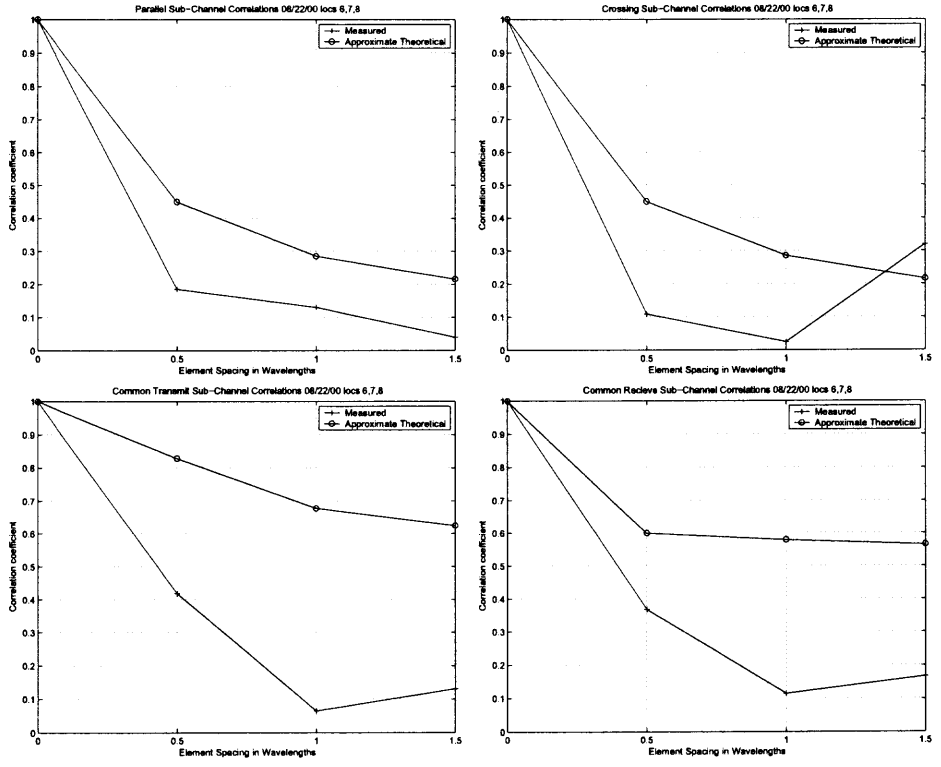

Figure B.11: Correlation Plots for 4×4 data collected on 08/22/00, location 6,7,8.

Table B.11: Parameters Taken from the Last Column of Table 3.19

Δ_U	Δ_{BS}	κ_U	κ_{BS}	μ_U	μ_{BS}
0°	57.3°	5	1	210.1°	87°

APPENDIX C

CAPACITY PLOTS

The remainder of the capacity plots are presented here. The transmit and receive correlation matrices for the one-ring Kronecker model may be found in Appendix E.

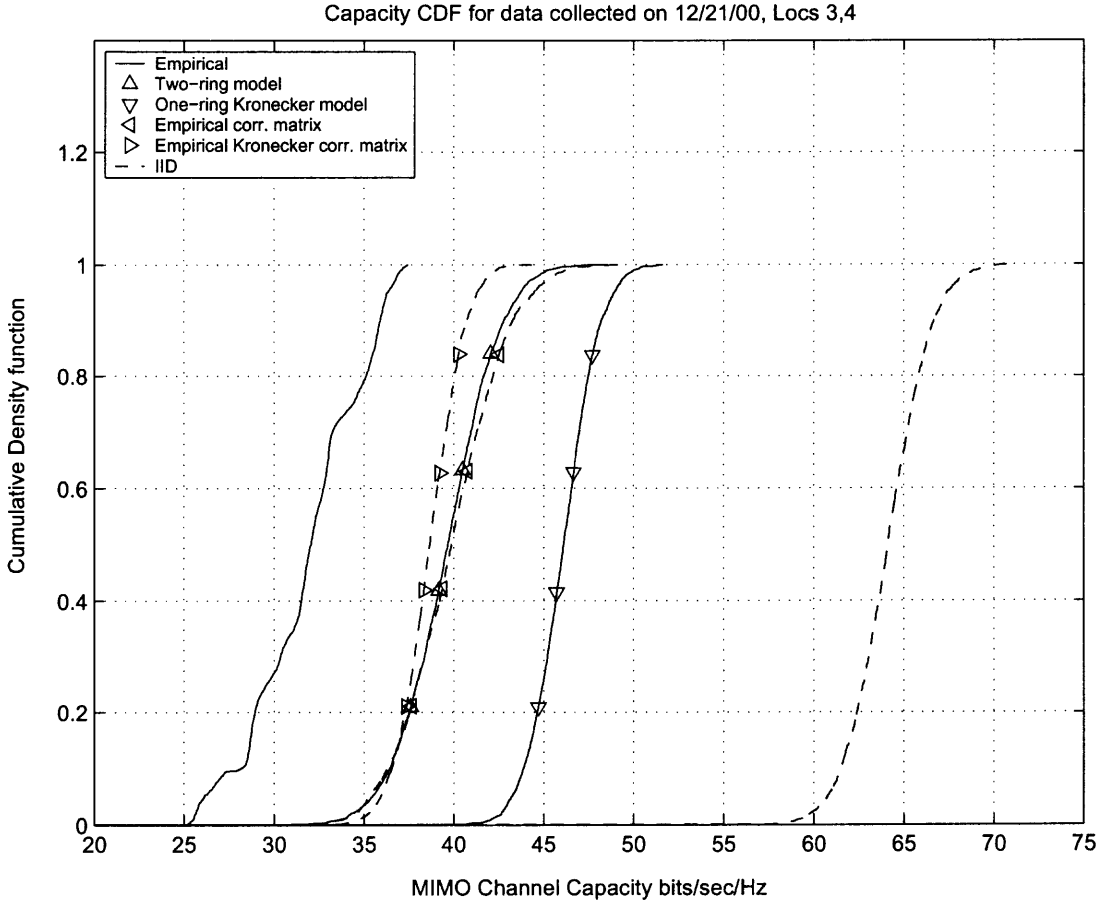

Figure C.1: Capacity CDF for 10×10 data collected on 12/21/00, locations 3,4.

Model	Δ_U	Δ_{BS}	κ_U	κ_{BS}	μ_U	μ_{BS}
Two-ring (Table 3.14)	43°	57.3°	1.6	0	305.6°	0°
One-ring Kronecker	–	–	0.53	0	189°	0°

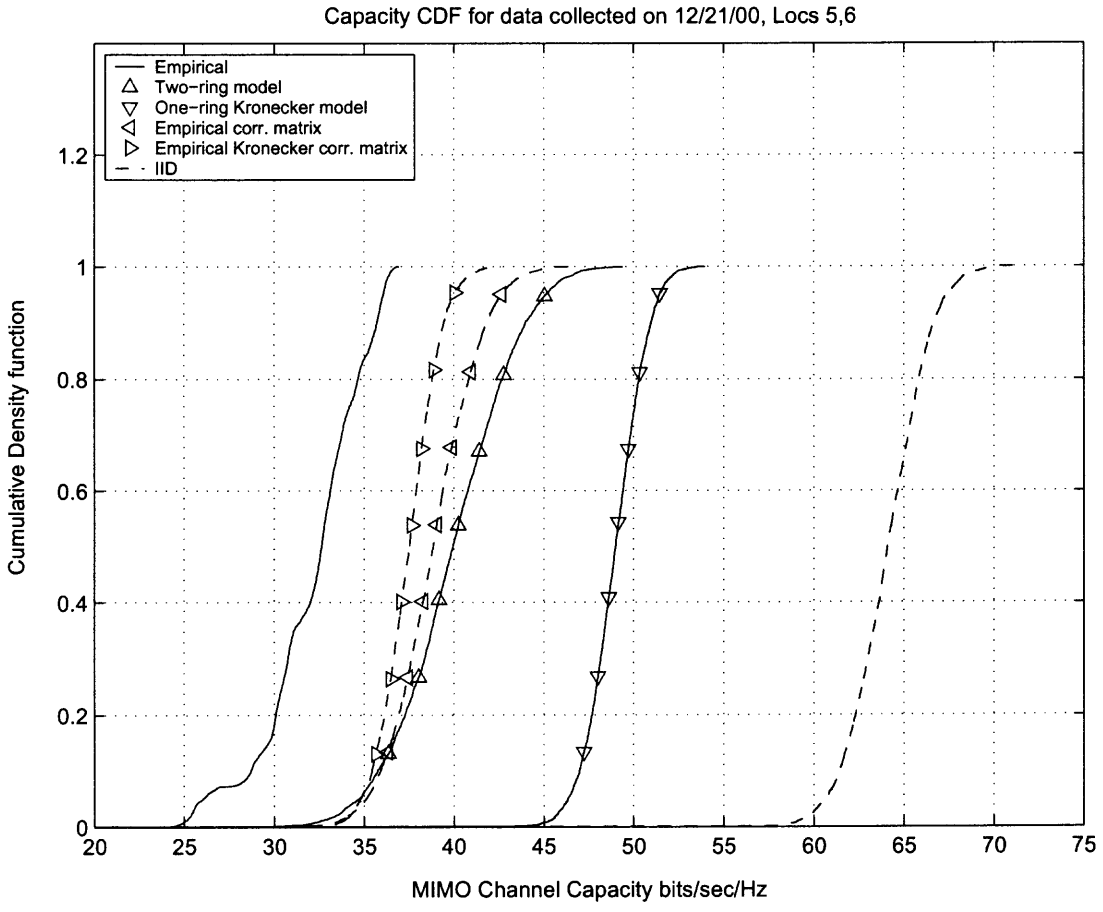

Figure C.2: Capacity CDF for 10×10 data collected on 12/21/00, locations 5,6.

Model	Δ_U	Δ_{BS}	κ_U	κ_{BS}	μ_U	μ_{BS}
Two-ring (Table 3.15)	11.5°	37.24°	1.13	0	76.3°	0°
One-ring Kronecker	–	–	1.93	0	10.5°	0°

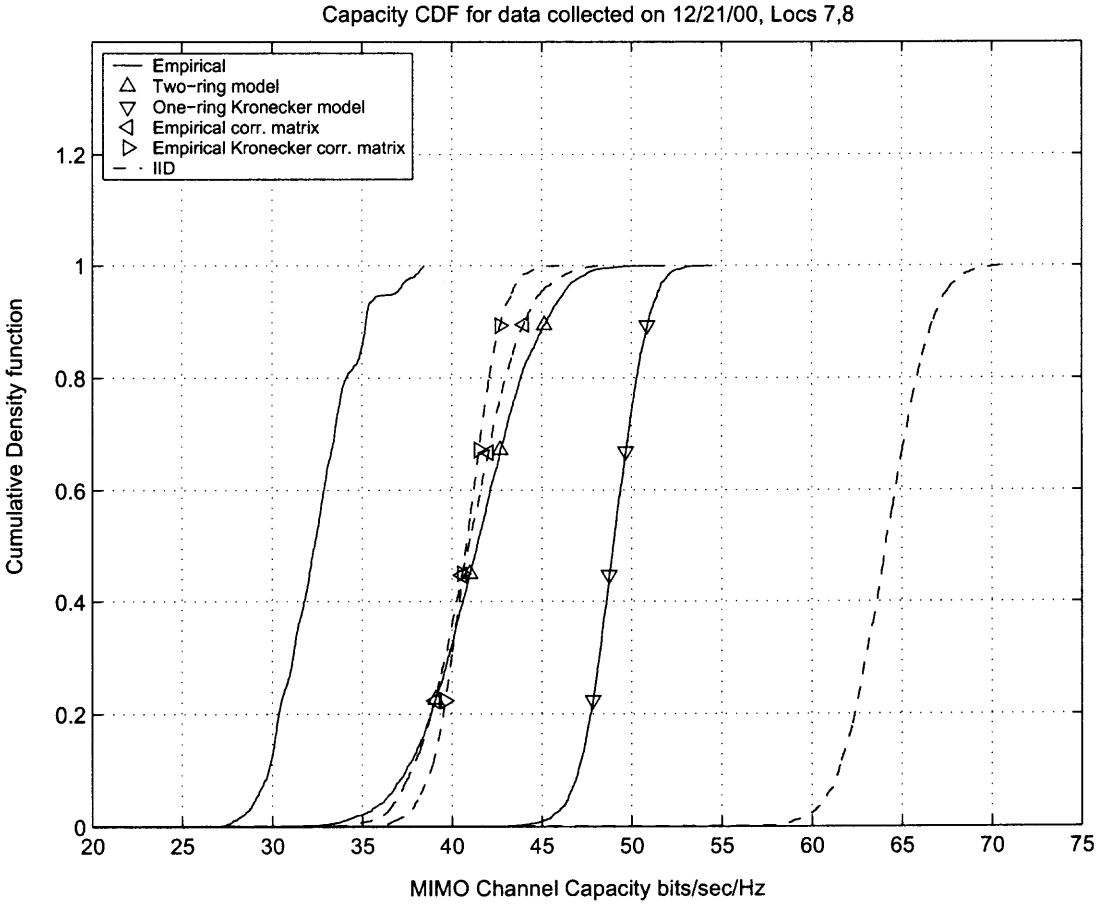

Figure C.3: Capacity CDF for 10×10 data collected on 12/21/00, locations 7,8.

Model	Δ_U	Δ_{BS}	κ_U	κ_{BS}	μ_U	μ_{BS}
Two-ring (Table 3.16)	28.65°	32.5°	1.6	0	171.9°	0°
One-ring Kronecker	–	–	0.73	0	42.97°	0°

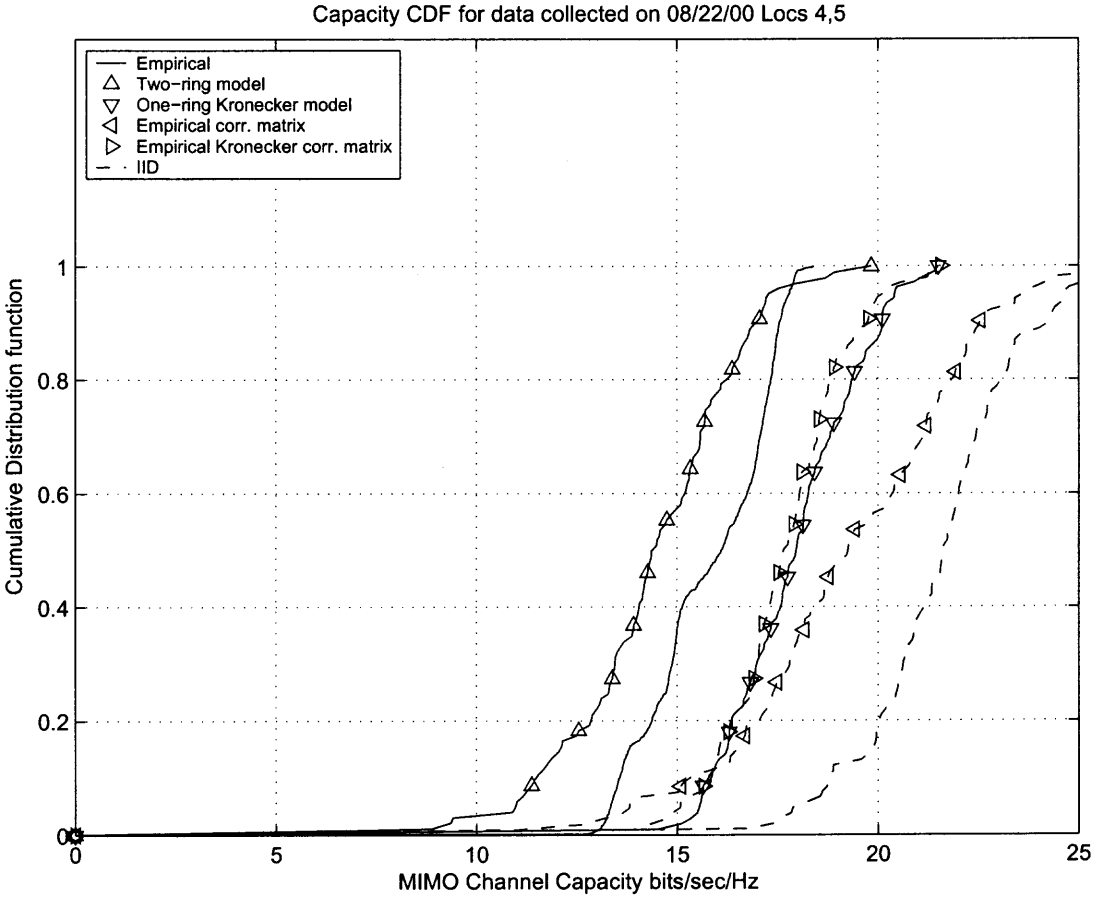

Figure C.4: Capacity CDF for 4×4 data collected on 08/22/00, locations 4,5.

Model	Δ_U	Δ_{BS}	κ_U	κ_{BS}	μ_U	μ_{BS}
Two-ring (Table 3.18)	22.92°	28.65°	3.66	1	248.3°	87°
One-ring Kronecker	–	–	3.2	1	104.1°	87°

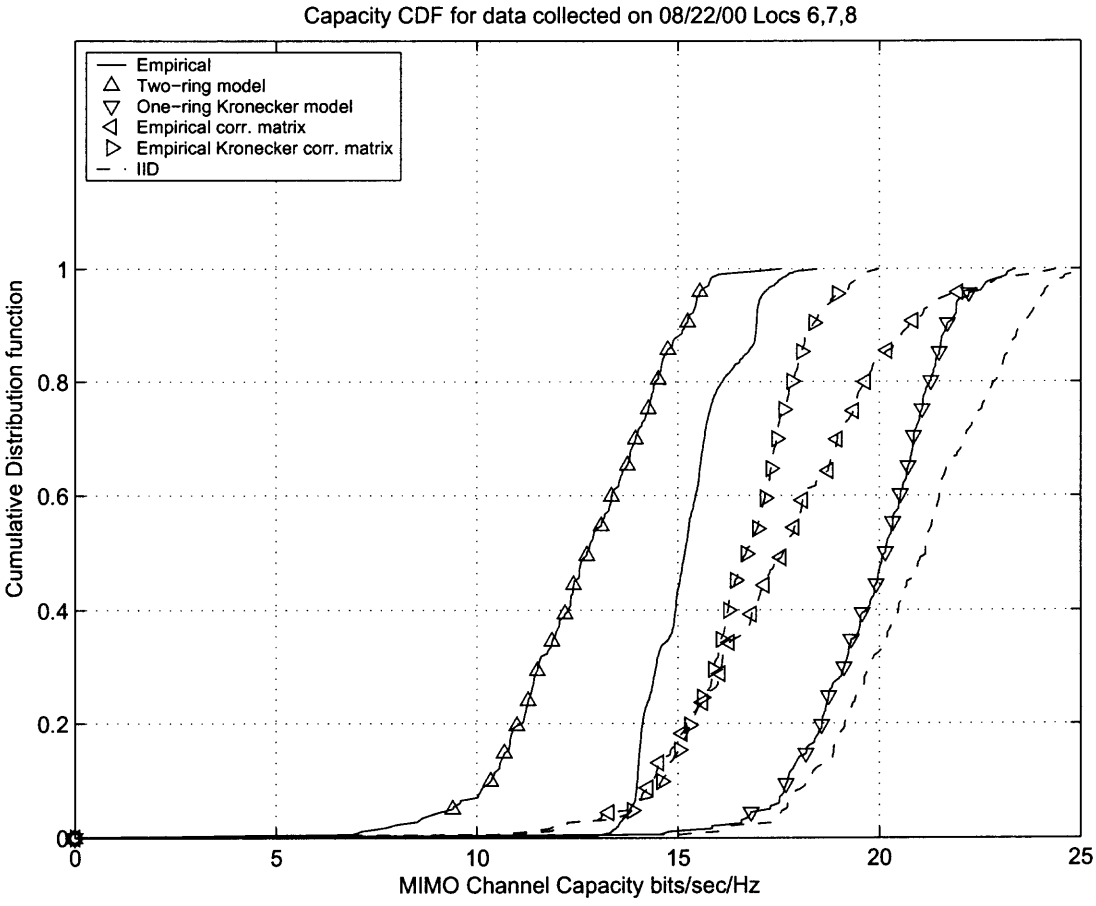

Figure C.5: Capacity CDF for 4×4 data collected on 08/22/00, locations 6,7,8.

Model	Δ_U	Δ_{BS}	κ_U	κ_{BS}	μ_U	μ_{BS}
Two-ring (Table 3.19)	0°	57.3°	5	1	210.1°	87°
One-ring Kronecker	–	–	3.1	1	35.33°	87°

APPENDIX D

TRANSMIT AND RECEIVE CORRELATION MATRICES USED TO CALCULATE ONE-RING KRONECKER CORRELATION MATRIX

Due to the wide popularity of the Kronecker model in literature, it is informative to view the transmit and receive correlation matrices for the one-ring Kronecker model. For a 10×10 scenario, each of the transmit and receive correlation matrices are 10×10 matrices, and the Kronecker product of the two results in a 100×100 correlation matrix.

The transmit and receive correlation matrices for the 10×10 measurements taken on 11/07/00, averaged across all locations, are listed below

The transmit *covariance* matrix is,

$$\mathbf{R}_{\mathbf{H}}^{Tx} = \begin{Bmatrix} 1.0000 & 0.4720 & 0.3042 & 0.2659 & 0.2203 & 0.2043 & 0.1812 & 0.1720 & 0.1575 & 0.1513 \\ 0.4720 & 1.0000 & 0.4720 & 0.3042 & 0.2659 & 0.2203 & 0.2043 & 0.1812 & 0.1720 & 0.1575 \\ 0.3042 & 0.4720 & 1.0000 & 0.4720 & 0.3042 & 0.2659 & 0.2203 & 0.2043 & 0.1812 & 0.1720 \\ 0.2659 & 0.3042 & 0.4720 & 1.0000 & 0.4720 & 0.3042 & 0.2659 & 0.2203 & 0.2043 & 0.1812 \\ 0.2203 & 0.2659 & 0.3042 & 0.4720 & 1.0000 & 0.4720 & 0.3042 & 0.2659 & 0.2203 & 0.2043 \\ 0.2043 & 0.2203 & 0.2659 & 0.3042 & 0.4720 & 1.0000 & 0.4720 & 0.3042 & 0.2659 & 0.2203 \\ 0.1812 & 0.2043 & 0.2203 & 0.2659 & 0.3042 & 0.4720 & 1.0000 & 0.4720 & 0.3042 & 0.2659 \\ 0.1720 & 0.1812 & 0.2043 & 0.2203 & 0.2659 & 0.3042 & 0.4720 & 1.0000 & 0.4720 & 0.3042 \\ 0.1575 & 0.1720 & 0.1812 & 0.2043 & 0.2203 & 0.2659 & 0.3042 & 0.4720 & 1.0000 & 0.4720 \\ 0.1513 & 0.1575 & 0.1720 & 0.1812 & 0.2043 & 0.2203 & 0.2659 & 0.3042 & 0.4720 & 1.0000 \end{Bmatrix}$$

The receive *covariance* matrix is,

$$\mathbf{R}_{\mathbf{H}}^{Rx} = \begin{Bmatrix} 1.0000 & 0.7049 & 0.1692 & 0.0846 & 0.0176 & 0.0614 & 0.0200 & 0.0484 & 0.0216 & 0.0407 \\ 0.7049 & 1.0000 & 0.7049 & 0.1692 & 0.0846 & 0.0176 & 0.0614 & 0.0200 & 0.0484 & 0.0216 \\ 0.1692 & 0.7049 & 1.0000 & 0.7049 & 0.1692 & 0.0846 & 0.0176 & 0.0614 & 0.0200 & 0.0484 \\ 0.0846 & 0.1692 & 0.7049 & 1.0000 & 0.7049 & 0.1692 & 0.0846 & 0.0176 & 0.0614 & 0.0200 \\ 0.0176 & 0.0846 & 0.1692 & 0.7049 & 1.0000 & 0.7049 & 0.1692 & 0.0846 & 0.0176 & 0.0614 \\ 0.0614 & 0.0176 & 0.0846 & 0.1692 & 0.7049 & 1.0000 & 0.7049 & 0.1692 & 0.0846 & 0.0176 \\ 0.0200 & 0.0614 & 0.0176 & 0.0846 & 0.1692 & 0.7049 & 1.0000 & 0.7049 & 0.1692 & 0.0846 \\ 0.0484 & 0.0200 & 0.0614 & 0.0176 & 0.0846 & 0.1692 & 0.7049 & 1.0000 & 0.7049 & 0.1692 \\ 0.0216 & 0.0484 & 0.0200 & 0.0614 & 0.0176 & 0.0846 & 0.1692 & 0.7049 & 1.0000 & 0.7049 \\ 0.0407 & 0.0216 & 0.0484 & 0.0200 & 0.0614 & 0.0176 & 0.0846 & 0.1692 & 0.7049 & 1.0000 \end{Bmatrix}$$

The transmit and receive correlation matrices for the 10×10 measurements taken on 11/08/00, averaged across all locations, are listed below.

The transmit *covariance* matrix is,

$$\mathbf{R}_{\mathbf{H}}^{Tx} = \begin{Bmatrix} 1.0000 & 0.4720 & 0.3042 & 0.2659 & 0.2203 & 0.2043 & 0.1812 & 0.1720 & 0.1575 & 0.1513 \\ 0.4720 & 1.0000 & 0.4720 & 0.3042 & 0.2659 & 0.2203 & 0.2043 & 0.1812 & 0.1720 & 0.1575 \\ 0.3042 & 0.4720 & 1.0000 & 0.4720 & 0.3042 & 0.2659 & 0.2203 & 0.2043 & 0.1812 & 0.1720 \\ 0.2659 & 0.3042 & 0.4720 & 1.0000 & 0.4720 & 0.3042 & 0.2659 & 0.2203 & 0.2043 & 0.1812 \\ 0.2203 & 0.2659 & 0.3042 & 0.4720 & 1.0000 & 0.4720 & 0.3042 & 0.2659 & 0.2203 & 0.2043 \\ 0.2043 & 0.2203 & 0.2659 & 0.3042 & 0.4720 & 1.0000 & 0.4720 & 0.3042 & 0.2659 & 0.2203 \\ 0.1812 & 0.2043 & 0.2203 & 0.2659 & 0.3042 & 0.4720 & 1.0000 & 0.4720 & 0.3042 & 0.2659 \\ 0.1720 & 0.1812 & 0.2043 & 0.2203 & 0.2659 & 0.3042 & 0.4720 & 1.0000 & 0.4720 & 0.3042 \\ 0.1575 & 0.1720 & 0.1812 & 0.2043 & 0.2203 & 0.2659 & 0.3042 & 0.4720 & 1.0000 & 0.4720 \\ 0.1513 & 0.1575 & 0.1720 & 0.1812 & 0.2043 & 0.2203 & 0.2659 & 0.3042 & 0.4720 & 1.0000 \end{Bmatrix}$$

The receive *covariance* matrix is,

$$\mathbf{R}_{\mathbf{H}}^{Rx} = \begin{Bmatrix} 1.0000 & 0.6058 & 0.0597 & 0.1783 & 0.0818 & 0.1242 & 0.0764 & 0.0999 & 0.0701 & 0.0856 \\ 0.6058 & 1.0000 & 0.6058 & 0.0597 & 0.1783 & 0.0818 & 0.1242 & 0.0764 & 0.0999 & 0.0701 \\ 0.0597 & 0.6058 & 1.0000 & 0.6058 & 0.0597 & 0.1783 & 0.0818 & 0.1242 & 0.0764 & 0.0999 \\ 0.1783 & 0.0597 & 0.6058 & 1.0000 & 0.6058 & 0.0597 & 0.1783 & 0.0818 & 0.1242 & 0.0764 \\ 0.0818 & 0.1783 & 0.0597 & 0.6058 & 1.0000 & 0.6058 & 0.0597 & 0.1783 & 0.0818 & 0.1242 \\ 0.1242 & 0.0818 & 0.1783 & 0.0597 & 0.6058 & 1.0000 & 0.6058 & 0.0597 & 0.1783 & 0.0818 \\ 0.0764 & 0.1242 & 0.0818 & 0.1783 & 0.0597 & 0.6058 & 1.0000 & 0.6058 & 0.0597 & 0.1783 \\ 0.0999 & 0.0764 & 0.1242 & 0.0818 & 0.1783 & 0.0597 & 0.6058 & 1.0000 & 0.6058 & 0.0597 \\ 0.0701 & 0.0999 & 0.0764 & 0.1242 & 0.0818 & 0.1783 & 0.0597 & 0.6058 & 1.0000 & 0.6058 \\ 0.0856 & 0.0701 & 0.0999 & 0.0764 & 0.1242 & 0.0818 & 0.1783 & 0.0597 & 0.6058 & 1.0000 \end{Bmatrix}$$

The transmit and receive correlation matrices for the 10×10 measurements taken on 12/21/00, for locations 1,2, are listed below.

The transmit *covariance* matrix is,

$$\mathbf{R}_{\mathbf{H}}^{Tx} = \begin{Bmatrix} 1.0000 & 0.4720 & 0.3042 & 0.2659 & 0.2203 & 0.2043 & 0.1812 & 0.1720 & 0.1575 & 0.1513 \\ 0.4720 & 1.0000 & 0.4720 & 0.3042 & 0.2659 & 0.2203 & 0.2043 & 0.1812 & 0.1720 & 0.1575 \\ 0.3042 & 0.4720 & 1.0000 & 0.4720 & 0.3042 & 0.2659 & 0.2203 & 0.2043 & 0.1812 & 0.1720 \\ 0.2659 & 0.3042 & 0.4720 & 1.0000 & 0.4720 & 0.3042 & 0.2659 & 0.2203 & 0.2043 & 0.1812 \\ 0.2203 & 0.2659 & 0.3042 & 0.4720 & 1.0000 & 0.4720 & 0.3042 & 0.2659 & 0.2203 & 0.2043 \\ 0.2043 & 0.2203 & 0.2659 & 0.3042 & 0.4720 & 1.0000 & 0.4720 & 0.3042 & 0.2659 & 0.2203 \\ 0.1812 & 0.2043 & 0.2203 & 0.2659 & 0.3042 & 0.4720 & 1.0000 & 0.4720 & 0.3042 & 0.2659 \\ 0.1720 & 0.1812 & 0.2043 & 0.2203 & 0.2659 & 0.3042 & 0.4720 & 1.0000 & 0.4720 & 0.3042 \\ 0.1575 & 0.1720 & 0.1812 & 0.2043 & 0.2203 & 0.2659 & 0.3042 & 0.4720 & 1.0000 & 0.4720 \\ 0.1513 & 0.1575 & 0.1720 & 0.1812 & 0.2043 & 0.2203 & 0.2659 & 0.3042 & 0.4720 & 1.0000 \end{Bmatrix}$$

The receive *covariance* matrix is,

$$\mathbf{R}_{\mathbf{H}}^{Rx} = \begin{Bmatrix} 1.0000 & 0.5589 & 0.1420 & 0.2130 & 0.1279 & 0.1533 & 0.1113 & 0.1255 & 0.0993 & 0.1086 \\ 0.5589 & 1.0000 & 0.5589 & 0.1420 & 0.2130 & 0.1279 & 0.1533 & 0.1113 & 0.1255 & 0.0993 \\ 0.1420 & 0.5589 & 1.0000 & 0.5589 & 0.1420 & 0.2130 & 0.1279 & 0.1533 & 0.1113 & 0.1255 \\ 0.2130 & 0.1420 & 0.5589 & 1.0000 & 0.5589 & 0.1420 & 0.2130 & 0.1279 & 0.1533 & 0.1113 \\ 0.1279 & 0.2130 & 0.1420 & 0.5589 & 1.0000 & 0.5589 & 0.1420 & 0.2130 & 0.1279 & 0.1533 \\ 0.1533 & 0.1279 & 0.2130 & 0.1420 & 0.5589 & 1.0000 & 0.5589 & 0.1420 & 0.2130 & 0.1279 \\ 0.1113 & 0.1533 & 0.1279 & 0.2130 & 0.1420 & 0.5589 & 1.0000 & 0.5589 & 0.1420 & 0.2130 \\ 0.1255 & 0.1113 & 0.1533 & 0.1279 & 0.2130 & 0.1420 & 0.5589 & 1.0000 & 0.5589 & 0.1420 \\ 0.0993 & 0.1255 & 0.1113 & 0.1533 & 0.1279 & 0.2130 & 0.1420 & 0.5589 & 1.0000 & 0.5589 \\ 0.1086 & 0.0993 & 0.1255 & 0.1113 & 0.1533 & 0.1279 & 0.2130 & 0.1420 & 0.5589 & 1.0000 \end{Bmatrix}$$

The transmit and receive correlation matrices for the 10×10 measurements taken on 12/21/00, for locations 3,4, are listed below.

The transmit *covariance* matrix is,

$$\mathbf{R}_{\mathbf{H}}^{Tx} = \begin{Bmatrix} 1.0000 & 0.4720 & 0.3042 & 0.2659 & 0.2203 & 0.2043 & 0.1812 & 0.1720 & 0.1575 & 0.1513 \\ 0.4720 & 1.0000 & 0.4720 & 0.3042 & 0.2659 & 0.2203 & 0.2043 & 0.1812 & 0.1720 & 0.1575 \\ 0.3042 & 0.4720 & 1.0000 & 0.4720 & 0.3042 & 0.2659 & 0.2203 & 0.2043 & 0.1812 & 0.1720 \\ 0.2659 & 0.3042 & 0.4720 & 1.0000 & 0.4720 & 0.3042 & 0.2659 & 0.2203 & 0.2043 & 0.1812 \\ 0.2203 & 0.2659 & 0.3042 & 0.4720 & 1.0000 & 0.4720 & 0.3042 & 0.2659 & 0.2203 & 0.2043 \\ 0.2043 & 0.2203 & 0.2659 & 0.3042 & 0.4720 & 1.0000 & 0.4720 & 0.3042 & 0.2659 & 0.2203 \\ 0.1812 & 0.2043 & 0.2203 & 0.2659 & 0.3042 & 0.4720 & 1.0000 & 0.4720 & 0.3042 & 0.2659 \\ 0.1720 & 0.1812 & 0.2043 & 0.2203 & 0.2659 & 0.3042 & 0.4720 & 1.0000 & 0.4720 & 0.3042 \\ 0.1575 & 0.1720 & 0.1812 & 0.2043 & 0.2203 & 0.2659 & 0.3042 & 0.4720 & 1.0000 & 0.4720 \\ 0.1513 & 0.1575 & 0.1720 & 0.1812 & 0.2043 & 0.2203 & 0.2659 & 0.3042 & 0.4720 & 1.0000 \end{Bmatrix}$$

The receive *covariance* matrix is,

$$\mathbf{R}_{\mathbf{H}}^{Rx} = \begin{Bmatrix} 1.0000 & 0.4911 & 0.2762 & 0.2584 & 0.2040 & 0.1962 & 0.1689 & 0.1644 & 0.1473 & 0.1443 \\ 0.4911 & 1.0000 & 0.4911 & 0.2762 & 0.2584 & 0.2040 & 0.1962 & 0.1689 & 0.1644 & 0.1473 \\ 0.2762 & 0.4911 & 1.0000 & 0.4911 & 0.2762 & 0.2584 & 0.2040 & 0.1962 & 0.1689 & 0.1644 \\ 0.2584 & 0.2762 & 0.4911 & 1.0000 & 0.4911 & 0.2762 & 0.2584 & 0.2040 & 0.1962 & 0.1689 \\ 0.2040 & 0.2584 & 0.2762 & 0.4911 & 1.0000 & 0.4911 & 0.2762 & 0.2584 & 0.2040 & 0.1962 \\ 0.1962 & 0.2040 & 0.2584 & 0.2762 & 0.4911 & 1.0000 & 0.4911 & 0.2762 & 0.2584 & 0.2040 \\ 0.1689 & 0.1962 & 0.2040 & 0.2584 & 0.2762 & 0.4911 & 1.0000 & 0.4911 & 0.2762 & 0.2584 \\ 0.1644 & 0.1689 & 0.1962 & 0.2040 & 0.2584 & 0.2762 & 0.4911 & 1.0000 & 0.4911 & 0.2762 \\ 0.1473 & 0.1644 & 0.1689 & 0.1962 & 0.2040 & 0.2584 & 0.2762 & 0.4911 & 1.0000 & 0.4911 \\ 0.1443 & 0.1473 & 0.1644 & 0.1689 & 0.1962 & 0.2040 & 0.2584 & 0.2762 & 0.4911 & 1.0000 \end{Bmatrix}$$

The transmit and receive correlation matrices for the 10×10 measurements taken on 12/21/00, for locations 5,6, are listed below.

The transmit *covariance* matrix is,

$$\mathbf{R}_{\mathbf{H}}^{Tx} = \begin{Bmatrix} 1.0000 & 0.4720 & 0.3042 & 0.2659 & 0.2203 & 0.2043 & 0.1812 & 0.1720 & 0.1575 & 0.1513 \\ 0.4720 & 1.0000 & 0.4720 & 0.3042 & 0.2659 & 0.2203 & 0.2043 & 0.1812 & 0.1720 & 0.1575 \\ 0.3042 & 0.4720 & 1.0000 & 0.4720 & 0.3042 & 0.2659 & 0.2203 & 0.2043 & 0.1812 & 0.1720 \\ 0.2659 & 0.3042 & 0.4720 & 1.0000 & 0.4720 & 0.3042 & 0.2659 & 0.2203 & 0.2043 & 0.1812 \\ 0.2203 & 0.2659 & 0.3042 & 0.4720 & 1.0000 & 0.4720 & 0.3042 & 0.2659 & 0.2203 & 0.2043 \\ 0.2043 & 0.2203 & 0.2659 & 0.3042 & 0.4720 & 1.0000 & 0.4720 & 0.3042 & 0.2659 & 0.2203 \\ 0.1812 & 0.2043 & 0.2203 & 0.2659 & 0.3042 & 0.4720 & 1.0000 & 0.4720 & 0.3042 & 0.2659 \\ 0.1720 & 0.1812 & 0.2043 & 0.2203 & 0.2659 & 0.3042 & 0.4720 & 1.0000 & 0.4720 & 0.3042 \\ 0.1575 & 0.1720 & 0.1812 & 0.2043 & 0.2203 & 0.2659 & 0.3042 & 0.4720 & 1.0000 & 0.4720 \\ 0.1513 & 0.1575 & 0.1720 & 0.1812 & 0.2043 & 0.2203 & 0.2659 & 0.3042 & 0.4720 & 1.0000 \end{Bmatrix}$$

The receive *covariance* matrix is,

$$\mathbf{R}_{\mathbf{H}}^{Rx} = \begin{Bmatrix} 1.0000 & 0.6387 & 0.1788 & 0.2003 & 0.1196 & 0.1408 & 0.1013 & 0.1143 & 0.0897 & 0.0986 \\ 0.6387 & 1.0000 & 0.6387 & 0.1788 & 0.2003 & 0.1196 & 0.1408 & 0.1013 & 0.1143 & 0.0897 \\ 0.1788 & 0.6387 & 1.0000 & 0.6387 & 0.1788 & 0.2003 & 0.1196 & 0.1408 & 0.1013 & 0.1143 \\ 0.2003 & 0.1788 & 0.6387 & 1.0000 & 0.6387 & 0.1788 & 0.2003 & 0.1196 & 0.1408 & 0.1013 \\ 0.1196 & 0.2003 & 0.1788 & 0.6387 & 1.0000 & 0.6387 & 0.1788 & 0.2003 & 0.1196 & 0.1408 \\ 0.1408 & 0.1196 & 0.2003 & 0.1788 & 0.6387 & 1.0000 & 0.6387 & 0.1788 & 0.2003 & 0.1196 \\ 0.1013 & 0.1408 & 0.1196 & 0.2003 & 0.1788 & 0.6387 & 1.0000 & 0.6387 & 0.1788 & 0.2003 \\ 0.1143 & 0.1013 & 0.1408 & 0.1196 & 0.2003 & 0.1788 & 0.6387 & 1.0000 & 0.6387 & 0.1788 \\ 0.0897 & 0.1143 & 0.1013 & 0.1408 & 0.1196 & 0.2003 & 0.1788 & 0.6387 & 1.0000 & 0.6387 \\ 0.0986 & 0.0897 & 0.1143 & 0.1013 & 0.1408 & 0.1196 & 0.2003 & 0.1788 & 0.6387 & 1.0000 \end{Bmatrix}$$

The transmit and receive correlation matrices for the 10×10 measurements taken on 12/21/00, for locations 7,8, are listed below.

The transmit *covariance* matrix is,

$$\mathbf{R}_{\mathbf{H}}^{Tx} = \begin{Bmatrix} 1.0000 & 0.4720 & 0.3042 & 0.2659 & 0.2203 & 0.2043 & 0.1812 & 0.1720 & 0.1575 & 0.1513 \\ 0.4720 & 1.0000 & 0.4720 & 0.3042 & 0.2659 & 0.2203 & 0.2043 & 0.1812 & 0.1720 & 0.1575 \\ 0.3042 & 0.4720 & 1.0000 & 0.4720 & 0.3042 & 0.2659 & 0.2203 & 0.2043 & 0.1812 & 0.1720 \\ 0.2659 & 0.3042 & 0.4720 & 1.0000 & 0.4720 & 0.3042 & 0.2659 & 0.2203 & 0.2043 & 0.1812 \\ 0.2203 & 0.2659 & 0.3042 & 0.4720 & 1.0000 & 0.4720 & 0.3042 & 0.2659 & 0.2203 & 0.2043 \\ 0.2043 & 0.2203 & 0.2659 & 0.3042 & 0.4720 & 1.0000 & 0.4720 & 0.3042 & 0.2659 & 0.2203 \\ 0.1812 & 0.2043 & 0.2203 & 0.2659 & 0.3042 & 0.4720 & 1.0000 & 0.4720 & 0.3042 & 0.2659 \\ 0.1720 & 0.1812 & 0.2043 & 0.2203 & 0.2659 & 0.3042 & 0.4720 & 1.0000 & 0.4720 & 0.3042 \\ 0.1575 & 0.1720 & 0.1812 & 0.2043 & 0.2203 & 0.2659 & 0.3042 & 0.4720 & 1.0000 & 0.4720 \\ 0.1513 & 0.1575 & 0.1720 & 0.1812 & 0.2043 & 0.2203 & 0.2659 & 0.3042 & 0.4720 & 1.0000 \end{Bmatrix}$$

The receive *covariance* matrix is,

$$\mathbf{R}_{\mathbf{H}}^{Rx} = \begin{Bmatrix} 1.0000 & 0.5479 & 0.3384 & 0.2991 & 0.2445 & 0.2286 & 0.2012 & 0.1921 & 0.1749 & 0.1689 \\ 0.5479 & 1.0000 & 0.5479 & 0.3384 & 0.2991 & 0.2445 & 0.2286 & 0.2012 & 0.1921 & 0.1749 \\ 0.3384 & 0.5479 & 1.0000 & 0.5479 & 0.3384 & 0.2991 & 0.2445 & 0.2286 & 0.2012 & 0.1921 \\ 0.2991 & 0.3384 & 0.5479 & 1.0000 & 0.5479 & 0.3384 & 0.2991 & 0.2445 & 0.2286 & 0.2012 \\ 0.2445 & 0.2991 & 0.3384 & 0.5479 & 1.0000 & 0.5479 & 0.3384 & 0.2991 & 0.2445 & 0.2286 \\ 0.2286 & 0.2445 & 0.2991 & 0.3384 & 0.5479 & 1.0000 & 0.5479 & 0.3384 & 0.2991 & 0.2445 \\ 0.2012 & 0.2286 & 0.2445 & 0.2991 & 0.3384 & 0.5479 & 1.0000 & 0.5479 & 0.3384 & 0.2991 \\ 0.1921 & 0.2012 & 0.2286 & 0.2445 & 0.2991 & 0.3384 & 0.5479 & 1.0000 & 0.5479 & 0.3384 \\ 0.1749 & 0.1921 & 0.2012 & 0.2286 & 0.2445 & 0.2991 & 0.3384 & 0.5479 & 1.0000 & 0.5479 \\ 0.1689 & 0.1749 & 0.1921 & 0.2012 & 0.2286 & 0.2445 & 0.2991 & 0.3384 & 0.5479 & 1.0000 \end{Bmatrix}$$

The transmit and receive correlation matrices for the 4×4 measurements taken on 08/22/00, for locations 2,3, are listed below.

The transmit *covariance* matrix is,

$$\mathbf{R}_{\mathbf{H}}^{Tx} = \begin{Bmatrix} 1.0000 & 0.5994 & 0.3703 & 0.3236 \\ 0.5994 & 1.0000 & 0.5994 & 0.3703 \\ 0.3703 & 0.5994 & 1.0000 & 0.5994 \\ 0.3236 & 0.3703 & 0.5994 & 1.0000 \end{Bmatrix}$$

The receive *covariance* matrix is,

$$\mathbf{R}_{\mathbf{H}}^{Rx} = \begin{Bmatrix} 1.0000 & 0.7251 & 0.3996 & 0.3174 \\ 0.7251 & 1.0000 & 0.7251 & 0.3996 \\ 0.3996 & 0.7251 & 1.0000 & 0.7251 \\ 0.3174 & 0.3996 & 0.7251 & 1.0000 \end{Bmatrix}$$

The transmit and receive correlation matrices for the 4×4 measurements taken on 08/22/00, for locations 4,5, are listed below.

The transmit *covariance* matrix is,

$$\mathbf{R}_{\mathbf{H}}^{Tx} = \begin{Bmatrix} 1.0000 & 0.5859 & 0.3432 & 0.3064 \\ 0.5859 & 1.0000 & 0.5859 & 0.3432 \\ 0.3432 & 0.5859 & 1.0000 & 0.5859 \\ 0.3064 & 0.3432 & 0.5859 & 1.0000 \end{Bmatrix}$$

The receive *covariance* matrix is,

$$\mathbf{R}_{\mathbf{H}}^{Rx} = \begin{Bmatrix} 1.0000 & 0.9063 & 0.7495 & 0.6309 \\ 0.9063 & 1.0000 & 0.9063 & 0.7495 \\ 0.7495 & 0.9063 & 1.0000 & 0.9063 \\ 0.6309 & 0.7495 & 0.9063 & 1.0000 \end{Bmatrix}$$

The transmit and receive correlation matrices for the 4×4 measurements taken on 08/22/00, for locations 6,7,8, are listed below.

The transmit *covariance* matrix is,

$$\mathbf{R}_{\mathbf{H}}^{Tx} = \begin{Bmatrix} 1.0000 & 0.5770 & 0.3245 & 0.2952 \\ 0.5770 & 1.0000 & 0.5770 & 0.3245 \\ 0.3245 & 0.5770 & 1.0000 & 0.5770 \\ 0.2952 & 0.3245 & 0.5770 & 1.0000 \end{Bmatrix}$$

The receive *covariance* matrix is,

$$\mathbf{R}_{\mathbf{H}}^{Rx} = \begin{Bmatrix} 1.0000 & 0.8476 & 0.6015 & 0.4566 \\ 0.8476 & 1.0000 & 0.8476 & 0.6015 \\ 0.6015 & 0.8476 & 1.0000 & 0.8476 \\ 0.4566 & 0.6015 & 0.8476 & 1.0000 \end{Bmatrix}$$

REFERENCES

[1] G. J. Foschini and M. J. Gans, "On limits of wireless communications in a fading environment", *Wireless Pers. Commun.,* vol. 6, pp. 311-335, 1998.

[2] I. E. Telatar, "Capacity of multi-antenna Gaussian channels", *European Trans. Telecommun. Related Technol.,* vol. 10, pp. 585- 595, 1999.

[3] V. Tarokh, N. Seshadri, and A. R. Calderbank, "Space-time codes for high data rate wireless communication: Performance criterion and code construction", *IEEE Trans. Infor. Theory,* vol. 44, pp. 744-765, 1998.

[4] G. Golden, C. Foschini, R. Valenzuela, and P. Wolniansky, "Detection algorithm and initial laboratory results using V-BLAST space- time communication architecture," *Electron. Letters.,* vol. 35, no. 1, pp. 14-15, Jan. 1999.

[5] K. Yu, M. Bengtsson, B. Ottersen, D. McNamara, P. Karlson and M. Beach, "Second order statistics of NLOS indoor MIMO channels based on 5.2 GHz measurements", in *Proc. IEEE Global Telecommun. Conf.,* San Antonio, Texas, 2001, pp. 156-160.

[6] A. Abdi and M. Kaveh, "A space-time correlation model for multielement antenna systems in mobile fading channels", *IEEE J. Select. Areas Commun.,* vol. 20, pp. 550-560, 2002.

[7] B. A. Bjerke and J. G. Proakis, "Multiple-antenna diversity techniques for transmission over fading channels", in *Proc. IEEE Wireless Commun. & Networking Conf.,* New Orleans, LA, 1999, vol. 3, pp. 461-465.

[8] R. H. Clark, "A statistical theory of mobile radio reception", *Bell Syst. Tech. J.,* vol. 47, no. 6. pp. 957-1000, July- Aug, 1968.

[9] R. B. Ertel, P. Cardieri,K. S. Sowerby, and T. S. Rappaport, "Overview of spatial channel models for antenna array communication systems", *IEEE Pers. Commun. Mag.,* vol. 5, no.1, pp. 10-22,1998.

[10] D. Shiu, G. J. Foschini, M. J. Gans, J. M. Kahn, "Fading correlation and its effect on the capacity of multi-element antenna systems," *IEEE Trans. Commun.,* vol. 48, no. 3, pp. 502-513, March 2000.

[11] W. C. Jakes, Jr., "Multipath Interference,", *Microwave Mobile Communications,* W. C. Jakes, Jr., Ed., New York, Wiley, 1974, pp. 11-78.

[12] K. Yu and B. Ottersen, "Models for MIMO propagation channels, A review", *Wiley Journal on Wireless Commun. and Mobile Comp., Special Issue of Adaptive Antennas and MIMO Systems,* 2002.

[13] J. C. Liberti and T. S. Rappaport, "A geometrically based model for line of sight multipath radio channels", in *Proc. IEEE Vehicular Technology Conference.*, Atlanta, Georgia, April 1996, vol. 2, pp. 844-848.

[14] D. Gesbert, H. Bölcskei, D. Gore, and A. Paulraj, "MIMO wireless channels: capacity and performance", in *Proc. Global Telecommunications Conference.*, San Francisco, CA, November 2000, vol. 2, pp. 1083-1088.

[15] D. Shiu, *Wireless Communication Usng Dual Antenna Arrays,* Kluwer Academic Publishers, 2000.

[16] J. J. Blanz and P. Jung, "A flexibly configurable spatial model for mobile radio channels", *IEEE Trans. on Commun.,* vol. 46, pp. 366-371, 1998.

[17] A. G. Burr, "Wide-band channel modeling using a spatial model", in *Proc. IEEE 5th Int. Symp. on Spread Spectrum Techniques Applications,* Sun City, South Africa, 1998, vol. 1, pp. 255-257.

[18] L. Hanlen and M. Fu, "Multiple antenna wireless communication systems: limits to capacity growth", in *Proc. IEEE Wireless Commun. Networking Conf.,* 2002, vol. 1, pp. 173-176.

[19] H. Asplund, A. F. Molisch, M. Steinbauer and N. Mehta, "Clustering of scatterers in mobile radio channels- Evaluation and modeling in the COST259 directional channel model", in *Proc. IEEE Int.Conf. Commun.,* New York, 2002, vol. 3. pp. 901-905.

[20] D. Gesbert, H. Bölcskei, D. A. Gore and A. J. Paulraj, "Performance evaluation for scattering MIMO channel models", in *Proc. Asilomar Conf. Signals, Systems and Computers,* Pacific Grove, California, CA, 2000, vol. 1, pp. 748-752.

[21] J. Fuhl, A. F. Molisch and E. Bonek, "Unified channel model for mobile radio systems with smart antennas", *IEE Proc. Radar, Sonar, Navig.,* vol. 145, pp. 32-41, 1998.

[22] J. W. Wallace and M. A. Jensen, "Measured Characteristics of the MIMO wireless channel", in *Proc. of IEEE Vehic. Technol. Conf.,* Atlantic City, NJ, 2001, vol. 4, pp. 2038-2042.

[23] J. W. Wallace and M. A. Jensen, "Modeling the indoor MIMO wireless channel", *IEEE Transactions on Antennas and Propagation,* vol. 50, no. 5, pp. 591-599, May 2002.

[24] G. J. Byers and Fambirai Takawira, "The influence of spatial and temporal correlation on the capacity of MIMO channels", in *Wireless Commun. and Networking Conf.,* New Orleans, LA, 2003.

[25] I. S. Gradshteyn and I. M. Ryzhik, in *Tables of Integrals, Series, and Products,* 5th ed., A. Jeffrey, Ed., San Diego, CA: Academic, 1994.

[26] H. Hashemi, "The indoor radio propagation channel", in *Proc. of the IEEE*, vol. 81, no. 7, pp. 943-968, July 1993.

[27] Linda. M. Davis, "Scaled and decoupled Cholesky and QR decompositions with application to spherical MIMO detection", in *press.*